

IVW - Schriftenreihe Band 129

Institut für Verbundwerkstoffe GmbH - Kaiserslautern

Gihune Jung

**Development of continuous fiber-
and long fiber reinforced thermo-
plastic materials with multilayered
hybrid structure, and then crash
application thereof**

Bibliografische Information Der Deutschen Bibliothek

Die Deutsche Bibliothek verzeichnet diese Publikation in der Deutschen Nationalbibliografie; detaillierte bibliografische Daten sind im Internet über <<http://dnb.ddb.de>> abrufbar.

Bibliographic information published by Die Deutsche Bibliothek

Die Deutsche Bibliothek lists this publication in the Deutsche Nationalbibliografie; detailed bibliographic data is available in the Internet at <<http://dnb.ddb.de>>.

Herausgeber: Institut für Verbundwerkstoffe GmbH
Prof. Dr.-Ing. Ulf Breuer
Erwin-Schrödinger-Straße
TU Kaiserslautern, Gebäude 58
67663 Kaiserslautern
<http://www.ivw.uni-kl.de>

Verlag: Institut für Verbundwerkstoffe GmbH

Druck: Technische Universität Kaiserslautern
ZBT – Abteilung Foto-Repro-Druck

D 386

© Institut für Verbundwerkstoffe GmbH, Kaiserslautern 2018

Alle Rechte vorbehalten, auch das des auszugsweisen Nachdrucks, der auszugsweisen oder vollständigen Wiedergabe (Photographie, Mikroskopie), der Speicherung in Datenverarbeitungsanlagen und das der Übersetzung.

Als Manuskript gedruckt. Printed in Germany.
ISSN 1615-021X
ISBN 978-3-944440-24-8

Development of continuous fiber- and long fiber reinforced thermoplastic materials with multilayered hybrid structure, and then crash application thereof

Vom Fachbereich Maschinenbau und Verfahrenstechnik
der Technischen Universität Kaiserslautern
zur Verleihung des akademischen Grades

Doktor-Ingenieur (Dr.-Ing.)

genehmigte Dissertation

von

M. Eng. Gihune Jung

aus Boseong (KOR)

Tag der mündlichen Prüfung: 31. August 2018

Prüfungsvorsitzender: Prof. Dr.-Ing. Paul Ludwig Geiß

1. Berichterstatter: Prof. Dr.-Ing. Peter Mitschang

2. Berichterstatter: Prof. Dr.-Ing. Ralf Schledjewski

D386

Preface

The present work was intensively conducted in the years of 2012 to 2016 during my occupation as a research associate in the Department of Manufacturing Science at the Institut für Verbundwerkstoffe (IVW) GmbH, Kaiserslautern, Germany.

I would like to express my gratitude to the supervisor Prof. Dr.-Ing. Peter Mitschang for the comprehensive guidance and the excellent research environment. Besides, I really appreciate Prof. Dr.-Ing. Ralf Schledjewski making the second appraisal, and Prof. Dr.-Ing. Paul Ludwig Geiß taking over the chairman of the examination board.

The IVW life was very comfortable in the kindness of Mrs. Andrea Hauck, Dr. Luisa Medina, Mr. Matthias Bendler, Mr. Steven Brogdon, Dr. Miro Duhovic, Mr. Holger Franz, Dr. Sergiy Grishchuk, Dr. Liudmyla Gryschchuk, Mr. Sven Hennes, Dr. Robert Lahr, Mr. Michael Päßler, Dr. Jens Schlimbach, Mr. Uwe Schmitt, Mr. Roman Schüler, Mr. Thomas Schütz and Mr. Torsten Weick. Many thanks for having shared ideas and scientific issues frequently with the colleagues in the department, who are Matthias Arnold, Markus Brzeski, Marcel Christmann, Mirja Didi, Karsten Grebel, Timo Grieser, Klaus Hildebrandt, René Holschuh, Jens Mack, Dennis Maurer, David May, Jovana Džalto and Martina Hümbert, as well as Matthias Domm, Florian Gortner, Oliver McGregor, Wolfgang Koch, Florian Kühn, Stephan Becker, Christian Goergen, Oliver Rimmel and Jan Eric Semar. Of course, I owe to the well-developed competence of Mr. Mark Dully and Mr. Harald Weber at the workshop, Mr. Stefan Giehl, Mr. Peter Mang, Mr. Michael Nast, Mr. Erhard Natter and Mr. Eric Schott for processing, Mr. Hermann Giertzsch and Mr. Ralf Schimmele for characterization, and Mr. Jan Rehra, Dr. Sebastian Schmeer and Mr. Ralph Schneider for crash application.

Finally, the most important ones are my wife Songyi Chong and two daughters Jiwoo and Seoyeon, not to mention my parents and parents-in-law. They have encouraged me always, and then are more pleased with my achievement than I am.

Contents

Contents I

Abbreviation and Nomenclature III

Kurzfassung..... VII

Abstract..... VIII

1 Introduction and Objective 1

 1.1 Motivation 1

 1.2 Structure and Objective 3

2 State of the Art 5

 2.1 Fiber Reinforced Thermoplastic Materials 5

 2.1.1 Continuous fiber reinforcement..... 9

 2.1.2 Long fiber reinforcement..... 16

 2.2 Crash Behavior and Performance..... 24

 2.2.1 Crashworthy structure..... 25

 2.2.2 Material and crash behavior..... 27

3 Material Development..... 33

 3.1 Impregnation..... 34

 3.1.1 General Kozeny-Carman equation 34

 3.1.2 Modified equation for packed bed of fibers 37

 3.1.3 Permeability and tortuous degree 39

 3.1.4 Controllable parameters 43

 3.2 Continuous Fiber Reinforcement 45

 3.2.1 Concept of multilayered hybrid roving..... 45

 3.2.2 Newly derived spreading equation..... 48

 3.2.3 Verification on impregnation quality 53

3.2.4	Characterization on major direction	56
3.2.5	Variation in minor direction.....	60
3.3	Long Fiber Reinforcement	63
3.3.1	Concept of multilayered hybrid mat	63
3.3.2	Changes of porosity along pressure	65
3.3.3	Preparation and impregnation.....	71
3.3.4	Evaluation and characterization	75
4	Crash Application	85
4.1	Dynamic Crash Test.....	85
4.1.1	Specimen preparation.....	85
4.1.2	Test and evaluation method	89
4.2	Woven Fabric of PP/GF	91
4.3	Random Mat of PP/GF	97
4.4	Random Mat of PA6/GF	101
5	Conclusions	105
6	References	108
7	Appendix	123
	Betreute studentische Arbeiten.....	124
	Publikationen	125
	Lebenslauf.....	127

Abbreviation and Nomenclature

Abbreviation	Description
Al	Aluminum
ANOVA	Analysis of variance
BMC	Bulk molding compound
CAGR	Compound annual growth rate
CBT	Cyclic butylene terephthalate
CCM	Continuous compression molding
CF	Carbon fiber
CFRP	Carbon fiber reinforced plastic
CR	Controlled rheology
CV	Coefficient of variation
DMC	Dough molding compound
GF	Glass fiber
GFRP	Glass fiber reinforced plastic
GMT	Glass mat reinforced thermoplastic
HDPE	High-density polyethylene
IR	Infrared
LFT	Long fiber reinforced thermoplastic
LFT-D	Long fiber reinforced thermoplastic through direct process
LFT-D/ILC	LFT-D process by inline compounding
LFT-D/IMC	LFT-D system with injection molding compounder
LFT-P	Long fiber reinforced thermoplastic of pellet shape
LWRT	Lightweight reinforced thermoplastic
MD	Machine direction
Mg	Magnesium
MLH-mat	Multilayered hybrid mat
MLH-roving	Multilayered hybrid roving
PA12	Polyamide 12

Abbreviation	Description
PA6	Polyamide 6
PA66	Polyamide 66
PEEK	Polyether ether ketone
PEKK	Polyetherketoneketone
PP	Polypropylene
PPS	Polyphenylene sulfide
SEA	Specific energy absorption (J/g)
SFT	Short fiber reinforced thermoplastic
SMC	Sheet molding compound
TD	Transverse direction
TEX	Unit of linear density for fiber bundle (g/km)
Ti	Titanium
TPU	Thermoplastic polyurethane
UD	Unidirectional
VEA	Volumetric energy absorption (J/cm ³)
vol. %	Volume percent
wt. %	Weight percent

Notation	Unit	Description
Impregnation and rule of mixtures		
d	m	Fiber diameter or equivalent cylinder diameter
d_f	m	Individual fiber diameter
D	m	Equivalent sphere diameter
D_c	m	Diameter of cylindrical pipe or equivalent cylindrical pipe diameter
E_{11}	GPa	Modulus of unidirectional major (longitudinal direction)
E_{22}	GPa	Modulus of unidirectional minor (transverse direction)
E_f	GPa	Modulus of fiber
E_m	GPa	Modulus of matrix
h_c	m	Height of cylindrical pipe or actual path length
Δh	m	Height of packed bed
K	m ²	Permeability
l	m	Fiber length
m	-	Number of rows
n	-	Number of columns
ΔP	Pa	Pressure drop
s	μm	Inter-fiber spacing
S_c	m ²	Surface area of capillaries
S_p	m ²	Surface area of particles
V_c	m ³	Volume of capillaries
V_f	-	Fiber volume fraction
V_p	m ³	Volume of particles
ε	-	Porosity of packed bed
η	Pa.s	Viscosity of fluid
λ	-	Degree of agglomeration
v	m/s	Superficial or empty-tower velocity
v_c	m/s	Mean velocity in cylindrical pipe

Notation	Unit	Description
Spreading		
H	mm	Vertical distance
L_R	mm	Tangent length intersecting two supports at center line
L_r	mm	Tangent length intersecting two supports at arbitrary position
R	mm	Radius of spreading support at center line
R_s	mm	Radius of starting support
r	mm	Radius of spreading support at arbitrary position
S	mm	Horizontal distance
x	mm	Half width after spreading
x_i	mm	Half width before spreading
θ_R	°	Acute angle with vertical line at center line
θ_r	°	Acute angle with vertical line at arbitrary position

Notation	Unit	Description
Crash		
$A(l)$	mm ²	Function of cross-sectional area
E	J	Applied impact energy
L	mm	Length of test specimen
W	g	Weight of test specimen
δ	mm	Maximum displacement
ρ	g/cm ³	Density of test specimen

Kurzfassung

Der Fokus der vorliegenden Arbeit liegt auf endlosfaser- und langfaserverstärkten thermoplastischen Materialien. Hierfür wurde das „multilayered hybrid (MLH)“ Konzept entwickelt und auf zwei Halbzeuge, den MLH-Roving und die MLH-Mat angewendet. Der MLH-Roving ist ein Roving (bestehend aus Endlosfasern), der durch thermoplastische Folien in mehrere Schichten geteilt wird. Der MLH-Roving wird durch eine neuartige Spreizmethode mit anschließender thermischer Fixierung und abschließender mehrfacher Faltung hergestellt. Dadurch können verschiedene Faser-Matrix-Konfigurationen realisiert werden. Die MLH-Mat ist ein glasmattenverstärktes thermoplastisches Material, das für hohe Fasergehalte bis 45 vol. % und verschiedene Matrixpolymere, z.B. Polypropylen (PP) und Polyamide 6 (PA6) geeignet ist. Sie zeichnet sich durch eine hohe Homogenität in der Flächendichte und in der Faserrichtung aus. Durch dynamische Crashversuche mit auf MLH-Roving und MLH-Mat basierenden Probekörpern wurden das Crashverhalten und die Performance untersucht. Die Ergebnisse der Crashkörper basierend auf langfaserverstärktem Material (MLH-Mat) und endlosfaserverstärktem Material (MLH-Roving) waren vergleichbar. Die PA6-Typen zeigten eine bessere Crashperformance als PP-Typen.

Abstract

The present work deals with continuous fiber- and long fiber reinforced thermoplastic materials. The concept of multilayered hybrid (MLH) structure was developed and applied to the so-called MLH-roving and MLH-mat. The MLH-roving is a continuous fiber roving separated evenly into several sublayers by thermoplastic films, through the sequential processes of spreading with a newly derived equation, thermal fixing, and folding. It was aimed to satisfy the variety of material configuration as well as the variety in intermediate product. The MLH-mat is a glass mat reinforced thermoplastic (GMT)-like material that is suitable for high fiber contents up to 45 vol. % and various matrix polymers, e.g. polypropylene (PP), polyamide 6 (PA6). It showed homogeneity in areal density, random directional fiber distribution, and reheating stability required for molding process. On the MLH-roving and MLH-mat materials, the crash behavior and performance were investigated by dynamic crash test. Long fiber reinforced materials (MLH-mat) were equivalent to continuous fiber reinforced materials (MLH-roving), and PA6 grades showed higher crash performance than PP grades.

1 Introduction and Objective

1.1 Motivation

The present work deals with continuous fiber- and long fiber reinforced thermoplastic materials that are becoming more and more important today in automotive industry. Due to an inverse relationship between intrinsic stiffness and shape complexity (see Figure 1.1), the hybridization of materials should be considered as an essential point to achieve more efficient components. It accompanies a sort of integrated processes. There are several types of continuous fiber- and long fiber reinforced thermoplastic materials already available in the market. However, those materials are insufficient to fully satisfy a wider choice of materials as well as so-called hybrid molding processes.

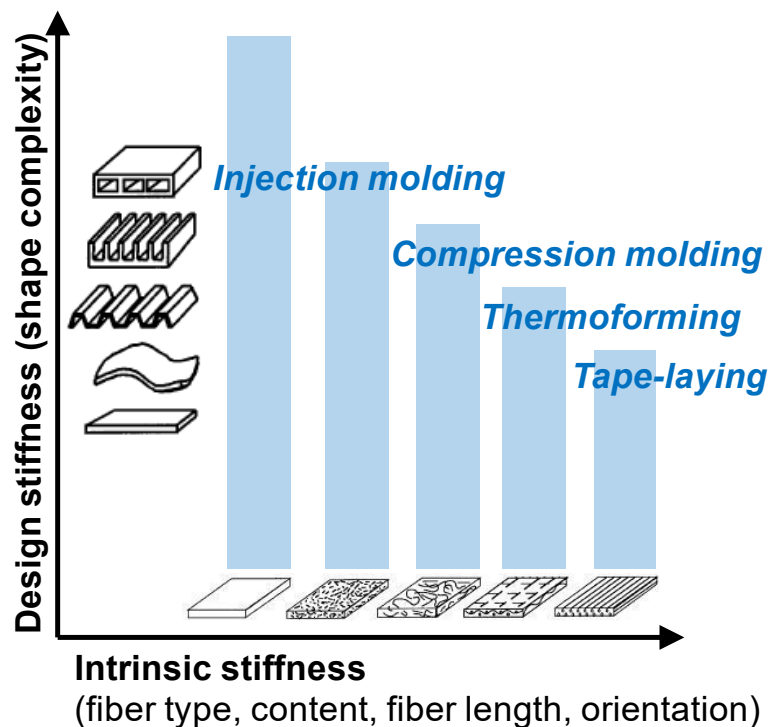


Figure 1.1: Inverse relationship between intrinsic stiffness and shape complexity [1]

Many attempts to develop continuous fiber reinforced thermoplastic materials could not fill up all the needs of the varieties in both material configuration and intermediate product completely; e.g. somewhat limited variety in matrix polymer if using powder or filament form, nothing but consolidated plates if produced by film stacking method, too thin but inflexible pre-impregnated tapes and so on. The fiber contents of these materials are relatively high ranging from 35 vol. % to 60 vol. %. Meanwhile, most of

long fiber reinforced thermoplastic materials can trace back to the traditional attempts of short fiber reinforcement commonly using screw systems to compound matrix resin with fiber and to mold into a component. So, it is difficult to increase the fiber content up to the level of continuous fiber reinforcement on a commercial scale. No attention paid to the gap of fiber contents might have brought about the prejudice that long fiber reinforcement is weaker than continuous fiber reinforcement. On the other hand, the manufacturing process of glass mat reinforced thermoplastic (GMT) material also uses an extruder, but this is just to melt a matrix resin of lowered viscosity and then feed onto glass mats [2][3]; there is no conceivable reason why the fiber contents are so low now in GMT materials, except for ensuring flowability to mold a component.

In the field of lightweight applications, fiber reinforced thermoset and thermoplastic materials have competed against metallic materials for a long time, with lower density and better formability. Nevertheless, there are some peerless cases to use metallic materials of ductile behavior, where structural parts should not be failed suddenly by brittle fractures. But, this ductile behavior can be undesirable in crash application due to a reduced length-efficiency (refer to Figure 1.2 (a)) led by full compaction in folded zones. When reinforced with brittle fibers, such as glass and carbon, thermoset and thermoplastic materials are providing the obviously different crash behaviors named fragmentation mode and splaying mode [4] (refer to Figure 1.2 (b) and Figure 1.2 (c)). Furthermore, the tough behavior of thermoplastic materials would make an important contribution toward the splaying mode to be free from pulverized particles.

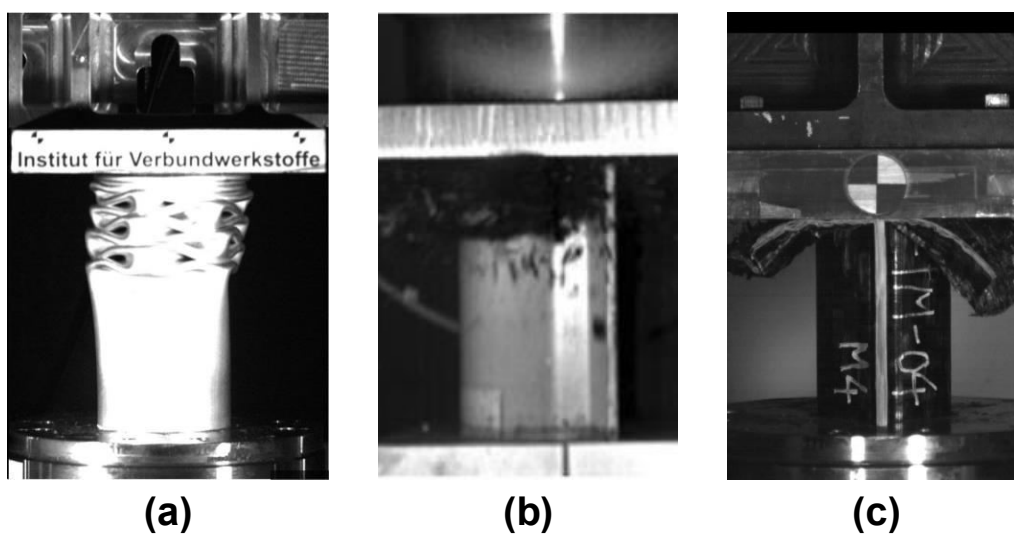


Figure 1.2: Crash behaviors of (a) metallic material, (b) fiber reinforced thermoset material [5], and (c) fiber reinforced thermoplastic material

1.2 Structure and Objective

The structure of present work is organized into two parts, as schematized in Figure 1.3. The first part is about the material development with the concept of multilayered hybrid structure; continuous fiber- and long fiber reinforced thermoplastic materials consisting of several sublayers of matrix polymer film and fiber reinforcement. The second part is about the crash application using those two materials especially for deformable components not only to dissipate impact energy as far as possible, but also to follow a stable, progressive and controlled crushing behavior.

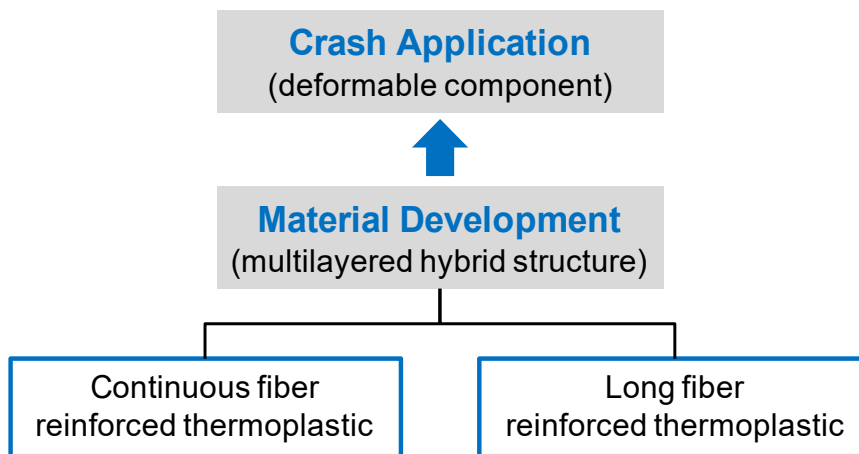


Figure 1.3: Structure of present work: material development and crash application

Each objective is as follows and summarized in Table 1.1. The development strategy for continuous fiber reinforced thermoplastic material is to pick the variety of material configuration from organic sheets as well as the variety in intermediate product from commingled rovings (refer to Table 1.2 for basic features of these two materials).

Table 1.1: Objectives of present work

Crash Application	
Influence of matrix polymer (PP vs. PA6) on crash behavior and performance	
Comparison between continuous fiber- and long fiber reinforcements	
Material Development	
Continuous fiber reinforcement	Long fiber reinforcement
Variety of material configuration	High GF content (e.g. 45 vol. %)
Variety in intermediate product	Various polymers (e.g. PP and PA6)
Spreading fibers without splitting	Maintaining impregnation quality

Meanwhile, the development strategy for long fiber reinforced thermoplastic material is to keep a feature similar to conventional GMT materials. But it aims to be suitable for high fiber contents, like 45 vol. % glass fiber (GF), and for various matrix polymers including polypropylene (PP) used for conventional GMT materials (refer to Table 1.2) and polyamide 6 (PA6). Here the concept of multilayered hybrid structure is simply based on the minimized unit-height of fiber reinforcement, in consideration of good balances between easy impregnation and cost aspects in a wide range of circumstances. Thus, the key issue for continuous fiber reinforcement is how to spread the continuous fibers into a given width without center-splitting-problem. And the key issue for long fiber reinforcement is to see if the impregnation quality is acceptable even at high fiber contents.

Table 1.2: Basic features of current materials for benchmarking

Material	Features
Organic sheet (TEPEX [®]) [6]	Woven fabric of fiber reinforcement with thermoplastic resin Impregnated and consolidated plate or simple profile shape
Commingled roving (TwinTEX [®]) [7]	Suitable for various processes (e.g. winding, weaving, etc.) Various material configuration by offline commingling
GMT (StrongLite [®]) [3]	PP/GF15 wt. % to PP/GF45 wt. % (6 vol. % to 22 vol. %) Limited matrix resin of lowered viscosity in a chemical way

The crash behavior and performance are investigated by dynamic crash test which takes into account true circumstances as well as the material sensitivity to strain rate, obeying a short-time scale behavior of substance governed by elastic modulus and strain limit [5][8]. For this reason, long fiber reinforcement would be very worthy of attention if reaching the same level of fiber content as continuous fiber reinforcement. In general, long fiber reinforcement has a random directional fiber distribution and accompanies a cheaper price, at least no need of weaving or placement, as well as an excellent design-flexibility compared to continuous fiber reinforcement. Therefore, the key issue in crash application is set as the comparison of crash behaviors and performances between continuous fiber- and long fiber reinforcements, including the influence of matrix polymer.

2 State of the Art

The global demand for glass fiber reinforced plastic (GFRP) materials is continuously increasing every year like 8,800 kilo tonnes in 2014 and above 10,000 kilo tonnes in 2016; it is about 100 times as great as the global demand for carbon fiber reinforced plastic (CFRP) materials [9][10]. GFRP and CFRP materials are further segmented not only by fiber length into short fiber, long fiber and continuous fiber reinforcements, but also by matrix type into thermoset and thermoplastic materials.

This chapter will focus on current status and limitations of continuous fiber- and long fiber reinforced thermoplastic materials commercially available in the market. A basic prerequisite is that continuous fiber reinforced thermoplastic materials are being used for local reinforcement through hybrid molding processes with a species of flowable materials. Moreover, it would be better if the flowable materials are reinforced with long fiber rather than short fiber. Certainly, thermoplastic materials have outstanding advantages such as recycling, eco-friendly manufacturing, shorter processing time, lower costs for mass production, and impact resistance. Also the tough behaviors of thermoplastic materials, even if reinforced with brittle fibers, will serve as a promising point in the field of crash application. One possibility is that crash energy absorbers are dissipating impact energies by their sacrifice in crashworthy structures. However, it is not so easy to impregnate woven or nonwoven fabrics of fiber reinforcement with any thermoplastic resin of high melt viscosity.

2.1 Fiber Reinforced Thermoplastic Materials

The production of GFRP materials in Europe is 2,800 kilo tonnes in 2016, and short fiber reinforced thermoplastic (SFT) materials take the biggest proportion with 49% (1,360 kilo tonnes) [10]. Due to short fiber-length less than 1 mm, SFT materials have been restricted to the specific purposes like modulus dominant applications. A useful guideline, as depicted in Figure 2.1, suggests that fiber length in molded components should roughly be over 1 mm for modulus, 5 mm for strength, and 25 mm for impact resistance. This leads to an increased demand for long fiber reinforced thermoplastic (LFT) materials, with a high compound annual growth rate (CAGR) of 7.6% in Europe, from 121 kilo tonnes in 2014 to 140 kilo tonnes in 2016 [10]. So far it takes a small

proportion in the GFRP materials with 5%. Thus the sum of SFT and LFT materials becomes 54% (1,500 kilo tonnes). The remaining 46% (1,300 kilo tonnes) is mainly assigned to thermoset materials of continuous fiber and long fiber reinforcements, including a very little amount of continuous fiber reinforced thermoplastic materials.

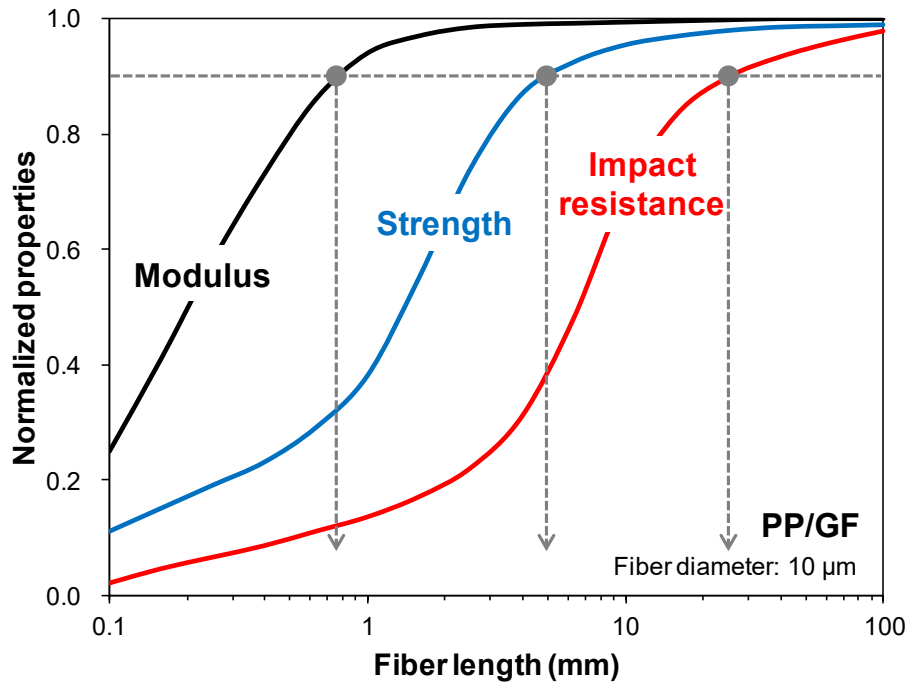


Figure 2.1: Normalized mechanical properties along with fiber length: glass fiber (GF) reinforced polypropylene (PP) [11][12][13]

Some automotive components of high volume production have been hybrid-molded for the best performance, commonly by the aid of local reinforcement with continuous fiber reinforced thermoplastic materials (refer to Figure 2.2); clockwise from top left, steering column holders, airbag modules, brake pedals, and door side-impact beams. Typically, SFT and LFT materials take charge of shape complexity (or design stiffness) with flowability, and continuous fiber reinforced materials contribute toward intrinsic stiffness but with a limited drapability [14][15][16][17].

The manufacturing process involves several steps, such as heating a sheet blank of continuous fiber reinforced thermoplastic material in an oven and then placing it in an injection mold or on a compression mold as quickly as possible using a robot system. Thereafter, the sheet blank is simultaneously thermoformed and overmolded with the flowable thermoplastic material reinforced with long fiber, short fiber, or unfilled. In the whole range of manufacturing processes, however, careful attention should be taken

to the mechanical properties at overmolded interfaces not being weakened by dusts, residues of releasing agent and oil, thermal decomposition of resin (the most serious one) and so on.



Figure 2.2: Hybrid-molded automotive components by the aid of local reinforcement with continuous fiber reinforced thermoplastic materials [18][19][20]

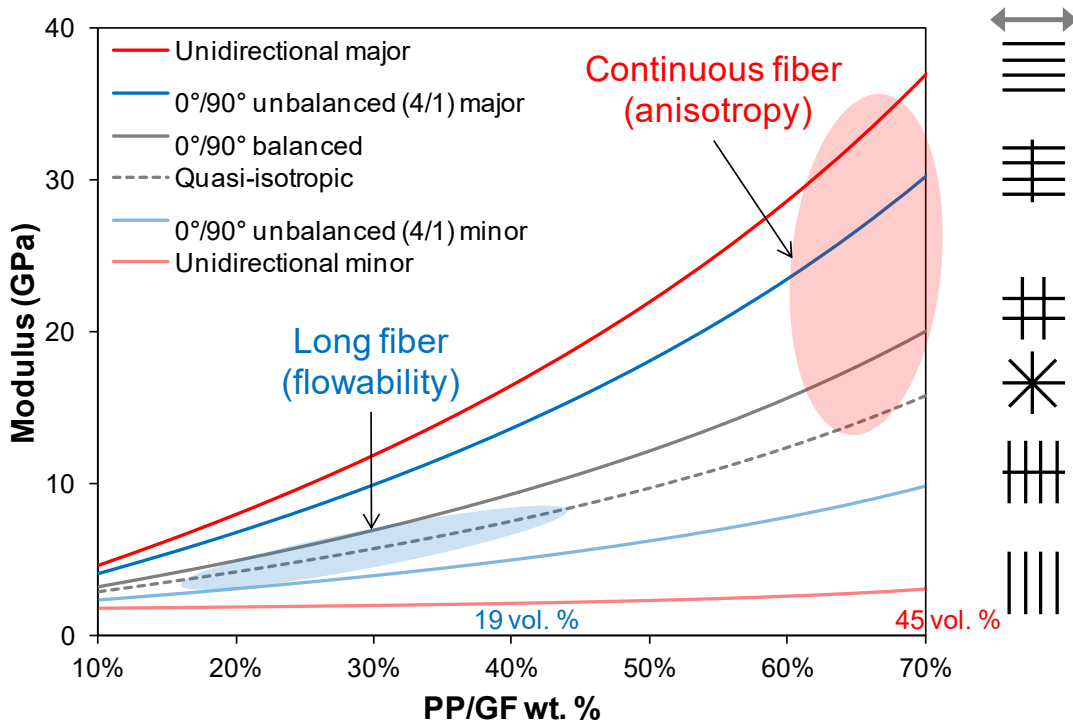


Figure 2.3: Modulus curves of PP/GF along with fiber content and fiber orientation

The modulus of fiber reinforced polymeric materials can be theoretically estimated by the rule of mixtures [21][22]. It is highly dependent not only on fiber type, but also on fiber content and fiber orientation. Thus, the modulus of a given matrix-fiber system normally increases with fiber content, and it varies with fiber orientation as shown in Figure 2.3; curves based on PP of 1.72 GPa [23] for the modulus of matrix (E_m) and GF of 80.5 GPa [24] for the modulus of fiber (E_f) with the fiber volume fraction (V_f) (refer to Table 2.1 for each layup).

Table 2.1: Modulus estimation by the rule of mixtures on different layups

Modulus	Equation
Unidirectional (UD) major	$E_{11} = V_f E_f + (1 - V_f) E_m$
Unidirectional (UD) minor	$E_{22} = \frac{E_f E_m}{V_f E_m + (1 - V_f) E_f}$
0°/90° unbalanced (4/1) major and minor	$\frac{4}{5} E_{11} + \frac{1}{5} E_{22}$ and $\frac{1}{5} E_{11} + \frac{4}{5} E_{22}$
0°/90° balanced	$\frac{1}{2} E_{11} + \frac{1}{2} E_{22}$
Quasi-isotropic	$\frac{3}{8} E_{11} + \frac{5}{8} E_{22}$

The general level of fiber content in PP/GF materials available in the market is below 40 wt. % (19 vol. %) for long fiber reinforcement and short fiber reinforcement of a random directional fiber distribution (refer to quasi-isotropic curve in Figure 2.3). Meanwhile, for continuous fiber reinforcement, it ranges from 60 wt. % (35 vol. %) to 72 wt. % (47 vol. %) [7][25]. Toward the best performance-to-price ratio, it is often recommended that these materials have an anisotropic reinforcement starting from 0°/90° balanced weaving up to unidirectional major, much more strongly if reinforced with expensive carbon fiber (CF). The gap of fiber contents, also fiber orientation, might induce the prejudice that long fiber reinforcement is weaker than continuous fiber reinforcement, although there is no link between fiber length and modulus; e.g. when above 5 mm in fiber length. This is why the present work aims to develop high content of long fiber reinforced thermoplastic materials equivalent to continuous fiber reinforcement.

2.1.1 Continuous fiber reinforcement

Some manufacturing processes for continuous fiber reinforced thermoplastic material, like pre-impregnated tows and film stacking (see Figure 2.4), are certainly derived from the ways that have been used for thermoset material. Yet these processes have much more difficulty in impregnation caused by high melt viscosity; 100–5,000 Pa.s of thermoplastic resin vs. 0.1–1 Pa.s of thermoset resin [26][27]. Consequently, other new approaches had to be designed, and each is named as powder-impregnated fiber bundle, commingled roving, and so on (see Figure 2.4); commonly making thermoplastic matrix physically premixed with fiber reinforcement before melting. And every attempt focuses on how to overcome the high viscosity of thermoplastic matrix and/or how to achieve the fast and reliable impregnation of fiber reinforcement.

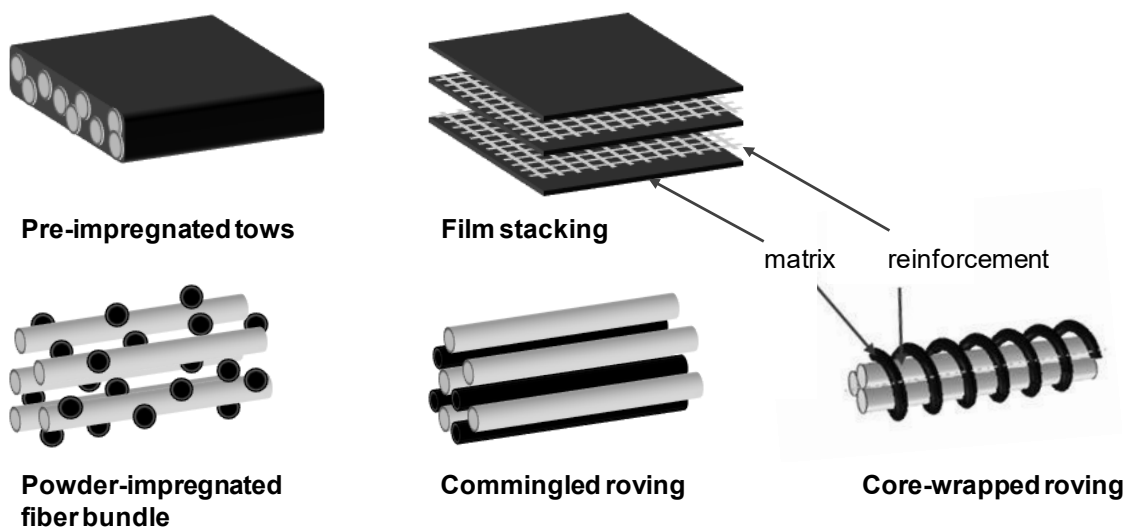


Figure 2.4: Manufacturing processes for continuous fiber reinforced thermoplastic material [1][28][29][30]

Several of the above attempts have successfully led to commercial products such as pre-impregnated tows the so-called tapes (e.g. SupremTM, Celstran[®], and Cetex[®])¹,

¹ SupremTM is the trade name originated from Suprem SA (Switzerland) for pre-impregnated tows in the shape of unidirectionally reinforced thermoplastic tapes, profiles, and rods. Celstran[®] is the trade name originated from Celanese AG (USA). TenCate Advanced Composites is a multi-national company (headquarters in the USA and Netherlands) that produces advanced thermoset and Cetex[®] branded thermoplastic composite materials from high-density polyethylene (HDPE) and polyamide 6 (PA6) to polyether ether ketone (PEEK) and polyetherketoneketone (PEKK).

fully impregnated plates the so-called organic sheets (e.g. TEPEX®) on the basis of film stacking between woven fabrics of reinforcement, and commingled rovings (e.g. TwinTEX®) of fiber-fiber system.

Pre-impregnated tow

Pre-impregnated tows can take several different shapes in response to a forming-die, such as tapes, profiles and rods as shown in Figure 2.5. And these are all commonly manufactured by means of a pultrusion process using extruders, through the specific series of steps that are impregnation, forming, cooling of thermoplastic material, and pulling. Hence, pre-impregnated tows are basically inflexible even in the case of thin tapes, not to mention profiles and rods.

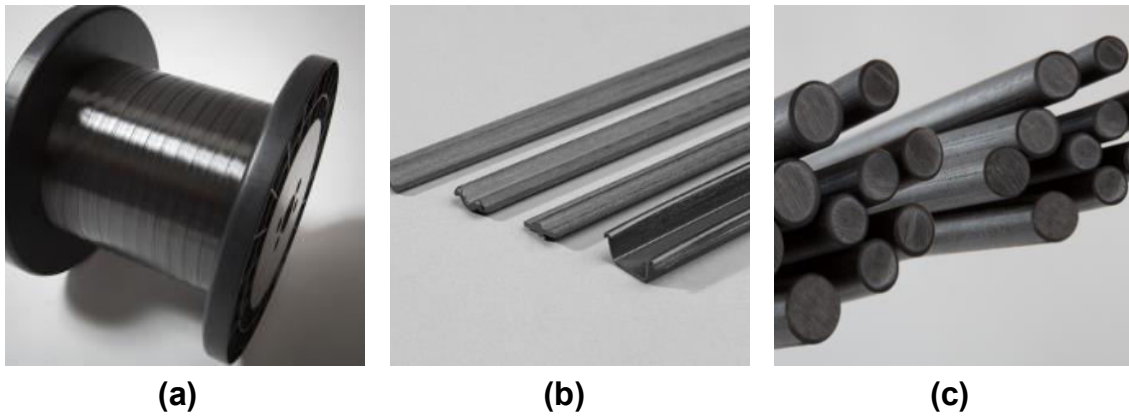


Figure 2.5: Pre-impregnated tows of Suprem™ [31] in the shapes of unidirectionally reinforced thermoplastic (a) tapes, (b) profiles, and (c) rods

Fiber reinforcements in pre-impregnated tows could be ideally characterized by the square and hexagonal models, as depicted in Figure 2.6, to define the relationships of the fiber volume fraction (V_f), the individual fiber diameter (d_f), and the inter-fiber spacing (s) [21]. In addition, those are associated with the macroscopic information about the unit thickness of tape as well as the nominal roving width. A fiber array is expressed in terms of the number of rows (m) by the number of columns (n), thus, the unit thickness of tape and the nominal roving width are calculated by the following equations. However, the reverse calculations to obtain the values of m and n are more useful for the characterization of a fiber array.

$$\text{Square model: } md_f + (m-1)s \quad \text{and} \quad nd_f + (n-1)s \quad (2.1)$$

$$\text{Hexagonal model: } (m-1)(d_f + s)\cos(\pi/6) + d_f \quad \text{and} \quad nd_f + (n-1)s \quad (2.2)$$

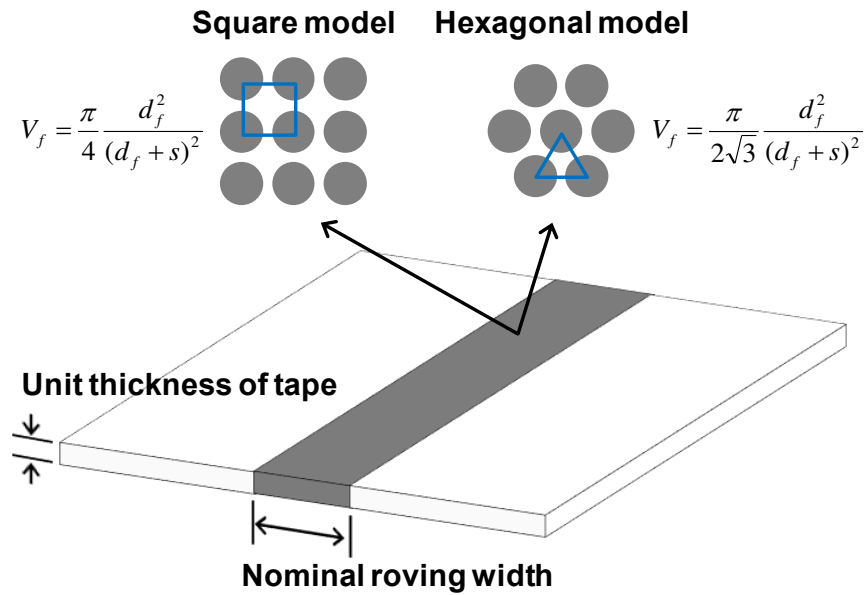


Figure 2.6: Characterization of fiber array by square and hexagonal models

For example, PA6/CF45 vol. % (56 wt. %) unidirectional tape of SGL Carbon SE² is described with the data of 0.18 mm in unit thickness (or 255 g/m² in areal density and 1.42 g/cm³ in density), using SIGRAFIL[®] 50k CF rovings of 7.0 μm in fiber diameter [32][33]. The values of inter-fiber spacing are returned, respectively 2.25 and 2.94 μm, by entering the fiber volume fraction and the individual fiber diameter into the square and hexagonal models. Then, the number of rows in CF array is calculated to be 20–21 rows from 0.18 mm the unit thickness of tape. Moreover, the nominal roving width becomes 23–24 mm based on 50k the number of fibers in a CF roving. This means that a single CF roving forms an array of about 20 by 2500.

As for the unidirectional Cetex[®] tapes of TenCate Advanced Composites (see Table 2.2), the CF grades have the similar numbers of rows in CF array with AS-4 roving of 7.1 μm in fiber diameter [34]. But, the GF grade has the smaller number of rows in GF array with S2 GF roving of 10 μm in fiber diameter [35]. It is not clear whether each level of the number of rows in fiber array is differently designed for CF and GF from the first.

² SGL Carbon SE is a German chemical company manufacturing carbon-related products from carbon fibers to composites preferably with polyamide 6 (PA6) matrix resin. It has operated on the market as SGL Group-The Carbon Company since March 2007.

Table 2.2: Number of rows in array for unidirectional Cetex[®] tapes

Grade	No. of rows	Information on composite
PA6/CF49 vol. % (60 wt. %)	18–19	0.16 mm in unit thickness [36] 232 g/m ² in areal density
PEEK/CF59 vol. % (66 wt. %)	17–18	0.14 mm in unit thickness 218 g/m ² in areal density [37]
PEEK/GF56 vol. % (71 wt. %)	13–14	0.15 mm in unit thickness 289 g/m ² in areal density [37]

In short, the pre-impregnated tows in the shape of unidirectional tape have 15–20 rows in fiber array as the overall value, or up to 21 rows for CF grade and 14 rows for GF grade, when ideally characterized by the square and hexagonal models.

Organic sheet

As shown in Figure 2.7, a manufacturing process of the so-called organic sheets, a kind of fully impregnated plates, starts with the step where thermoplastic films and woven fabrics are alternatively stacked on top of one another. Continuously, woven fabrics are fully impregnated with melted resin and consolidated on a double belt press, then cut to a given length. The organic sheets are quite easy to design with various material configurations on fiber reinforcement (glass, carbon, and aramid) and thermoplastic matrix (PA66, PA6, PP, PA12, PPS, PC, and TPU)³ [6][38], like TEPEX[®]. The fiber contents are normally in the range of 45 vol. % to 55 vol. %.

However, the product type is limited to consolidated plates when manufactured by a double belt press; cf. sometimes it can be shaped into uncomplicated profiles [39] by continuous compression molding (CCM). Most fiber reinforcements of TEPEX[®] are of the balanced woven fabrics with twill pattern having an areal density of 200 g/m² with 3k CF rovings (200 TEX⁴) [40] or 600 g/m² with 1200 TEX GF rovings [41]. The unit-

³ Polyamide 66 (PA66), Polyamide 6 (PA6), Polypropylene (PP), Polyamide 12 (PA12), Polyphenylene sulfide (PPS), Polycarbonate (PC), and Thermoplastic polyurethane (TPU)

⁴ TEX is a unit of measure, g/km, for the linear density of fibers, yarns and thread.

thickness of TEPEX[®] plates is of one ply of the woven fabrics being impregnated with a relevant matrix polymer. Instead of actual weaving patterns, an approach with 0°/90° laminated tapes will be used here for simplification as depicted in Figure 2.8.

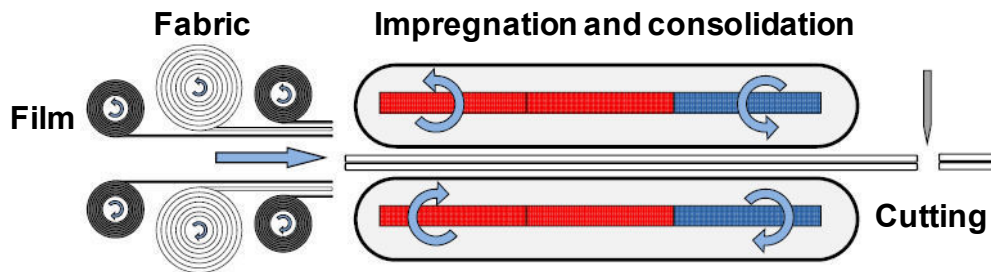


Figure 2.7: Manufacturing process of fully impregnated plate (TEPEX[®]): continuous production on a double belt [38][42]

Each areal density and TEX of the above fiber reinforcements signifies 500 m and 500 m CF rovings, and 250 m and 250 m GF rovings being used in square meter for 0° and 90° directions. So the nominal roving widths can be calculated simply to be 2.0 mm of CF and 4.0 mm of GF. Furthermore, by the square and hexagonal models, the numbers of rows in fiber array per a roving are calculated to be 14–15 rows for PA66/CF45 vol. % with half the unit thickness of 0.25 mm [40] and GF of 7.0 μm in diameter, and be 11–12 rows for PA6/GF47 vol. % with half the unit thickness of 0.50 mm [41] and GF of 18 μm in diameter [43]. But, it would be reasonable to double the above numbers, like 20–30 rows, considering the actual impregnation of TEPEX[®] on a fabric basis (refer to Figure 2.8). The lateral flow is much longer for the aspect ratio of fiber array per a roving is about 16:1. And the melt flow between rovings is more unlikely as the pressure increases. Thus, the impregnation at many crossing points of warp and weft is getting more difficult and time-consuming.

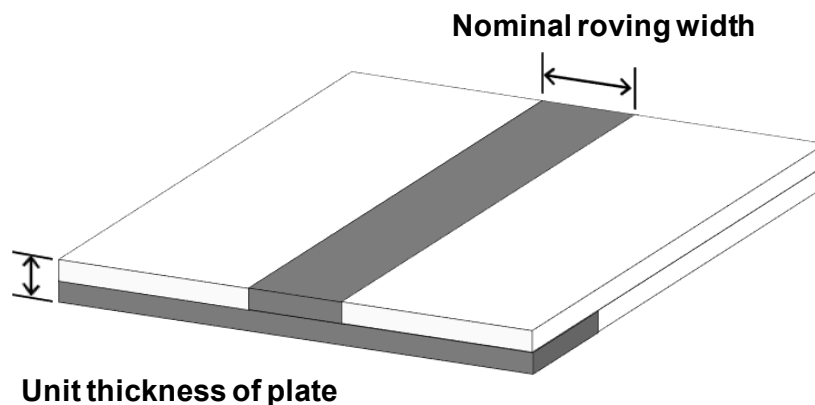


Figure 2.8: Simplified approach with 0°/90° laminated tapes for a woven fabric

Commingled roving

Commingled rovings, on the contrary, are un-impregnated and ready-to-impregnate products. As being a commingled roving of fiber-fiber system, it is suitable for various processes such as filament winding, woven or non-crimp fabric, and pultrusion [7]. Originally TwinTEX[®] process was developed in the way of commingling the two kinds of fibers at the melt spinning stage of the GF production line as depicted in Figure 2.9. Afterwards, the so-called offline commingling processes emerged as an alternative way to provide more diversity in material configurations. Two kinds of fibers start from each bobbin and then usually pass through an air-nozzle to open and intensively mix them [28][44][45].

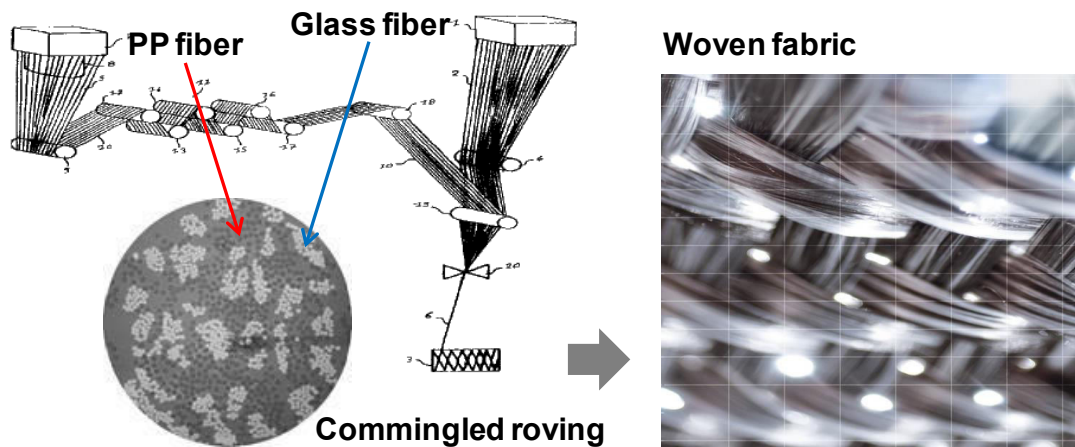


Figure 2.9: Online commingling [28][46] and woven fabric of TwinTEX[®] [47]

The main grade of TwinTEX[®] is PP/GF35 vol. % (60 wt. %) having a linear density of 1870 TEX [7]. It consists of PP fibers and glass fibers. PP fiber has a common melt viscosity of 880 to 360 Pa.s at 220°C in the range of 0.1 to 10 s⁻¹ shear rate [48]. And glass fiber has a linear density of 1120 TEX with 17 μm in diameter, which is on the same level with TEPEX[®] GF grades. The balanced woven fabrics with twill pattern have the typical areal densities of 745, 980 and 1485 g/m² [49]; these are designed for a fully impregnated and consolidated plate to be respectively 0.5, 0.7 and 1.0 mm in thickness. Through the same procedures used for TEPEX[®] and ignoring PP fibers, the above fabrics (or consolidated plates) can be characterized respectively with the nominal roving width and the number of rows in GF array per a commingled roving; 5.0 mm width and 10–11 rows for 745 g/m², 3.8 mm width and 13–14 rows for 980 g/m², and 2.5 mm width and 20–21 rows for 1485 g/m², changing aspect ratios from 20:1 to 5:1. TwinTEX[®] has 10–20 rows in GF array per a commingled roving as an

overall value. However, the actual impregnation environment would be better than above numbers of rows represent. As depicted in Figure 2.10, it depends on commingling quality in a roving that can be conceptually classified into three types; homogeneous, agglomerated, and side-by-side distributions. TwinTEX[®] is much easier to impregnate than TEPEX[®], even in the worst case of side-by-side distribution. But, TwinTEX[®] has uncontrollable high risks which are most likely to be caused by irregularly distributed and movable fibers.

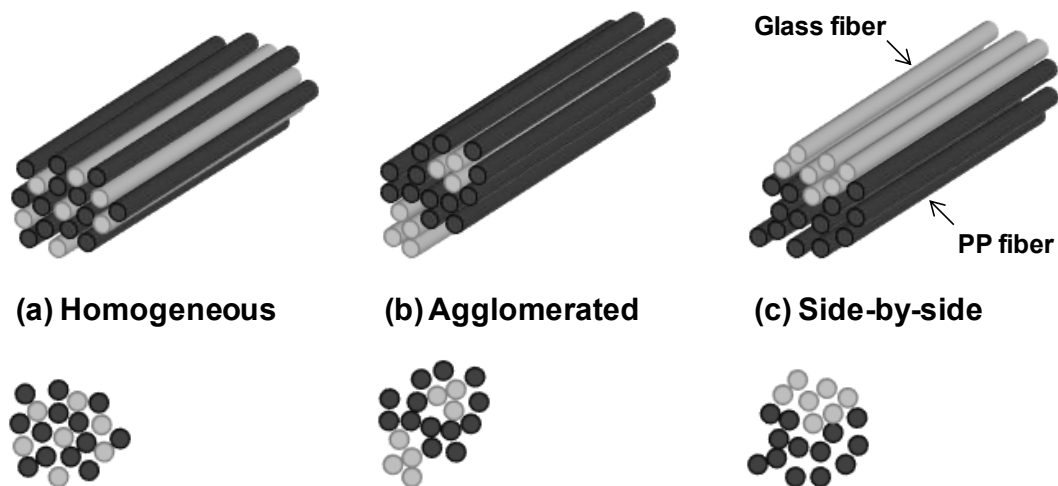


Figure 2.10: Commingling quality in a roving conceptually classified into three types

In summary, the impregnation becomes easier as the number of rows in fiber array is smaller. The current materials are characterized as being composed of more than 10 rows; 15–20 for pre-impregnated tows in the shape of unidirectional tape, 20–30 for organic sheets (TEPEX[®]) that will be impregnated and consolidated on a fabric basis, and 10–20 for commingled rovings of irregularly distributed and movable fiber-fiber system (TwinTEX[®]). Furthermore, the specific features of each material are listed as follows; flexibility for various processes with ready-to-impregnate TwinTEX[®], wider variety in matrix polymer of TEPEX[®] by using thermoplastic film rather than powder or fiber form, and stable impregnation quality of pre-impregnated tow. There are risks of poor impregnation at crossing points in TEPEX[®] and by commingling irregularity of TwinTEX[®], which have to be overcome and seriously considered for developing new types of materials.

2.1.2 Long fiber reinforcement

Generally, long fiber reinforced thermoplastic (LFT) materials could be classified into three groups like glass mat reinforced thermoplastic (GMT) materials, LFT materials of pellet shape (LFT-P), and LFT materials through direct process (LFT-D). And their mechanical properties are primarily determined by the types of fiber reinforcement and matrix polymer, and subject to variation by the process induced fiber-orientation and by the reduction of fiber-length in a molded component [2][12][50]. In the light of cost, property, and design flexibility, customers are often confronted with the question which kind of LFT material and its related process is the right decision [11].

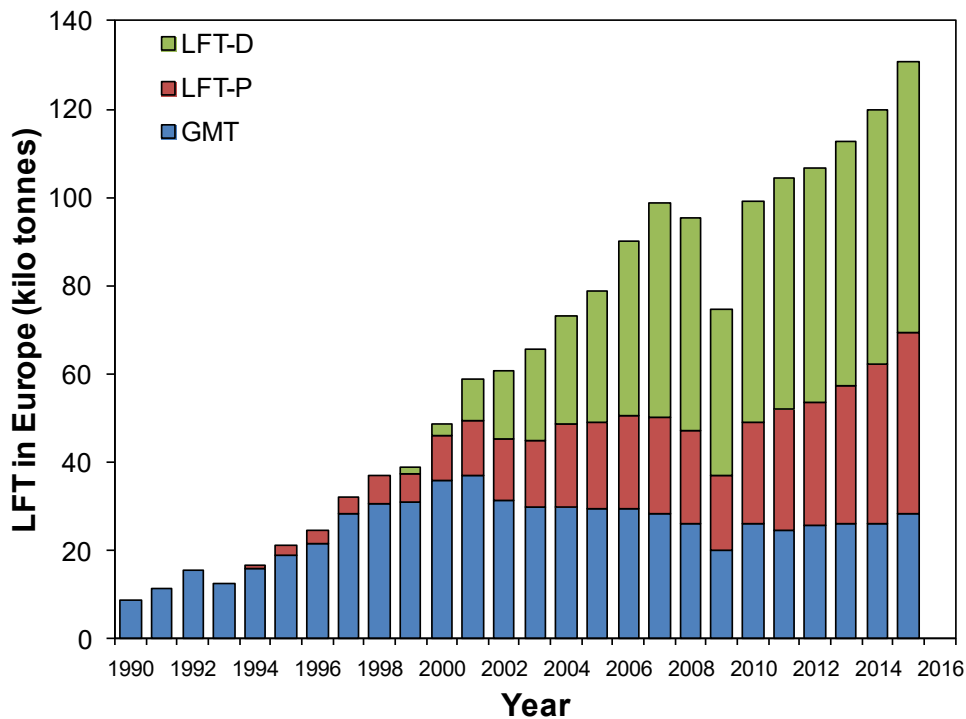


Figure 2.11: Market demand for LFT materials in Europe [2][13]

Glass mat thermoplastic (GMT) material

GMT materials have acted as a notable pioneer for lightweight solution in automotive industry, and sometimes treated as the nearly matchless option for relatively big and thin structural components, e.g. spare wheel well and underbody shield. Since 1972 after the first market launch in the USA under the brand name Azdel[®], GMT materials had continuously grown for about 30 years as the exclusive option [2][51][52] in those days. But, they faced the serious stagnancy from the year 2002 by the emergence of LFT-P and LFT-D materials up to the present time (refer to Figure 2.11). Still there is

no tangible evidence of extinction, despite GMT materials defending themselves with the single item of PP/GF configuration.

GMT materials are commercially manufactured by either of the two distinct processes [2][11]. One is a dry process done by melt-impregnation of nonwoven GF mats, which uses an extruder and a double belt press as schematized in Figure 2.12. The other is a wet process derived from a sort of papermaking process, which starts by mixing both chopped glass fibers and polymer powder in a fluid medium. A continuous web formation as a result of filtration on the screens is then followed by heat drying and consolidation [11]. The most dominant GMT materials are made by a dry process [2][3] into the fully impregnated and consolidated sheets of 3–4 mm thickness. But the GF contents in current products are usually low, being in the range of PP/GF15 wt. % to PP/GF45 wt. %.

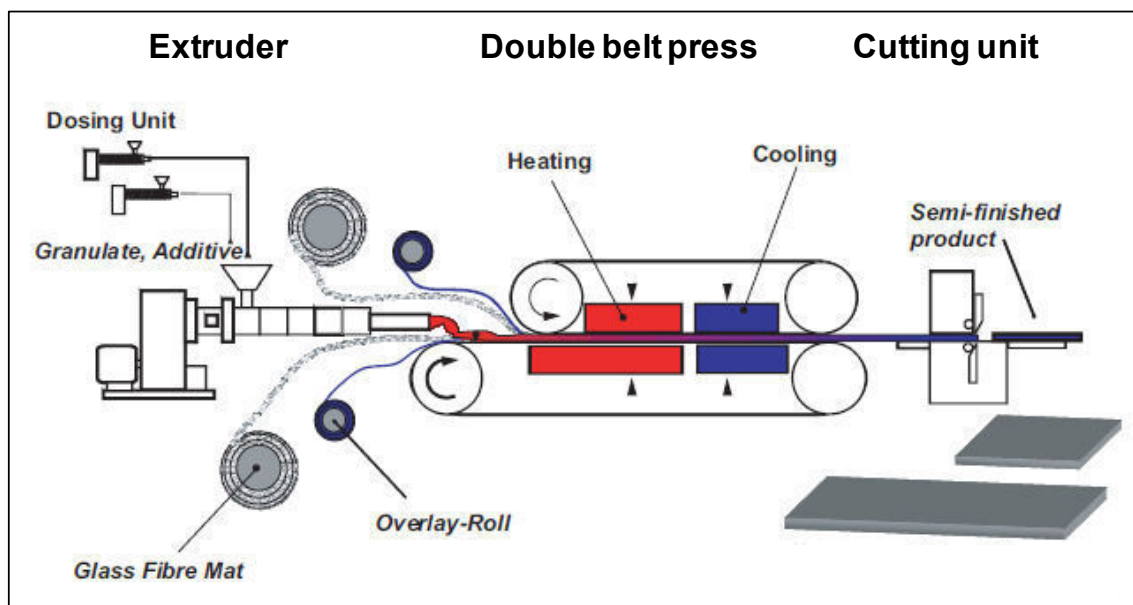


Figure 2.12: Dry process for GMT materials using extruder and double belt press [2]

The chop and needle mat line of a dry process is to prepare nonwoven GF mats by chopping multi-end GF rovings into mixed lengths like 25 and 37 mm; cf. a multi-end GF roving of 2400 TEX is composed of 40 sub-bundles, and there are 100 fibers in each sub-bundle. Here the chopped glass fibers are being scattered on a conveyor belt as evenly as possible, and then needle-matted into a specific areal density like $1,000 \text{ g/m}^2$ [3]. The other detailed specifications of GF mat have been optimized for a long time, with consideration not only for manufacturing costs and handling, but also for impregnation quality crucial in the next process of double belt press. As expected,

it is difficult to impregnate such a thick GF mat due to high viscosity of thermoplastic resin that could not be suitably lowered by increasing temperature and/or shear rate. Therefore, the viscosity of PP resin has to be reduced significantly in a chemical way, e.g. by using some peroxides, named the controlled rheology (CR) [53]; cf. the most widely used peroxide is 2,5-Dimethyl-2,5-di(tert-butylperoxy)hexane that has a high molecular weight and is good for high flash point as well as limited volatility. This is one of the reasons why current GMT materials are limited to PP/GF grade.

Besides, there are consolidated but partially impregnated GMT materials that consist of glass fiber (or basalt fiber) and polymer fiber, the so-called lightweight reinforced thermoplastic (LWRT) materials [2][3]. LWRT materials can be more various in matrix polymer as well as fiber reinforcement, but used for the purpose of noise absorbing.

Furthermore, since 1998 the so-called 'Advanced GMT' materials have been used for heavy-duty underbody shields and bumper beams [2], which are of combining woven fabrics (or unidirectional layers) during GMT production. At the inlet of a double belt press, continuous fiber reinforced thermoplastic materials, such as fabrics or rovings of TwinTEX[®], are put together with conventional GMT materials either continuously for being sandwich skins or discontinuously for local reinforcements. So, 'Advanced GMT' materials could also be compression-molded in the same way as conventional GMT materials, after heating in an oven enough to thermoform. Namely, this is a kind of hybrid molding with continuous fiber and long fiber reinforcements by means of a tailored blank at a stage of material production. And GMT materials, conventional or advanced, are produced commercially into a sheet of 1300–1400 mm in width [52] and cut to a given size for molding big and thin components maintaining fiber length.

LFT material of pellet shape (LFT-P)

LFT-P materials were commercialized in the mid-to-late 1990s by thermoplastic resin producers to increase the mechanical properties much better than those of short fiber reinforced thermoplastic (SFT) materials [52]. In appearance, SFT materials are of pellets cut into normally 6 mm (1/4 inch) length for injection molding, whereas LFT-P materials are of the longer pellets cut into like 10–15 mm (about 1/2 inch) for injection molding or 25 mm (1 inch) for compression molding. Such LFT-P materials are cut from the rods of small diameter manufactured by a pultrusion process of continuous fiber with melted resin. So, the fiber length is equal to the pellet length or a little bit

longer in the case of the twisted LFT [54]. LFT-P materials are very easy to provide various combinations of fiber and matrix [55] offering an intermediate level between SFT and GMT in performance and also price [50].

As a way to reduce cost burdens coming from LFT-P process itself, sometimes, it is recommended to blend the so-called LFT-P concentrates of 60 wt. % to 75 wt. % in fiber content, with resin pellets to achieve a desired level of fiber content [56][57]. Also, the concentrates cannot be used alone as being too harsh to melt by a screw system, and too viscous to mold into a component. Moreover, LFT-P materials do not necessarily have to be fully impregnated, for there are other chances in an injection molding or compression molding machine. This leads to another cost down with an increase in the production rate of LFT-P materials.

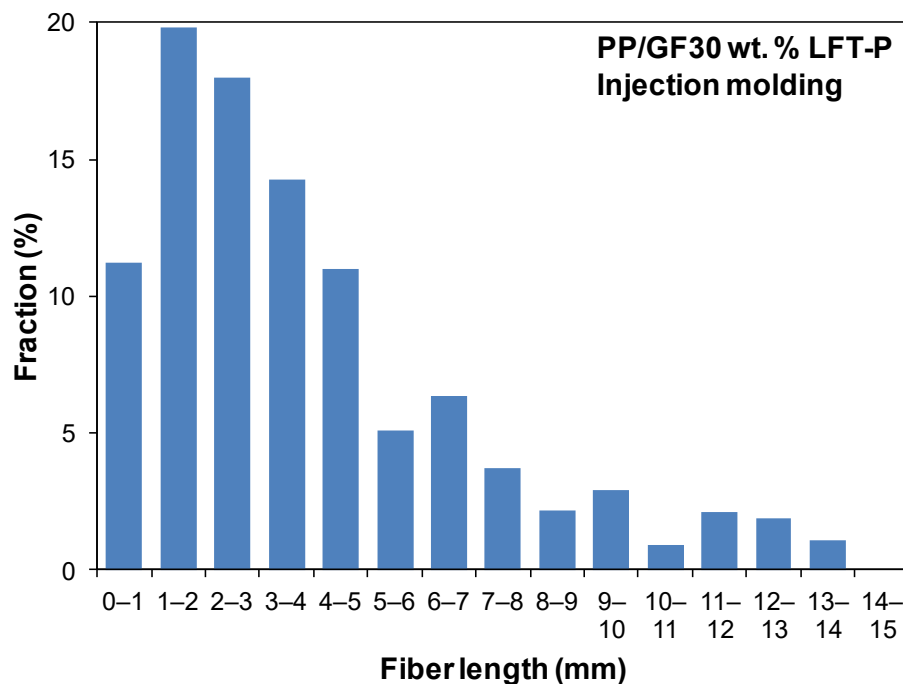


Figure 2.13: Typical fiber length distribution in injection-molded component [11]

However, it is quite unavoidable that the reduction of fiber length is mainly caused by screw geometries and process conditions during injection or compression molding process. In spite of using pellets of 15 mm length (PP/GF30 wt. % LFT-P material), the fiber length distribution in an injection-molded component is represented with the median value of merely 2–3 mm (see Figure 2.13). Similarly, PP/GF40 wt. % LFT-P material of 25 mm in pellet length accompanies the reduction of fiber length about 8 mm at extruder head, further 4–5 mm in a compression-molded component [2][11].

In general, the fiber length of LFT-P materials becomes below 5 mm remaining in a molded component. In the end, they are suitable for modulus and strength dominant applications rather than impact resistance (refer to Figure 2.1). The influence of fiber length on impact resistance can be experimentally distinguished by the relationship between flexural modulus and Charpy impact, as shown in Figure 2.14.

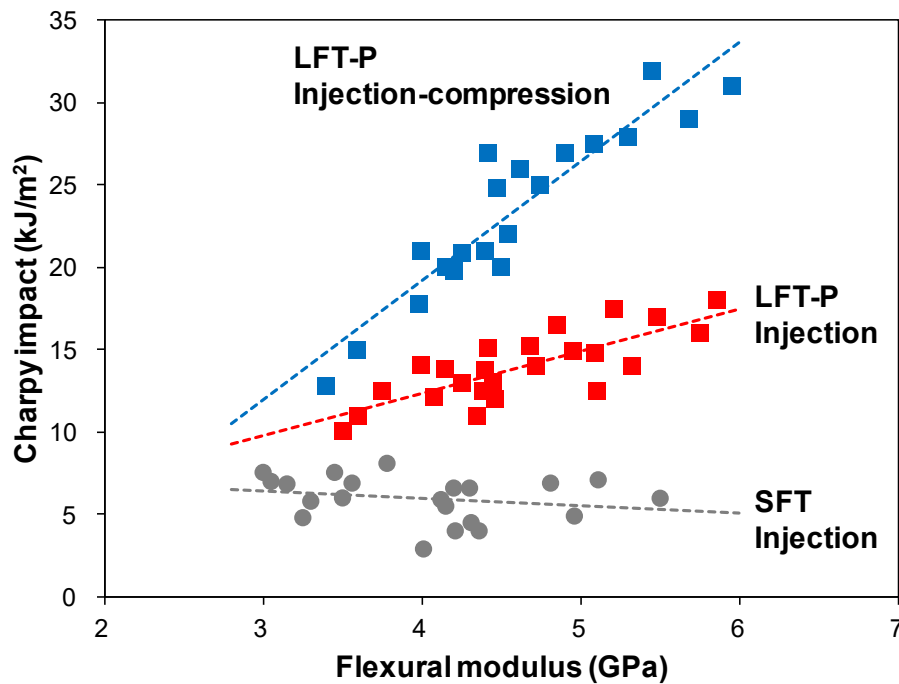


Figure 2.14: Different slopes of Charpy impact-to-flexural modulus related to fiber length remaining in a molded component [11]; PP/GF30 wt. % SFT and LFT-P by injection or injection-compression molding

The broad distributions in flexural modulus and Charpy impact are related to locally different fiber orientation as a result of excessive flow, having 14%–23% in coefficient of variation (CV)⁵. It is obvious that the slopes of the linear trend lines are different and the ‘LFT-P Injection-compression’ case has the highest slope. The higher flexural modulus in each case is for the fiber orientation heading much more toward the test direction. And the slope of Charpy impact-to-flexural modulus becomes higher as the fiber length is longer, because the Charpy impact is more sensitive to the fiber length.

⁵ The coefficient of variation (CV) is defined as the ratio of the standard deviation to the mean, which is often expressed as a percentage for the purpose of a standardized measure of dispersion.

LFT material through direct process (LFT-D)

LFT-D means LFT materials produced through direct processes, starting from basic materials such as fiber reinforcement, matrix polymer, and additives if necessary [58]. At least by skipping an additional heating to mold a component, this direct approach could be definitely a real breakthrough in cost aspects. But, LFT-D processes require higher investment costs, skilled personnel, and too much consideration ranging from material to final part. In the beginning, LFT-D processes were used with compression molding but are now growing more with injection molding. Several LFT-D processes are then respectively named 'LFT-D system with injection molding compounder (LFT-D/IMC)' [56] for continuous compounding and discontinuous injection molding (refer to Figure 2.15) by Krauss-Maffei (Germany) and ENGEL (Austria), 'LFT-D process by inline compounding (LFT-D/ILC)' [12] for compression molding (refer to Figure 2.16) by Dieffenbacher (Germany), and Pushtusion™ technology for direct compounding [56][59] by PlastiComp (USA) that can be easily integrated with an existing injection or compression molding machine.

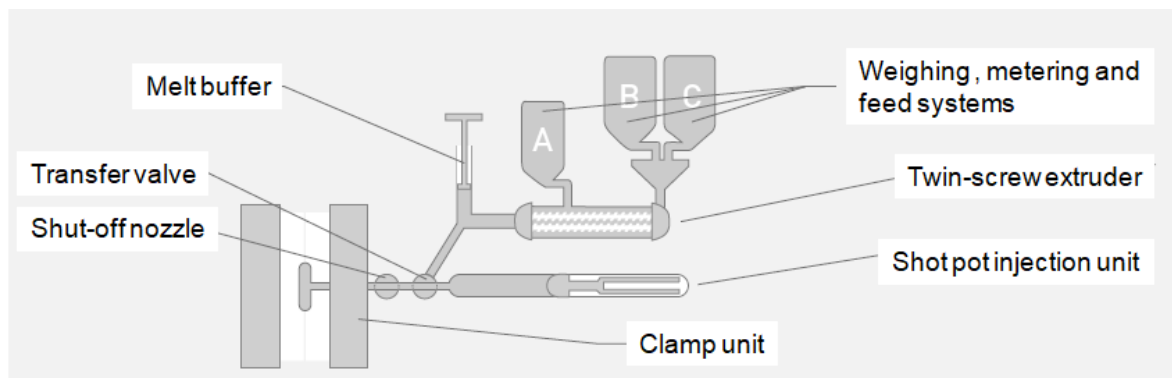


Figure 2.15: LFT-D/IMC process developed by Krauss-Maffei GmbH (Germany) [60]

In every LFT-D process, the level of controlling fiber length and fiber dispersion is a very important matter. Thus, LFT-D/ILC has taken a significant improvement by the cutting before mixing (see Figure 2.17); old one is the cutting along with mixing in a twin-screw extruder. And Pushtusion™ technology (refer to Figure 2.18) is inherently excellent due to the rotary cutter located at the exit of the entrainment die where continuous fiber rovings are partially or fully impregnated with molten resin. The fiber length in LFT-D process can be maintained long enough to fulfill the criterion for impact resistance dominant applications, depending somewhat on the downstream processes. However, the fiber content is constrained, e.g. up to PP/GF40 wt. %, on

account of using a twin-screw or a single-screw system to gently mix or for injection molding.

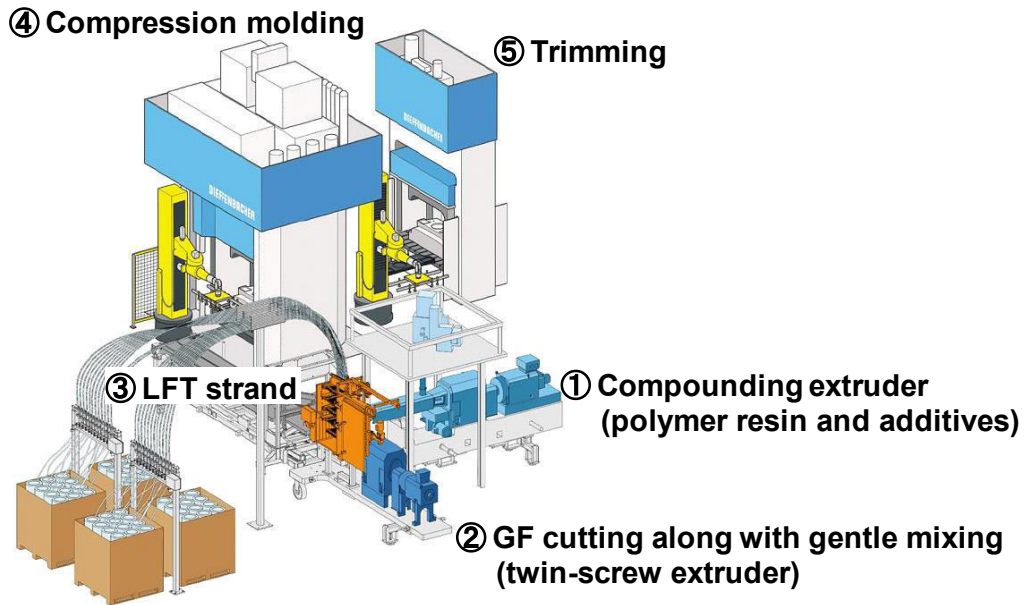


Figure 2.16: LFT-D/ILC process developed by Dieffenbacher GmbH (Germany) [61]

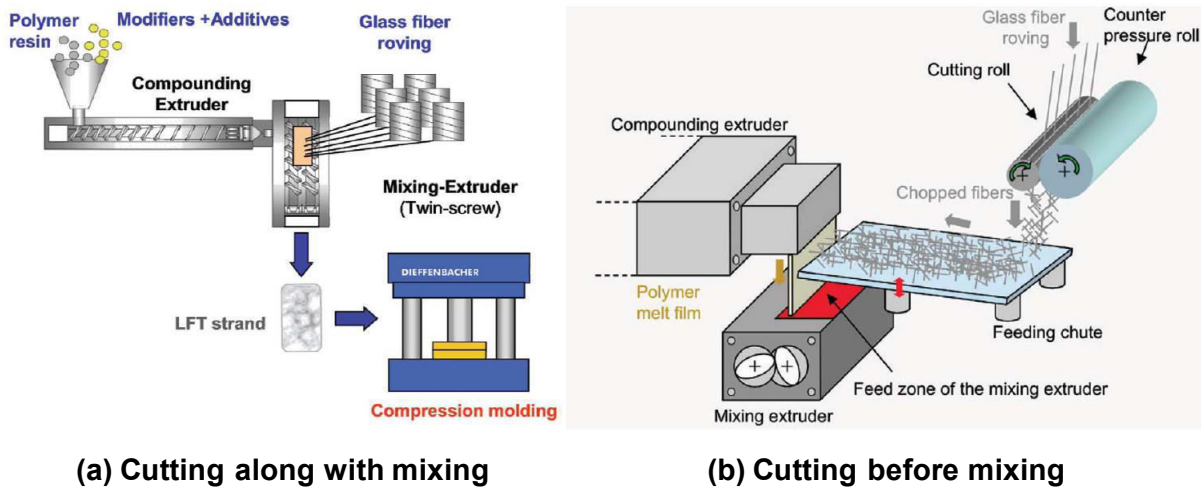


Figure 2.17: Improvement in LFT-D/ILC for better quality of fiber dispersion [58]

In summary, for all the current LFT materials (GMT, LFT-P, and LFT-D), the level of fiber content is below 20 vol. %, equivalent to PP/GF40 wt. %. Such a level of fiber content is obviously low compared to around 45 vol. % of continuous fiber reinforced thermoplastic materials. GMT materials and LFT-D processes have the undeniable advantage of high impact resistance which can be achieved by the reinforcement of

really long fiber [2], e.g. over 25 mm in length, whereas LFT-P materials cannot reach it. In particular, GMT materials are very suitable for molding thin components up to 2.58 m² of less design complexity, with low tooling costs and fast cycle times [52]. But, GMT materials still lack diversity for matrix resin and fiber reinforcement compared to the other two LFT materials.

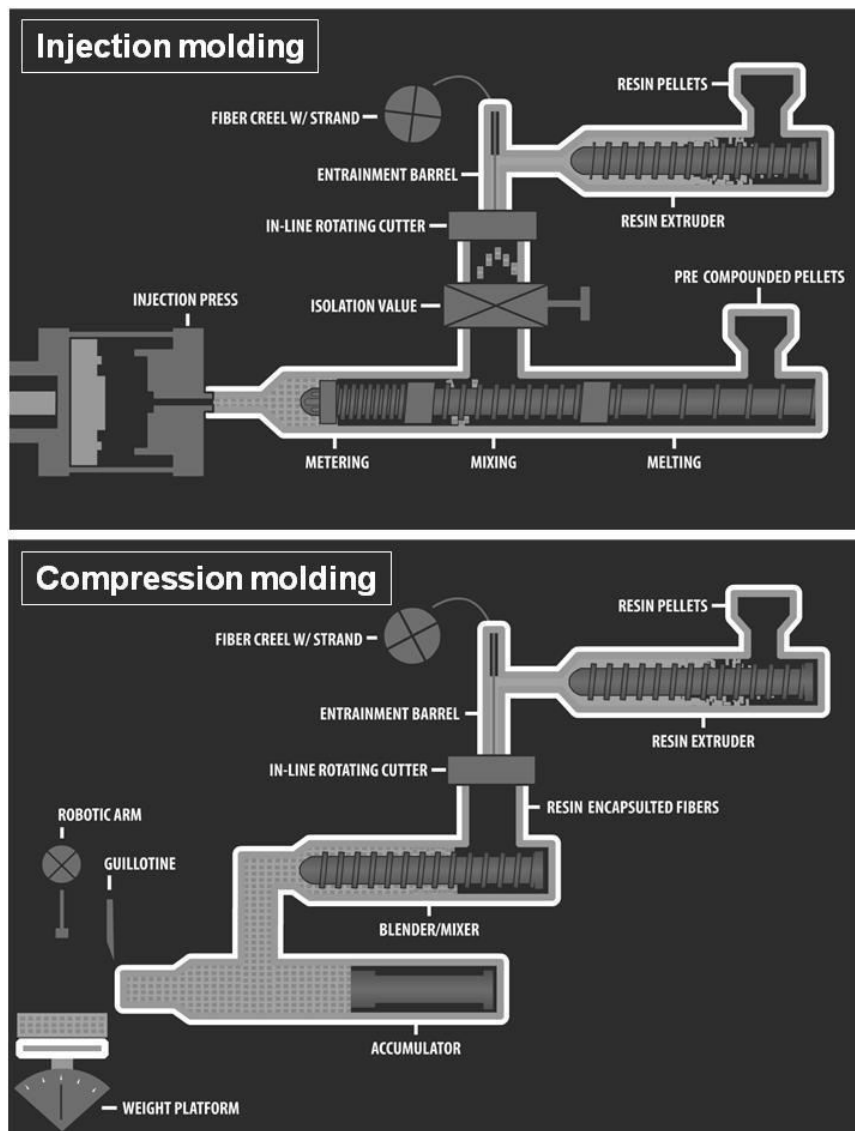


Figure 2.18: Pushtrusion™ technology developed by PlastiComp (USA) [59]

2.2 Crash Behavior and Performance

It has been believed that fiber reinforced thermoset and thermoplastic materials are good for lightweight applications. So, they might be substituted for metallic materials with no difficulty based on lower density and better formability; it seems half correct and half not. As shown in Figure 2.19, the densities of metallic materials range from 7.87 g/cm³ of steel to 1.74 g/cm³ of magnesium (Mg). In terms of density, glass fiber (GF) corresponds to aluminum (Al), and carbon fiber (CF) does to magnesium (Mg). Of course, the density of GFRP and CFRP materials can become lower. It looks quite incredible to have 38% and 18% lower density compared to each lightweight metallic material ultimately; GFRP to aluminum and CFRP to magnesium.

But, lower density is not everything necessary to compete against metallic material, whereas it is a well-known strong point of fiber reinforced plastic materials that they could regulate anisotropic reinforcement by intention more than metallic materials.

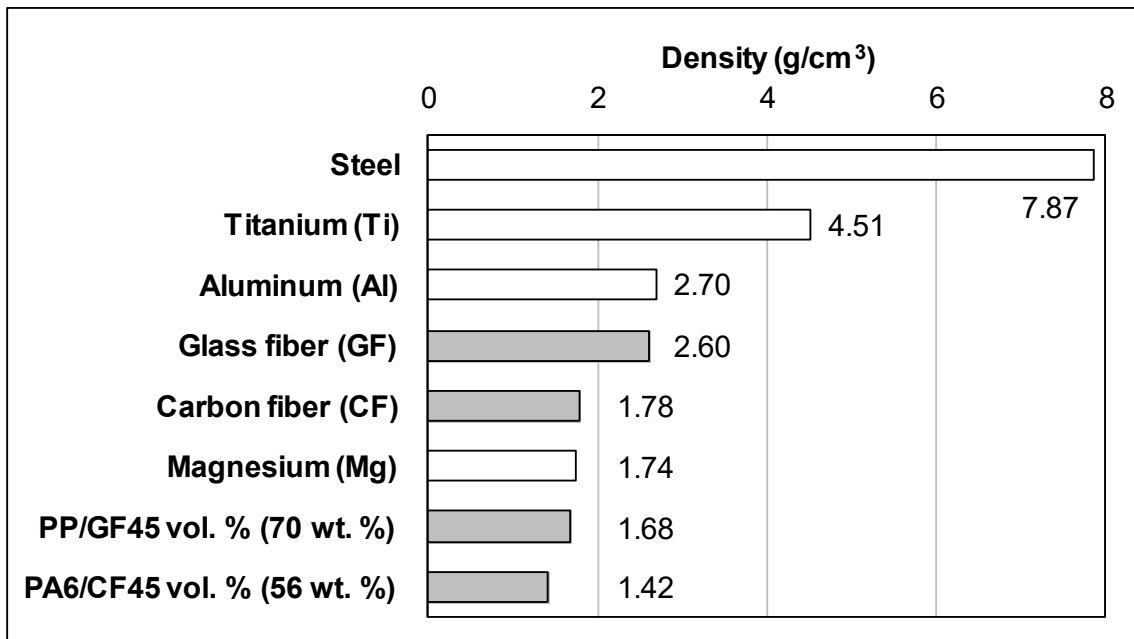


Figure 2.19: Comparison of densities between metallic materials and fiber reinforced thermoplastic materials

In the case of the Airbus A350 (first flight in 2013), the proportion of CFRP materials has increased dramatically to about 53%, which are primarily used for both fuselage and wing structures (anisotropic) [62]. The structural parts (such as ribs, floor beams, and pylons) still must be made of metallic materials, despite having high density, for the purpose of stiff and ductile characteristics; aluminum with 19%, titanium with 14%,

and steel with 7% in the Airbus A350. The Mercedes-Benz W205 (model years from 2015), DAIMLER C-Class model, achieved a weight reduction of 100 kg compared to the previous W204 (model years from 2008 to 2015) [63]. But, the weight reduction was done by using more amount of ultra high-strength steel for the safety cell, and by using aluminum for the outer skin panels (isotropic), not done by GFRP and CFRP materials of lower density. Thus, as a candidate for another strong point of GFRP and CFRP materials, the crash behavior and performance will be generally reviewed and compared with those of metallic materials.

2.2.1 Crashworthy structure

Crashworthy structures in automotive and aircraft industries are mainly divided into two kinds of subsystems (refer to Figure 2.20). These are rigid parts for the integrity and deformable parts for the sacrifice [64][65]. All the deformable parts, often called crash energy absorbers [66], should be designed to fully dissipate the impact energy in a stable, progressive and controlled manner. The main purpose is to prevent the rapid deceleration that could cause serious injuries of passenger and damages to cargo [67][68]. Moreover, such deformable parts should be concentrated in relatively narrow zones [69][70] and thus basically help most of the remainder to hold the integrity as far as possible.

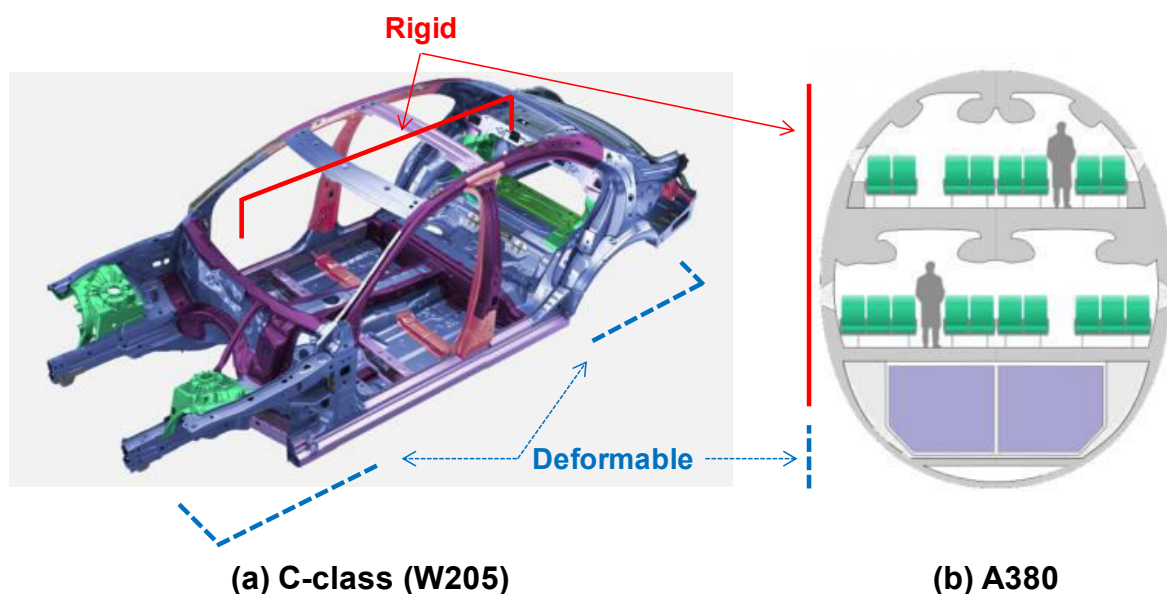


Figure 2.20: Crashworthy structures in (a) a car [63] and (b) an aircraft [71][72]

In the case of a car, there are a number of crash test programs around the world that should be conducted under rigorous standards, including frontal impact, side impact and roll-over tests. Considering the integrity in all directions, the safety cell (as a rigid part) prefers being made of ultra high-strength steel in these days. Moreover, it is mitigated by the sacrifice of deformable parts that are suitably installed in front and rear areas. For the purpose of protecting batteries in an electric vehicle, there was an attempt to dissipate the side impact energy by the concept of multiple crash-elements [73]. Furthermore, if manned drones are early commercialized in the near future, the concept of adaptive-crash-control system with various understructures will be a new matter of much account. Simply, the true meaning of crashworthy structure is to pour much money into what should not happen [74].

2.2.2 Material and crash behavior

Thin-walled metallic tubes have been widely used for the deformable parts, which are made of steel or aluminum alloys showing ductile behaviors of progressive folding as a result of plastic deformation [75][76]. Typical values of specific energy absorption (SEA) are in the range of 15–30 J/g, being absorbed by a non-symmetrical folding of diamond shape (refer to Figure 2.21) regardless of impact velocities. In other words, metallic materials show the same results in both dynamic crash test [75][77][78] and quasi-static test [77][79]. And such values tend to decrease below 10 J/g in the case of real parts, as pointed out with the frontal crash boxes that have a square hollow section and were assembled by various joining processes [65].

Above all, the behavior of progressive folding brings about a full compaction in folded zones which acts as a hindrance to effective displacements essential to maintain an endurable deceleration rate; it is no longer possible to dissipate impact energy, so that the residue of impact energy is just being transferred to rigid parts. This matter becomes more important when a feasible length (or space) is not so sufficient. As an example, the proportion of full compaction was calculated to be around 30% of the initial length of crash test specimen; it was roughly determined by dynamic crash test being done one more time with the same test condition [74].

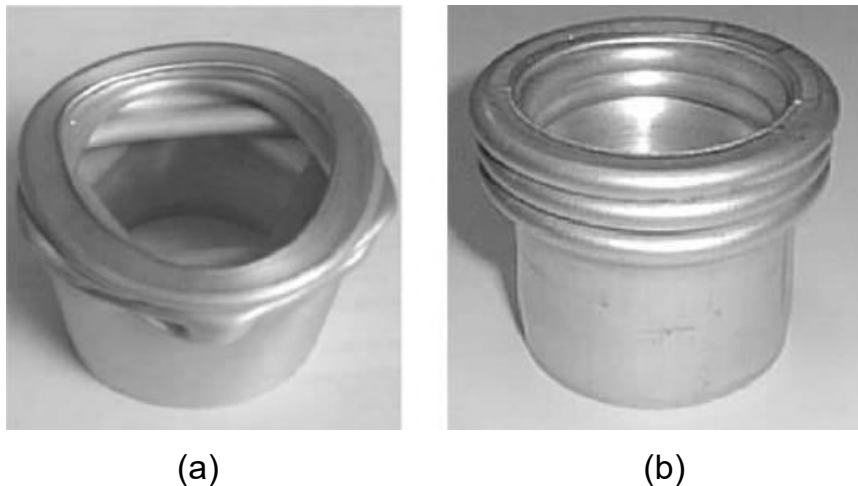


Figure 2.21: Crushing mode of aluminum tube [80] in (a) diamond or (b) concertina

Alternatively, brittle fiber reinforced polymeric materials can achieve higher values of SEA than metallic materials chiefly owing to low densities, but lead to quite different crash behaviors. Jacob et al. [68] comprehensively reviewed their performances and crash behaviors. These are dependent on many parameters such as types of matrix

and fiber, fiber content and its orientation, fiber architecture, specimen geometry and trigger, impact velocity, processing condition and so on. However, as shown in Figure 2.22, Hamada et al. [4] has categorized all the crash behaviors into three modes like progressive folding, fragmentation, and splaying; these modes are often described as local buckling, transverse shearing, and lamina-bending by Farley et al. [81][82][83]. Splaying is an expression from a viewpoint more focused on initial stage and a sort of wall splitting followed by lamina-bending. On the whole, every brittle fiber reinforced polymeric material shows the mode somewhere between fragmentation and splaying, whereas progressive folding is the typical mode of metallic materials.

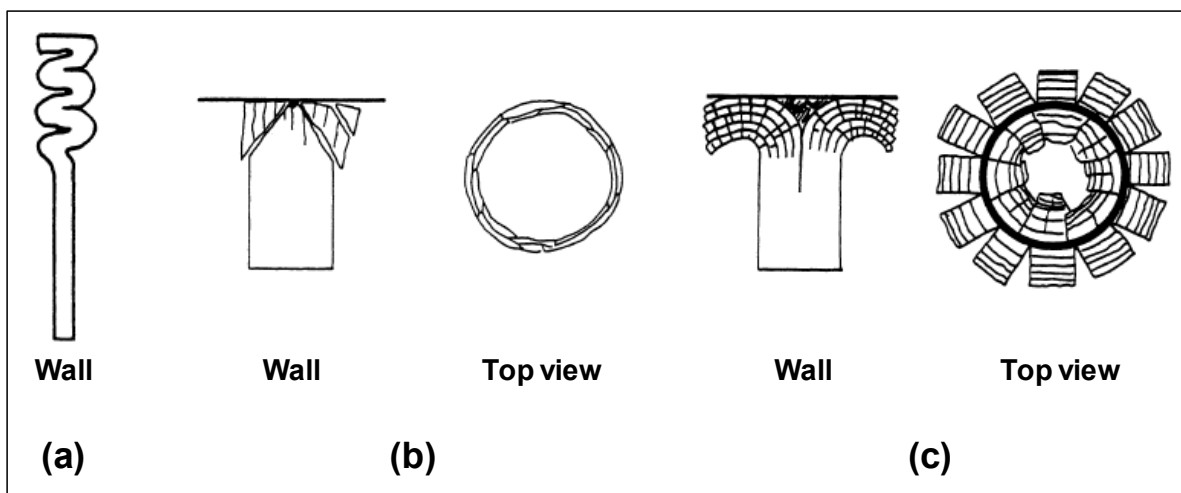


Figure 2.22: Typical modes of crash behavior categorized into (a) progressive folding, (b) fragmentation, and (c) splaying [4]

Up to this time, most of the research works have been inclined to thermoset materials (rather than thermoplastic materials) reinforced with continuous (rather than long or short) carbon-fiber (rather than glass-fiber). In the case of continuous carbon-fiber reinforced epoxy materials, typical values of SEA are about 75–90 J/g (see Table 2.3), with the mode of splaying (lamina-bending) in quasi-static test. In contrast to metallic materials, there are 20%–30% drops of SEA in dynamic crash test like 55–75 J/g (see Table 2.4), showing the different mode of fragmentation (transverse shearing); sometimes very close to pulverization. It is obviously compared in Figure 2.23 that the characteristic behavior is dependent on impact velocity. Since dynamic crash tests take into account circumstances of real crash events [68], it is appropriate to adopt the values of 55–75 J/g for SEA on continuous carbon-fiber reinforced epoxy materials. Nevertheless, these values are two or three times higher than 15–30 J/g of metallic materials.

Table 2.3: Values of SEA for CF reinforced epoxy materials in quasi-static test

SEA (J/g)	Material	Specimen identification
76.1	Epoxy/CF42 wt. % Woven fabric and UD	No. 2/3/14–17/21/22 [8] 0°/90°, Tube and truncated cone of 5°
77.6	Epoxy/CF Woven fabric	No. 1–8 [84] 0°/90°/±45°, Truncated cone of 5°
82.1	Epoxy/CF Winding	A3-0/100/200 h [85] 88°/17.6°/88°, Tube
87.1	Epoxy/CF55 vol. % Woven fabric	No. I [5] 0°/90°, DLR ⁶ specimen [86][87]
89.7	Epoxy/CF56 vol. % Woven fabric	AC9-1/2/3 [88] 0°/90°, Double hat tube

Table 2.4: Values of SEA for CF reinforced epoxy materials in dynamic test

SEA (J/g)	Material	Specimen identification
55.2	Epoxy/CF Woven fabric	No. 1–8 [84] 0°/90°/±45°, Truncated cone of 5°
60.3	Epoxy/CF58 wt. % Woven fabric	CL3 [89] 0°/90°, Cone
65.5	Epoxy/CF56 vol. % Woven fabric	100-1/2/3, 75-1/2/3 [90] 0°/90°, Double hat tube
67.5	Epoxy/CF55 vol. % Woven fabric	No. III [5] 0°/90°, DLR specimen
65 and 76	Epoxy/CF58 wt. % Woven fabric	80 mm and 50 mm diameter [91] 0°/90°, Tube

⁶ The DLR crush element is a kind of crash test specimens designed by Deutsches Zentrum für Luft- und Raumfahrt, being the shape of a chamfered tube.

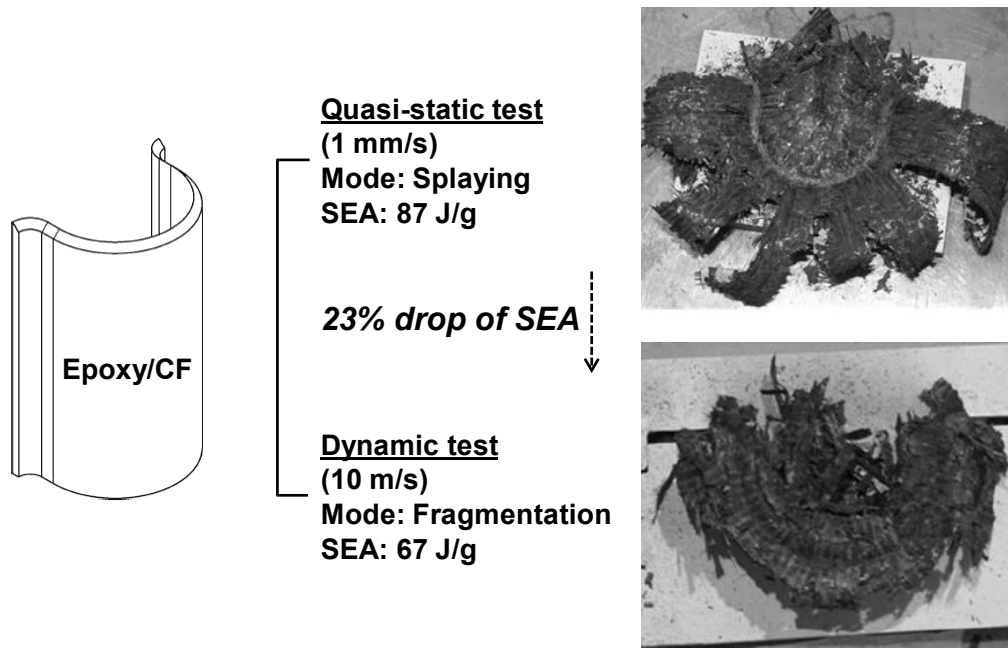


Figure 2.23: Crash behavior and performance dependent on impact velocity [5]

Meanwhile, considering cost aspects and crash behavior, more attention should be paid to glass fiber (rather than carbon fiber) reinforced thermoplastic materials (rather than thermoset materials). The typical values of SEA are about 35–70 J/g in dynamic crash test, which are significantly influenced by the type of thermoplastic material and absorbed by the mode of splaying (lamina-bending) (see Table 2.5).

Table 2.5: Values of SEA for GF reinforced thermoplastic materials in dynamic test

SEA (J/g)	Material	Specimen identification
36.4	PP/GF30 wt. % Chopped fiber	G: PP/GF30C [92] Random, Welded round-hat tube
39.4	PET/GF50 vol. % Knit	Weld (H) [92][93] Welded round-hat tube
41.1	PP/GF30 wt. % Long fiber (> 50 mm)	C: PP/GF30R [92] Random, Welded round-hat tube
41.7 and 48.8	PA/GF50 vol. % Woven fabric	H-4/5/6 and S-1/2/3/4/5 [69][70] 0°/90°, Hexagonal and square boxes
67.3	PA12/GF56 vol. % Woven fabric	At 20°C [94] 4/1 (0°/90°), Welded round-hat tube

When taking into account the higher density of glass fiber than of carbon fiber, e.g. 2.60 vs. 1.78 g/cm³, such values are very promising for performance. Above all things, the present work was motivated by the results, 13% betterment, conducted on two types of PP/GF30 wt. % materials different in fiber length. So, the assumption is that if fiber length is long enough, and fiber content can be as high as possible, then SEA will be on an equivalent level with continuous fiber reinforcement. Theoretically, this assumption is grounded on and supported by the short time-scale behavior [5][8] of substance mainly governed by elastic modulus and strain limit, such as in the case of crash circumstances.

Additionally, long fiber reinforcement can be free of delamination that occurs between plies where there are no fibers actually. Such delamination is very distinct when using relatively thick woven fabrics [89] of continuous fiber reinforcement, and it tends to weaken the contributions of splaying as well as lamina-bending in SEA. As shown in Table 2.6), the contributions can be determined by foam existence inside a specimen [70], higher inclinations of a truncated cone [84], and the nonresistant layer [85].

Table 2.6: Contributions of splaying and lamina-bending in SEA

Drop of SEA	Comparison	Description
22%	S67/68/69	Square tube, Dynamic test [70]
Mixed	F37/38/39	Hindrance to splaying formation by foam
23%	CL3 (200 g/m ²)	Cone, Dynamic test [89]
Mixed	CL6 (600 g/m ²)	Thick woven fabric
24%	Filament winding	Tube, Static test [4]
Mixed	Woven fabric	Woven fabric
23% and 27%	5°: No. 1–8	Truncated cone, Static and dynamic tests [84]
Mixed	15°: No. 18–25	See Figure 2.24 (a) and (b)
35%	A4 at 400 h	Tube, Static test [85]
Splaying	B5 at 400 h	See Figure 2.24 (c) and (d)

In summary, the contribution of splaying and laminar-bending in SEA can be guessed as high as 20%–35%. Hence, it is very worthy to investigate long fiber reinforcement that is inherently free of delamination. And the flowability of long fiber reinforcement

can contribute to the design flexibility like variation of wall thickness, making ribs for design-stiffness, and insert-molding for assembly.

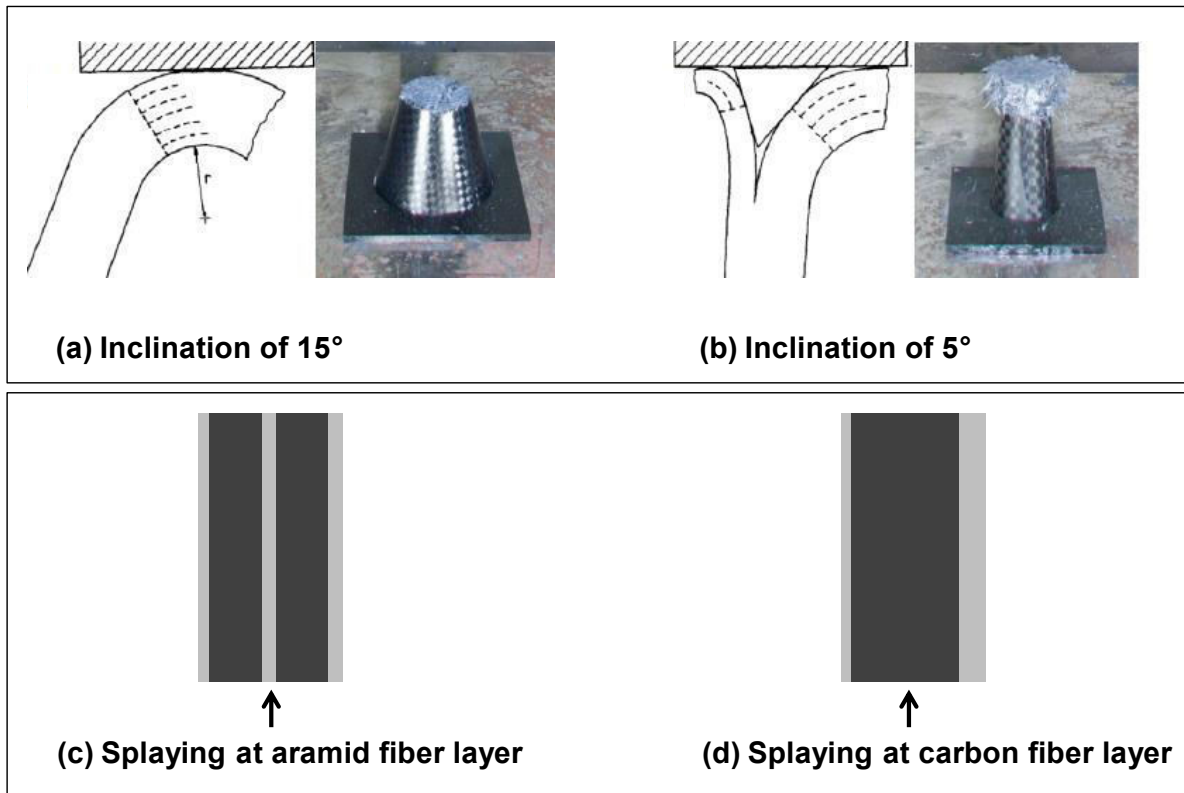


Figure 2.24: Alterations of splaying formation by inclination ((a) vs. (b)) [84] and by configuration of fiber layers ((c) vs. (d)) [85]

3 Material Development

Fundamentally, the Kozeny-Carman equation is quite a good screening method for checking every possible way to impregnate fiber reinforcements with thermoplastic resins of high melt viscosity. This equation has been commonly used in the field of chemical engineering for distillation, chemical reaction, and scrubber processes in order to describe a flow in a packed bed composed of Raschig rings⁷. And of course it is only valid at particle Reynolds numbers up to about 1.0. For packed bed systems of fibers, however, the Kozeny-Carman equation should be modified because of the length-to-diameter ratio being too far from 1; it is normally above 100.

This chapter starts with the derivation of the Kozeny-Carman equation. And then the equation is modified for the packed bed of fibers and examined with computational and experimental results in some other literatures. Based on the review, the concept of multilayered hybrid structure is suggested to develop each of continuous fiber- and long fiber reinforced thermoplastic materials, consisting of several thin sublayers of fiber reinforcement and polymer films. This concept basically heads toward the way to achieve a desirable level of impregnation quality, without lowering a melt viscosity of thermoplastic matrix resin. Moreover, it must satisfy cost aspects in manufacturing processes. For continuous fiber reinforcement, it is a critical point how to effectively spread the continuous fibers into a given width without center-splitting-problem. And for long fiber reinforcement, the key issue is to see if the impregnation quality can be maintained even at high fiber contents, e.g. 45 vol. % or above if possible.

The impregnation quality will be indirectly quantified by the three-point bending test for class II and III material in ISO 14125 [95]. The bending test sensitively grasps all kinds of failures arising from tensile, shear, and compression. Through the statistical analysis, all the representative values are determined, and the modulus is compared to the theoretical value calculated by the rule of mixtures. Especially, the persistence degree (or bias) will be used in order to characterize each stress-strain curve; it is the ratio of the experimental strength to the modulus-based strength [96][97].

⁷ Raschig rings are named after the German chemist Friedrich Raschig, which are pieces of tube approximately equal in length and diameter to provide a high surface area and isotopic packing.

3.1 Impregnation

3.1.1 General Kozeny-Carman equation

The Kozeny-Carman equation, named after Josef A. Kozeny and Philip C. Carman, can be derived from the capillary model schematized in Figure 3.1. Here the Hagen-Poiseuille equation basically describes the pressure drop (ΔP) of an incompressible and Newtonian fluid in steady laminar flow flowing through a long cylindrical pipe of constant cross section, assuming that there are no 'end effects' [98][99]. To take the macroscopic view on the flow, the mean velocity (v_c) in a cylindrical pipe should be expressed in terms of the superficial velocity (v) together with the porosity (ε) and the tortuous degree. The tortuous degree is simply defined as the ratio of the actual path length (h_c) to the height (Δh) of packed bed.

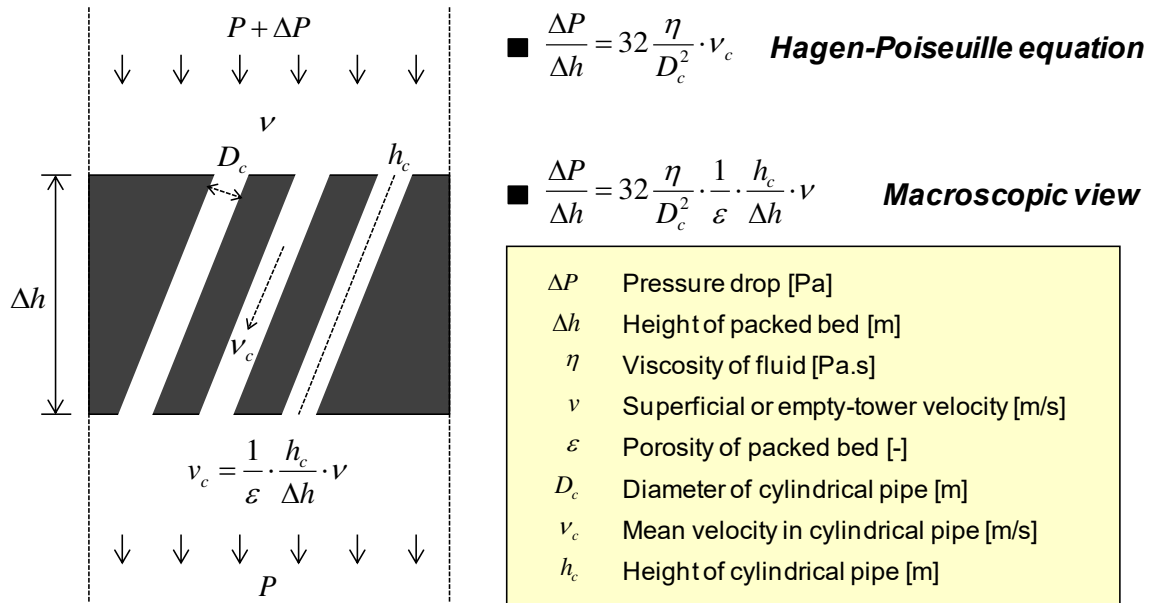


Figure 3.1: Capillary model for derivation of general Kozeny-Carman equation

The diameter (D_c) of the cylindrical pipe could be generalized and interpreted as the equivalent cylindrical pipe diameter that is defined as four times the volume (V_c) of the capillaries per those surface area (S_c) (see Figure 3.2). In this way, it becomes possible to cover all kinds of capillaries even having complicated and irregular cross sections along the same height (h_c) of cylindrical pipe.

$$D_c = \frac{4V_c}{S_c} \quad (3.1)$$

By shifting the viewpoint from capillary to particle [100][101] and through the definition of porosity (ε) in the packed bed system, the volume (V_c) of the capillaries can be expressed in terms of the volume (V_p) of the particles and with the related function of porosity. Meanwhile, the surface area (S_c) of the capillaries is simply substituted with the surface area (S_p) of the particles, since both are the same in essentials.

$$\varepsilon = \frac{V_c}{V_c + V_p}, \quad V_c = \frac{\varepsilon}{(1-\varepsilon)} \cdot V_p \quad (3.2)$$

$$D_c = \frac{4V_c}{S_c} = \frac{4\varepsilon}{(1-\varepsilon)} \cdot \frac{V_p}{S_c} = \frac{4\varepsilon}{(1-\varepsilon)} \cdot \frac{V_p}{S_p} \quad (3.3)$$

When the particles are very analogous to sphere, the 'volume to surface area of the particles' can be expressed in terms of the equivalent sphere diameter (D) that is defined as six times the volume (V_p) of the particles per those surface area (S_p) (see Figure 3.2). In short, the equivalent cylindrical pipe diameter (D_c) of the capillaries is completely shifted to the equivalent sphere diameter (D) of the particles.

$$D_c = \frac{4V_c}{S_c} = \frac{4\varepsilon}{(1-\varepsilon)} \cdot \frac{V_p}{S_p} = \frac{4\varepsilon}{(1-\varepsilon)} \cdot \frac{D}{6} = \frac{\varepsilon}{(1-\varepsilon)} \cdot \frac{2}{3} \cdot D \quad (3.4)$$

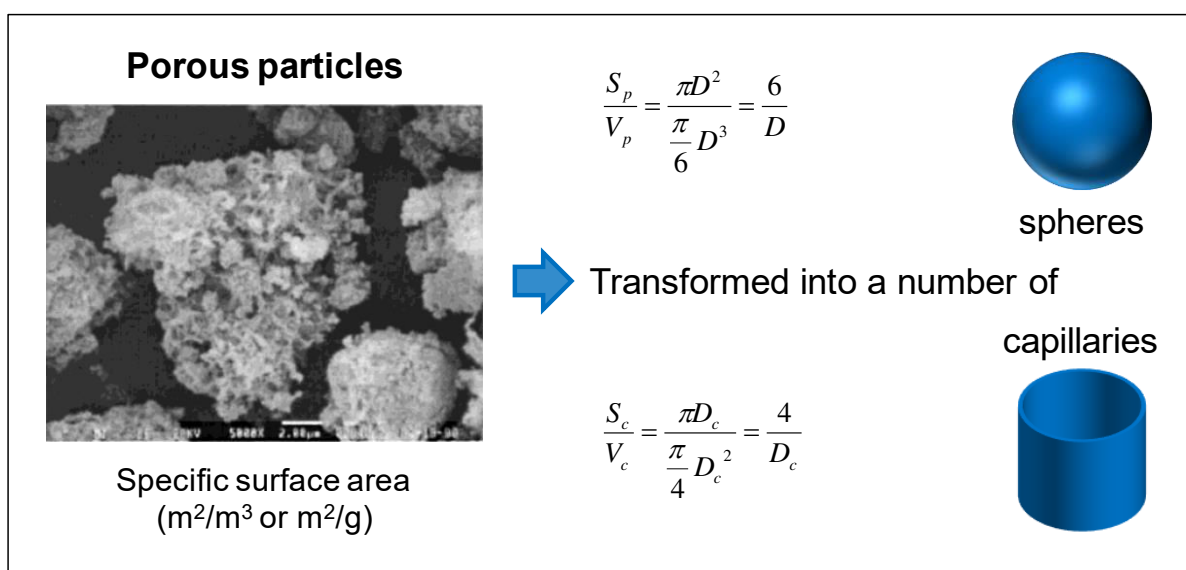


Figure 3.2: Transformation of porous particles [102] into equivalent sphere diameter [99][101] and equivalent cylindrical pipe diameter

Thus, the general Kozeny-Carman equation is another form of the Hagen-Poiseuille equation describing pressure drop in steady laminar flow, but it is substituted with the equivalent sphere diameter (D) for the packed bed of particles (see Figure 3.3).

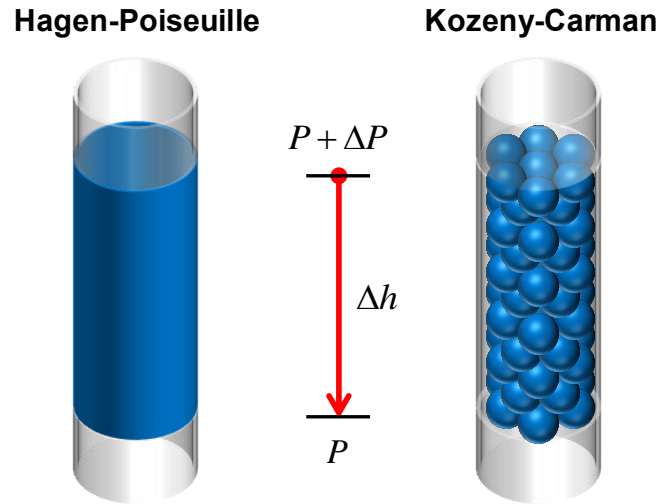


Figure 3.3: Pressure drop in Hagen-Poiseuille and Kozeny-Carman equations

$$\frac{\Delta P}{\Delta h} = 32 \frac{\eta}{D_c^2} \cdot v_c = 32 \frac{\eta}{D_c^2} \cdot \frac{1}{\varepsilon} \cdot \frac{h_c}{\Delta h} \cdot v = 32 \left(\frac{3}{2} \right)^2 \frac{\eta}{D^2} \cdot \frac{(1-\varepsilon)^2}{\varepsilon^2} \cdot \frac{1}{\varepsilon} \cdot \frac{h_c}{\Delta h} \cdot v \quad (3.5)$$

Often the above equation is rearranged and shortened with the permeability (K); the square of the equivalent sphere diameter (D), constant 72 and the tortuous degree in denominator, and the related function of porosity. Furthermore the general Kozeny-Carman equation is simply expressed in terms of the multiplied constant (150 or 180) by the empirical tortuous degree ($h_c / \Delta h$) in the range of 2.0 to 2.5 [100][101].

$$v = \left(\frac{D^2}{72(h_c / \Delta h)} \cdot \frac{\varepsilon^3}{(1-\varepsilon)^2} \right) \cdot \frac{1}{\eta} \cdot \frac{\Delta P}{\Delta h} = \frac{K}{\eta} \cdot \frac{\Delta P}{\Delta h} \quad (3.6)$$

$$v = \left(\frac{D^2}{150} \cdot \frac{\varepsilon^3}{(1-\varepsilon)^2} \right) \cdot \frac{1}{\eta} \cdot \frac{\Delta P}{\Delta h} \quad \text{or} \quad v = \left(\frac{D^2}{180} \cdot \frac{\varepsilon^3}{(1-\varepsilon)^2} \right) \cdot \frac{1}{\eta} \cdot \frac{\Delta P}{\Delta h} \quad (3.7)$$

3.1.2 Modified equation for packed bed of fibers

However, the shape of fiber is far from sphere so that the general Kozeny-Carman equation should be modified by being split up at the step of the 'volume to surface area of the particles'. The modified Kozeny-Carman equation for packed bed of fibers is expressed in terms of the fiber diameter (d) and the fiber length (l), instead of the equivalent sphere diameter (D). And then due to the fact that the fiber diameter (d) is very small compared with the fiber length (l) in most cases, the 'volume to surface area of the fibers' converges into a quarter of the fiber diameter.

$$D_c = \frac{4\varepsilon}{(1-\varepsilon)} \cdot \frac{V_p}{S_p} = \frac{4\varepsilon}{(1-\varepsilon)} \cdot \frac{\frac{\pi}{4} d^2 l}{\left(\pi d l + 2 \cdot \frac{\pi}{4} d^2\right)} = \frac{4\varepsilon}{(1-\varepsilon)} \cdot \frac{dl}{(4l+2d)} \quad (3.8)$$

$$D_c = \frac{4\varepsilon}{(1-\varepsilon)} \cdot \frac{dl}{(4l+2d)} \cong \frac{4\varepsilon}{(1-\varepsilon)} \cdot \frac{d}{4} = \frac{\varepsilon}{(1-\varepsilon)} \cdot d \quad (3.9)$$

Also, this can be intuitively explained by the terms of the equivalent cylinder diameter (d) that is defined as four times the volume (V_p) of the particles per those surface area (S_p), by neglecting the surface areas of both ends of fiber.

$$D_c = \frac{4\varepsilon}{(1-\varepsilon)} \cdot \frac{V_p}{S_p} \cong \frac{\varepsilon}{(1-\varepsilon)} \cdot d \quad (3.10)$$

Eventually, the modified Kozeny-Carman equation for packed bed of fibers consists of the constant 32, which is quite different from 72 in the general Kozeny-Carman equation for the packed bed of particles being very analogous to sphere.

$$\frac{\Delta P}{\Delta h} = 32 \frac{\eta}{D_c^2} \cdot v_c = 32 \frac{\eta}{D_c^2} \cdot \frac{1}{\varepsilon} \cdot \frac{h_c}{\Delta h} \cdot v \cong 32 \frac{\eta}{d^2} \cdot \frac{(1-\varepsilon)^2}{\varepsilon^2} \cdot \frac{1}{\varepsilon} \cdot \frac{h_c}{\Delta h} \cdot v \quad (3.11)$$

$$v \cong \left(\frac{d^2}{32(h_c / \Delta h)} \cdot \frac{\varepsilon^3}{(1-\varepsilon)^2} \right) \cdot \frac{1}{\eta} \cdot \frac{\Delta P}{\Delta h} \quad (3.12)$$

In principle, the constant in the modified Kozeny-Carman equation for packed bed of fibers is gradually decreasing from 72 and converging toward 32 along the length-to-diameter ratio of fiber as shown in the graph of Figure 3.4. The values of the constant

are 72 at the length-to-diameter ratio of 1 (ideal cylinder), 50 at 2, 40 at 4, and 35 at 10. Consequently, the value of the constant converges into 32, respectively with 99% level and 99.9% level when the length-to-diameter ratio is above 100 and 1000.

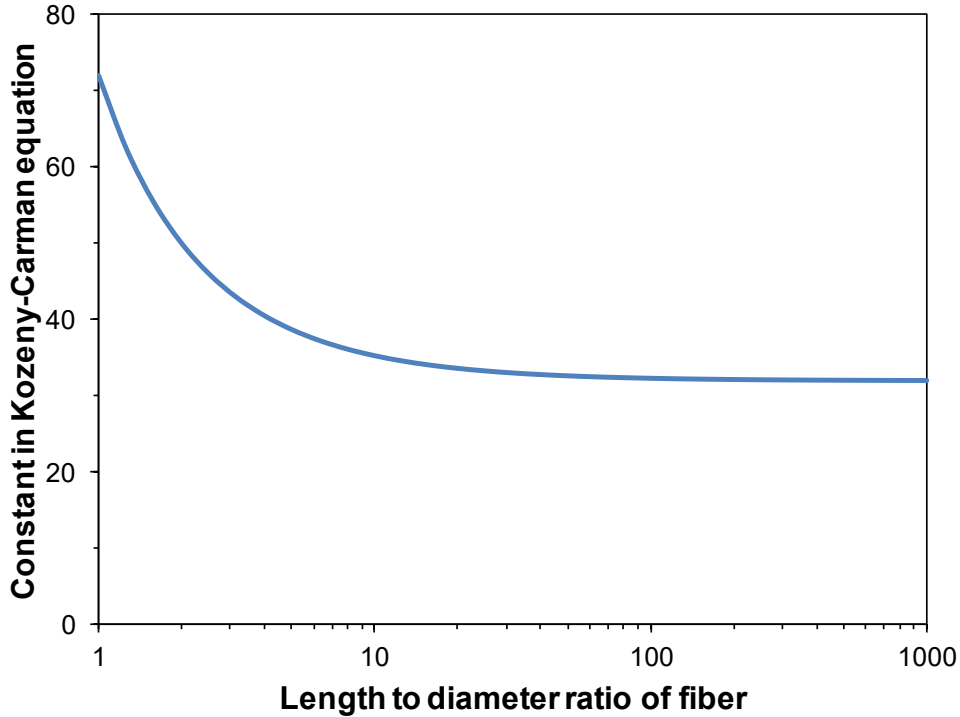


Figure 3.4: Convergence of constant in Kozeny-Carman equation for packed bed of fibers along length-to-diameter ratio of fiber

By the direct relationship that is linked to the 'volume to surface area of particles', the general Kozeny-Carman equation also can be substituted with the modified Kozeny-Carman equation for packed bed of fibers. This manner is the simplest way to apply to any shape of particles in a packed bed.

$$\frac{V_p}{S_p} = \frac{D}{6} \cong \frac{d}{4}, \quad D \cong \frac{6}{4}d \quad (3.13)$$

$$v = \left(\frac{D^2}{72(h_c / \Delta h)} \cdot \frac{\varepsilon^3}{(1-\varepsilon)^2} \right) \cdot \frac{1}{\eta} \cdot \frac{\Delta P}{\Delta h} \cong \left(\frac{d^2}{32(h_c / \Delta h)} \cdot \frac{\varepsilon^3}{(1-\varepsilon)^2} \right) \cdot \frac{1}{\eta} \cdot \frac{\Delta P}{\Delta h} \quad (3.14)$$

In the case of the packed bed of fibers, particularly the minimum tortuous degree of 1.0 can be assigned for the parallel direction to the fiber arrays. However, it should be guaranteed that the fibers are aligned very well and there is no channeling effect.

3.1.3 Permeability and tortuous degree

The permeability (K) in the Kozeny-Carman equation is a sort of intrinsic parameter that is already determined by a given packed bed system in steady laminar flow. So, it should not be influenced by the external variables like the pressure drop (ΔP), the viscosity (η), and the height (Δh) of the packed bed.

$$v = \frac{K}{\eta} \cdot \frac{\Delta P}{\Delta h}, \text{ where } K \cong \frac{d^2}{32(h_c / \Delta h)} \cdot \frac{\varepsilon^3}{(1-\varepsilon)^2} \quad (3.15)$$

Figure 3.5 shows the variation of permeability by fiber diameter, tortuous degree, and porosity from the modified Kozeny-Carman equation for packed bed of fibers. Each influence on permeability becomes smaller as the porosity decreases. This tendency implies that the permeability could not be a significant parameter for impregnation at low porosities, in other words, at high contents of fiber reinforcement. Nevertheless, at a given porosity, the permeability has a trend toward increasing with fiber diameter and decreasing with tortuous degree. Here the tortuous degree ($h_c / \Delta h$) should have a value above 1.0 in any case; not being affected by porosity and fiber diameter, but dependent on fiber orientation.

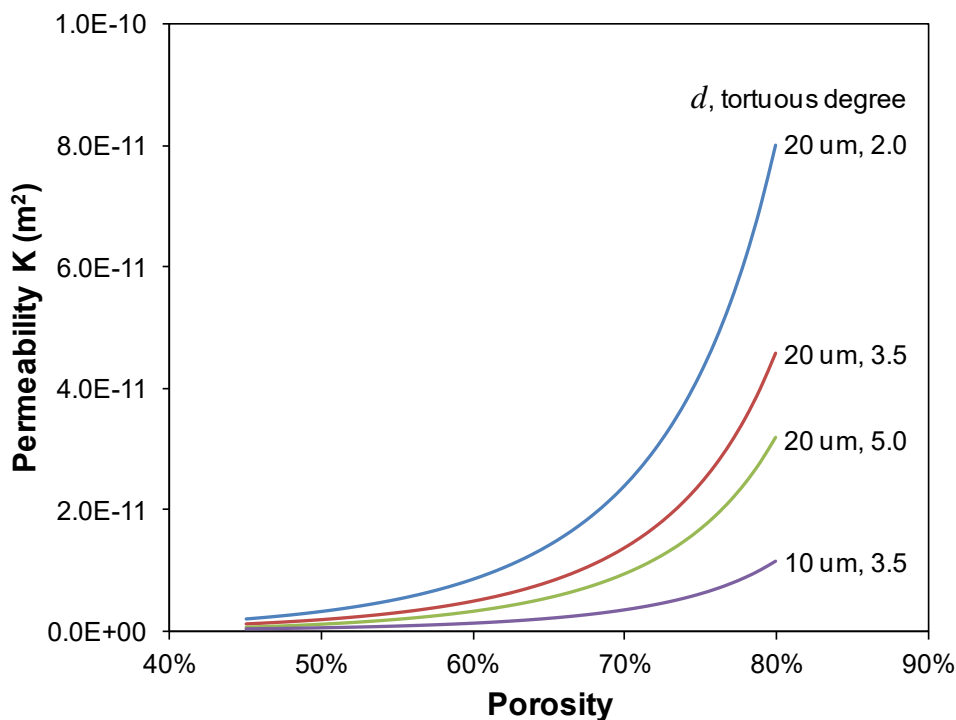


Figure 3.5: Variation of permeability influenced by fiber diameter, tortuous degree, and porosity in packed bed of fibers

Table 3.1: Tortuous degree for transverse direction to fiber arrays

Tortuous degree	Description in the literature	Literature
3.5	Porosity: 0.18–0.32 Experimental results: $k = 7$	Bates et al. (2001) [103]
5.2	Porosity: 0.45, 0.5, 0.6, 0.7, 0.8 Computational results: Table 2	Chen and Papathanasiou (2006) [104]
5.5	Porosity: 0.25–0.5 Experimental results: $k'_z = 11$	Lam and Kardos (1991) [105]
4.7–8.8	Porosity: 0.482 Computational results: Table 3	Bechtold and Ye (2003) [106]
9.0	Porosity: 0.28–0.31 Experimental results: $k_{zz} = 17.9$	Gutowski et al. (1987) [107]

Tortuous degree corresponds to half value of the constant in those literatures

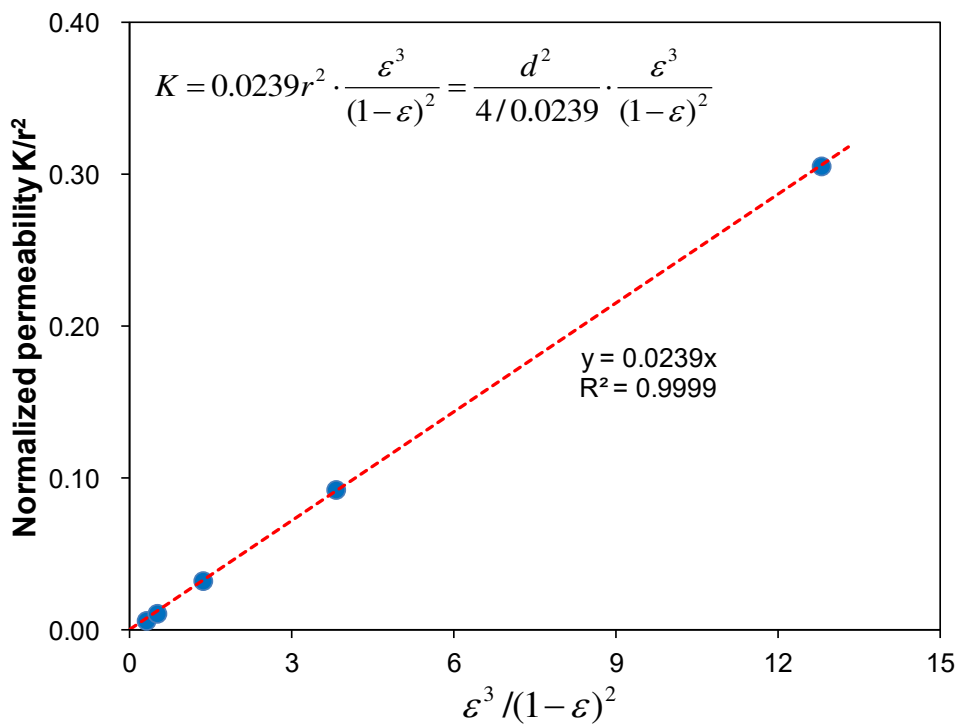


Figure 3.6: Tortuous degree calculation by least squares method on computational results [104] for transverse direction to fiber arrays

The maximum value of tortuous degree in packed bed of fibers could be suggested around 5, which is carefully chosen in Table 3.1. This is for the transverse direction to fiber arrays and especially for the practical porosity range of above 0.45. As shown in Figure 3.6, the most ideal and reasonable value of 5.2 could be calculated by least squares method on the computational results of Chen and Papathanasiou [104].

The tortuous degree for the woven fabric (HexForce[®] 01038), naturally a transverse direction to fibers, was experimentally determined as 3.5 ($k_0 = 7$ in the literature [108]). This is a somewhat reduced value from 5, which might be caused by the combination of macro and micro permeability (inter and intra bundles).

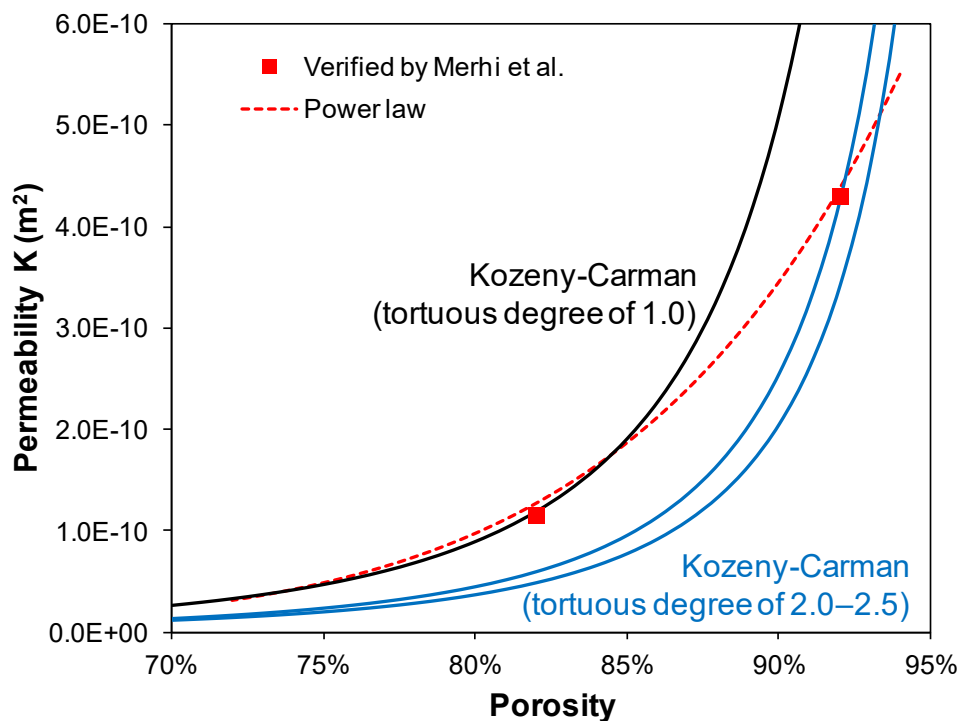


Figure 3.7: Permeability of random directional glass-fiber mat measured and fitted by power-law [109][110], and then compared with the modified Kozeny-Carman equation on tortuous degrees and fiber diameter of 15 μm [111]

Furthermore, the tortuous degree for random directional fiber mat is supposed to be in the range of 2.0 to 2.5, because it is very similar to the packed bed of particles. For example, the permeability had been measured by Michaud et al. [109] on the random directional glass-fiber mat (Quadrant Plastic Composites AG⁸ (Switzerland)), within

⁸ Quadrant Plastic Composite AG is one of GMT (glass mat reinforced thermoplastic) manufactures.

the porosity range of 0.72 to 0.94. However, there was no other option but to fit it by a power-law having no scientific ground (see the dotted line in Figure 3.7). This power-law fitting was again verified later by Merhi et al. [110] with the two additional data; the permeability of $1.15 \times 10^{-10} \text{ m}^2$ at the porosity of 0.82 and $4.3 \times 10^{-10} \text{ m}^2$ at 0.92. When these two data are processed by the modified Kozeny-Carman equation for packed bed of fibers, it is absolutely not possible to plot them on a single curve with the same tortuous degree. The permeability at the porosity of 0.92, nevertheless, seems to be more reasonable, for it is lying on the curve with the tortuous degree of 2.0; definitely the tortuous degree of 1.0 is assigned for the parallel direction to the fiber arrays.

This mismatch could be interpreted with the distortion of tortuous degree caused by fiber agglomeration. As schematized in Figure 3.8, in principle the fiber diameter (d) in the modified Kozeny-Carman equation is the individual fiber diameter (d_f) with no fiber agglomeration. But, if fibers are agglomerated, the fiber diameter (d) becomes a bigger value by multiplying the degree (λ) of agglomeration and there is no actual flow inside the agglomerated fibers. This agglomeration brings out the decrease in surface area without porosity change, so that it causes less flow resistance (tortuous degree) and leads to higher permeability eventually.

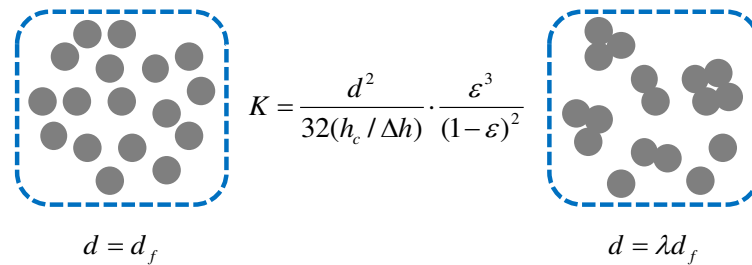


Figure 3.8: Fiber diameter (d) in Kozeny-Carman equation for packed bed of fibers considering fiber agglomeration

It is very hard to get actual information about the degree of agglomeration. But the tortuous degree is subject to get mistaken as shown in the following equation. Here the tortuous degree of 1.0 (at the porosity of 0.82) might be distorted by the degree of agglomeration in the range of 1.4–1.6, from an actual tortuous degree of 2.0–2.5 that is the very range for random directional fiber mat.

$$K = \frac{d^2}{32(h_c / \Delta h)} \cdot \frac{\epsilon^3}{(1 - \epsilon)^2} = \frac{d_f^2}{32[(h_c / \Delta h) / \lambda^2]} \cdot \frac{\epsilon^3}{(1 - \epsilon)^2} \quad (3.16)$$

3.1.4 Controllable parameters

As described in the previous section, the permeability (K) itself is not a controllable parameter because of being determined by a given packed bed system as a function of fiber diameter, tortuous degree, and porosity. Moreover, at low porosities (or high contents of fiber reinforcement), its variation becomes smaller and negligible.

$$v = \frac{K}{\eta} \cdot \frac{\Delta P}{\Delta h} \quad (3.17)$$

For the impregnation of fiber reinforcement with thermoplastic matrix resins, heating and pressurizing tools are universally used to melt the matrix resin by heat transfer and then to drive the melt flow into fiber reinforcement. Such processes bring about simultaneously the negative and positive effects on impregnation. The height (Δh) of fiber reinforcement and its porosity (ε) decrease due to the compaction caused by the pressurization (ΔP). Meanwhile, the viscosity (η) of thermoplastic matrix resin decreases as the temperature is higher, and as the shear rate increases due to shear-thinning behavior of non-Newtonian fluids (refer to Figure 3.9). Nevertheless, the viscosity of thermoplastic resin keeps at high level compared to that of thermoset matrix resin, and cannot decrease significantly by heating and pressurizing tools.

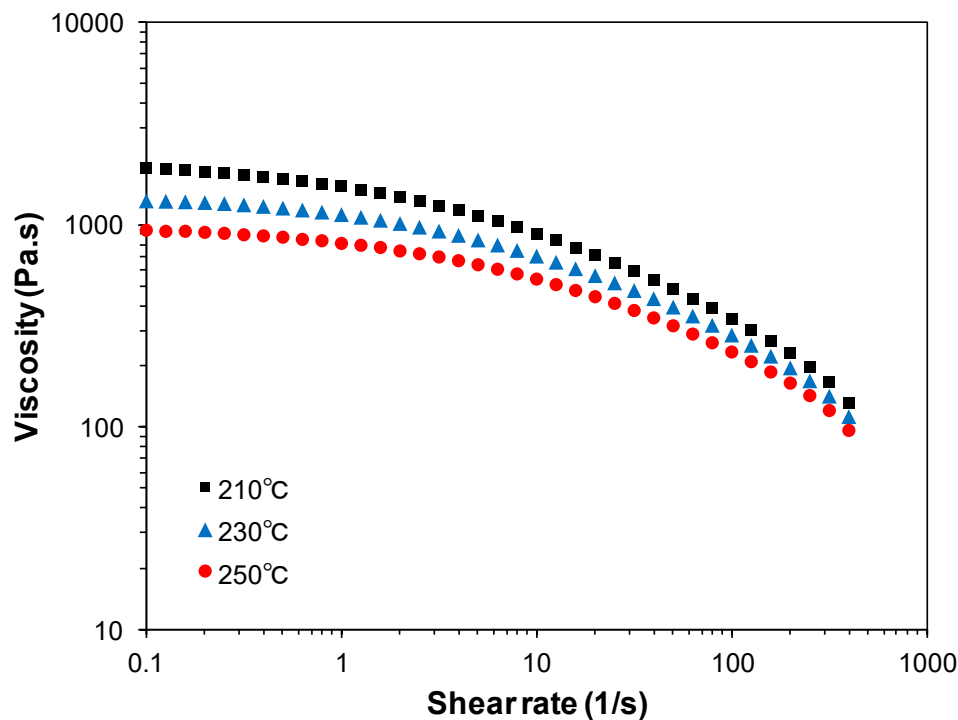


Figure 3.9: Viscosity changes of PP along with shear rate and temperature [112]

Accordingly, the pressure drop (ΔP), namely pressurization by heated tools, is not suitable to be an independent and a controllable parameter; it cannot help causing very complicated and manifold influences in the Kozeny-Carman equation.

In the denominator, there are still two possible parameters. One is the viscosity (η) of matrix resin, and the other is the height (Δh) of fiber reinforcement. On a case-by-case, a number of technologies in polymer chemistry have been tried to reach the viscosity of thermoplastic matrix resins at the equivalent level with thermoset matrix resins, such as in-situ-polymerization of cyclic butylene terephthalate (CBT) [113] and controlled rheology in GMT material. However, those approaches can cause many serious problems related to residues of thermally unstable and low-molecular-weight substances. Therefore, the present work finally selects the minimized height of fiber reinforcement as the controllable parameter which is being evolved into the concept of multilayered hybrid structure regarding commercial aspects.

3.2 Continuous Fiber Reinforcement

3.2.1 Concept of multilayered hybrid roving

The concept of multilayered hybrid roving (MLH-roving) was designed to combine the variety in intermediate product from commingled roving and the variety of material configuration from organic sheet. Namely, the MLH-roving is a fiber roving separated evenly into several sublayers by thermoplastic films, as schematized in Figure 3.10, through the three sequential processes [114][115][116][117] of spreading, fixing, and folding. Eventually, it takes the shape of a roving to meet the variety in intermediate product. It must be flexible enough to be suitable for general weaving processes, and be free from the risks caused by irregularly distributed and movable fibers.

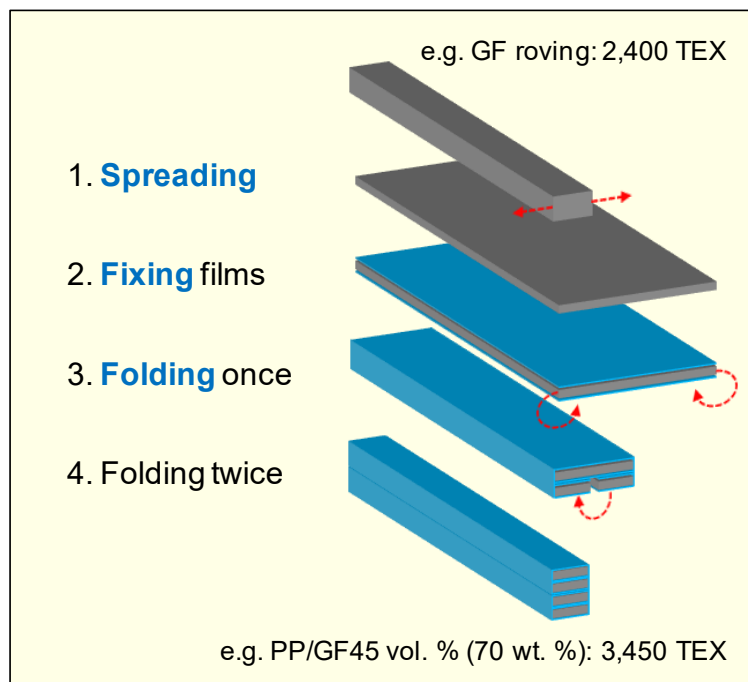


Figure 3.10: Manufacturing process of multilayered hybrid roving (MLH-roving) [118]

The MLH-roving of PP/GF45 vol. % (70 wt. %) was manufactured as follows for the present work. The GF roving of Advantex[®] boron-free ECR grade (Owens Corning, USA) was spread to 20 mm width; the GF roving is a single-end roving treated with PP compatible chemical sizing and has the linear density of 2400 TEX (g/km) with 4000 fibers of 17 μm in diameter [49]. On both sides (upper and under) of the spread GF roving, the PP films were thermally fixed by a double steel-belt press machine [119][120][121][122], being made of POLYPRO[®] homo PP (Korea Petrochemical Ind. Co., Ltd., Korea) by adding the concentrated master-batches for coupling, black color,

and heat stabilizing (see Figure 3.9 in Section 3.1.4 for the viscosity of base resin).

By means of the same procedures in Section 2.1.1, the number of rows in fiber array is calculated as follows. With the fiber diameter and the volume content, the square and hexagonal models return the values of the inter-fiber spacing into 5.46 and 7.13 μm respectively. Then, the spread width of 20 mm determines the number of columns (n) in fiber array to be 829 for square model or 891 for hexagonal model. As there are 4000 fibers in the fiber array, the number of rows (m) becomes 4–5 rows that is below half the level of continuous fiber reinforced thermoplastic materials available in the market. Furthermore, it matches 0.1 mm thickness when fully impregnated and consolidated. The MLH-roving of PP/GF45 vol. % (70 wt. %) has the linear density of 3450 TEX (g/km) and is multilayered with the same number of rows for impregnation regardless of final roving widths like 20 mm without folding, 10 mm by folding once, and 5 mm by folding twice. In other words, the MLH-roving is of 0.1 mm by 20 mm, 0.2 mm by 10 mm, or 0.4 mm by 5 mm.

For the better impregnation quality, fiber reinforcement should be minimized in height sufficiently to lead to a short flow-length and fast impregnation in accordance with the Kozeny-Carman equation. But, the level of minimum height must be considered in conjunction with the lower limit of film thickness which can be produced commercially. Almost all thermoplastic materials are available to MLH-roving, under the condition that it can be processed into film. Certainly, using film is a better prerequisite for the variety of material configuration rather than using fiber or powder. Besides, the MLH-roving is flexible enough to produce woven fabrics because it is not fully impregnated but merely fixed. The MLH-roving is more cost-effective in weaving process due to higher linear density than the GF roving of 1200 TEX for organic sheet TEPEX[®] and the commingled roving TwinTEX[®] of 1870 TEX. The MLH-roving is very comfortable in handling, for its fibers are wrapped with thermoplastic film [123][124][125].

One of the specific benefits to use continuous fiber reinforced materials is anisotropic reinforcement to optimize an intended performance of final components. For example, the unbalanced (2/1) woven fabric is the type of double reinforcement in warp to weft as shown in Figure 3.11. It can use the MLH-rovings of 5 mm width for warp with 5.0 picks per inch and of 10 mm width for weft with 2.5 picks per inch; this weaving type is better for a stable and tight weft than a conventional way using the MLH-roving of 5 mm width and spacing them apart with 2.5 picks per inch. So, the weaving density of

unbalanced (2/1) woven fabric made of PP/GF45 vol. % (70 wt. %) MLH-roving was experimentally adjusted in a way that one ply of the woven fabric will lead to a fully impregnated plate of 0.6 mm thickness. It is also possible to make more unbalanced (4/1) woven fabrics by using the MLH-roving of 20 mm width for weft.

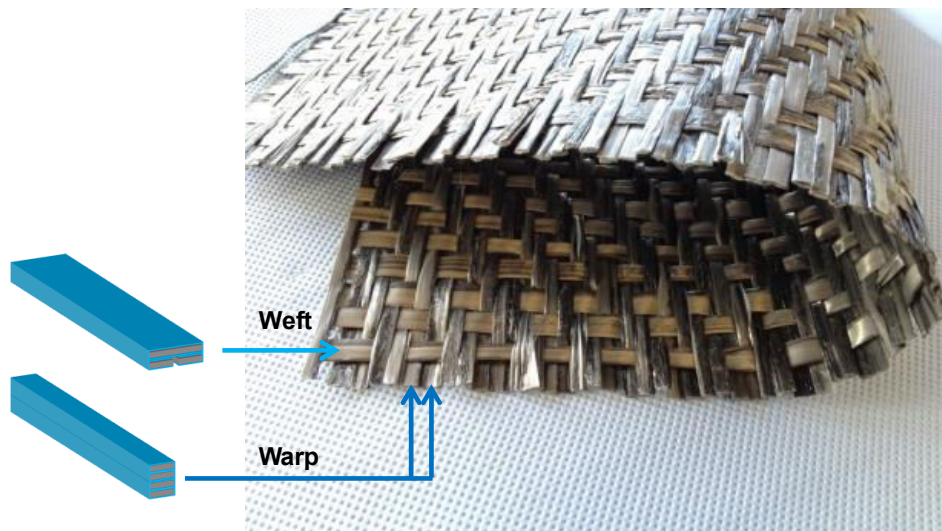


Figure 3.11: Unbalanced (2/1) woven fabric with twill pattern made of MLH-rovings

The woven fabric, if made of MLH-rovings, can reduce the risks of poor impregnation. As depicted in Figure 3.12, the outer film layers of a roving help to eliminate the risk of poor impregnation at every crossing point of warp and weft. Also, the outward flow from inner layers is the most outstanding behavior of MLH-roving that can overcome any kind of hindrances caused by fiber compaction under pressure.

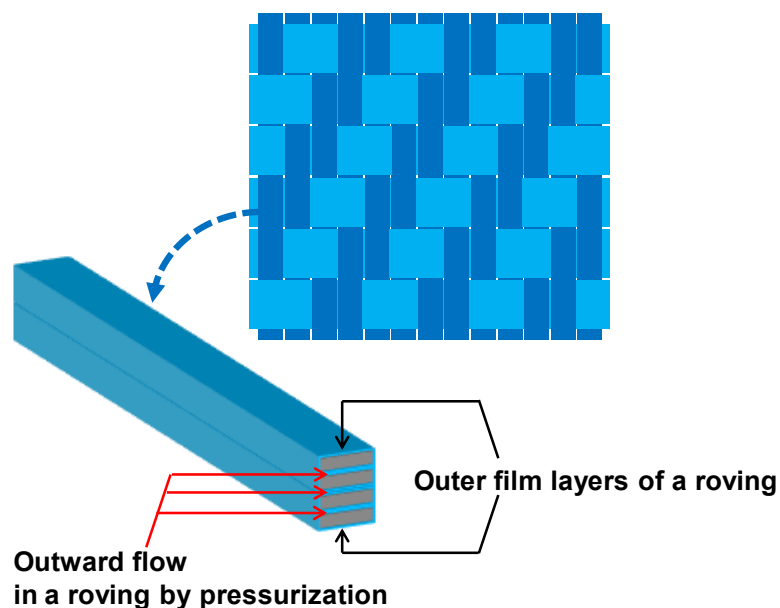


Figure 3.12: MLH-roving with outer film layers and having behavior of outward flow

3.2.2 Newly derived spreading equation

The spreading methodology is based on the very simple principle that every fiber has the same path length by a properly designed curvature on the spreading support, like in the schematic diagram of Figure 3.13. Thus, the spreading process implies that the fibers are seeking each of those more comfortable positions on the curved surface of spreading support to maintain the same path length; and the fibers are edging away gradually from the center line. Against the damages caused by excessive tension on fibers during any spreading process, it is better to weaken the firming agent in fiber rovings with the help of air flow or vibration, as well as by thermal or chemical way [126][127][128][129][130]. Most of all, the quality of fiber roving is so critical that it sometimes doesn't allow fibers to be spread continuously into a designed width, like when a fiber roving has any fully twisted point [129]. Such twisting of fiber roving frequently occurs during winding processes into bobbins, especially at a reciprocating linear-motion head. And it is widely affected by the head geometry, winding patterns, and process conditions.

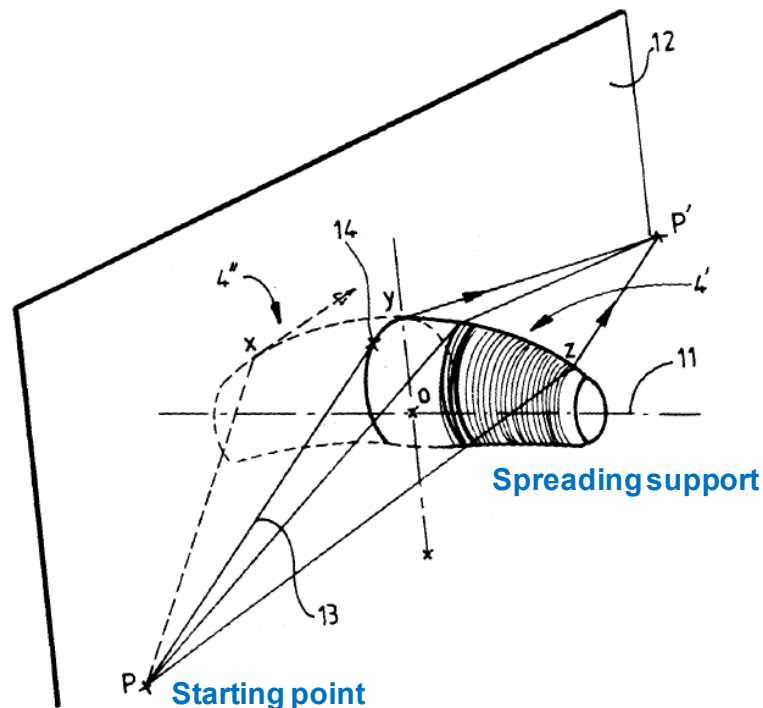


Figure 3.13: Spreading methodology on curved surface of spreading support [131]

As shown in Figure 3.13, the spreading equation in the patent of Bates and Charrier [131] has the restriction that every fiber is starting from a point. But from the practical point of view, it would be much better to take into account the half width (x_i) before

spreading and the radius (R_s) of the starting support as depicted in Figure 3.14. Even though this new spreading equation is getting more and more complex, it can prevent the serious center-splitting-problem of fibers on a spreading support which cannot be recovered naturally; cf. such a splitting is normally caused by an excessive curvature.

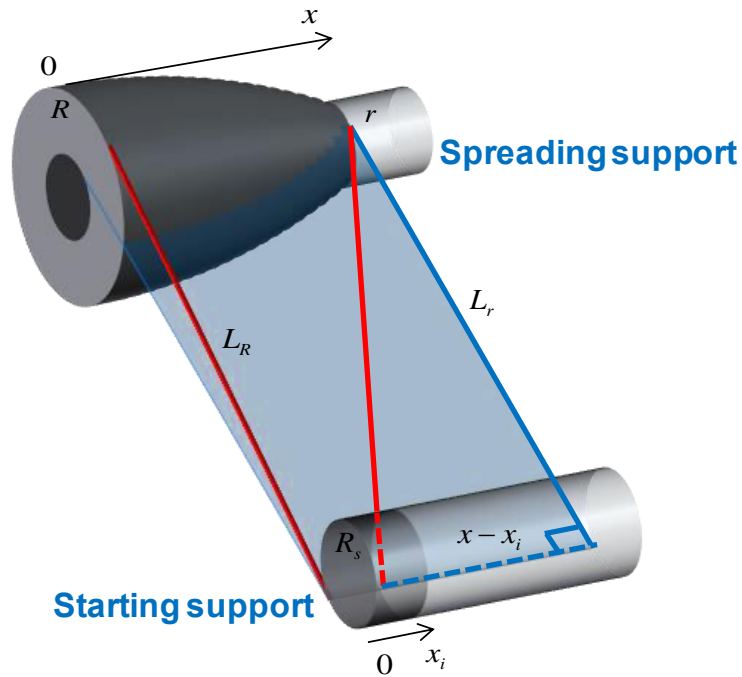


Figure 3.14: Schematic diagram for newly derived spreading equation

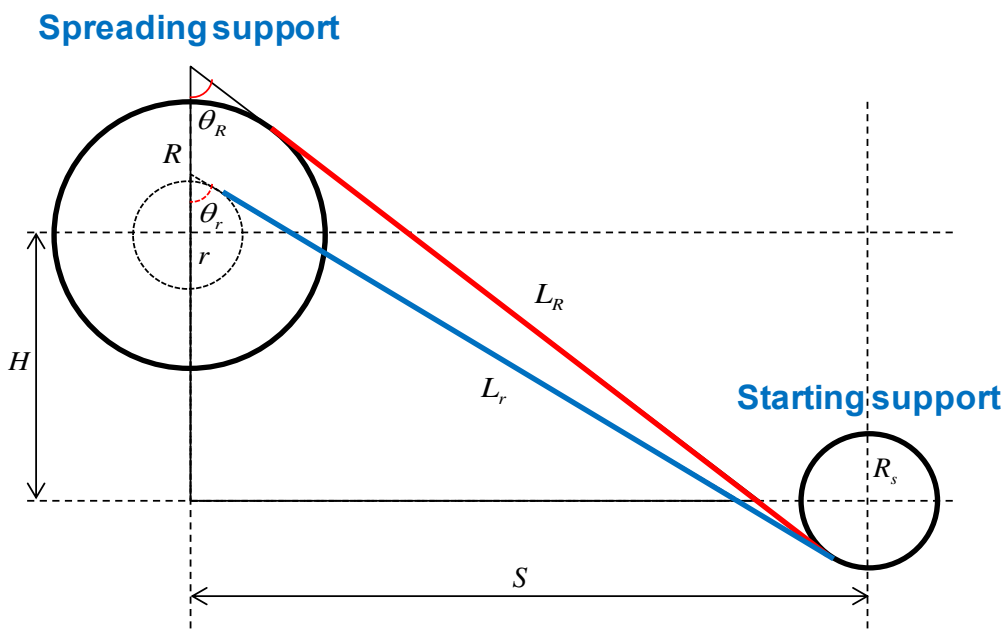


Figure 3.15: Cross-sectional diagram of spreading apparatus at center line

$$\text{Center line: } L_R + \left(\frac{\pi}{2} - \theta_R\right)R + \left(\frac{\pi}{2} - \theta_R\right)R_s \quad (3.18)$$

$$\text{Arbitrary line: } \sqrt{L_r^2 + (x - x_i)^2} + \left(\frac{\pi}{2} - \theta_r\right)r + \left(\frac{\pi}{2} - \theta_r\right)R_s \quad (3.19)$$

Accordingly, as shown in Figure 3.14 and Figure 3.15, the path length of the center line is the sum of a tangent length (L_R) intersecting two supports and continuing two arc lengths within the boundary of the horizontal distance (S). Also, in the same way, the path length of an arbitrary line is the sum of a diagonal tangent length intersecting two supports, which can be calculated from the hypotenuse of Pythagoras's theorem, and continuing two arc lengths in parallel to the center line.

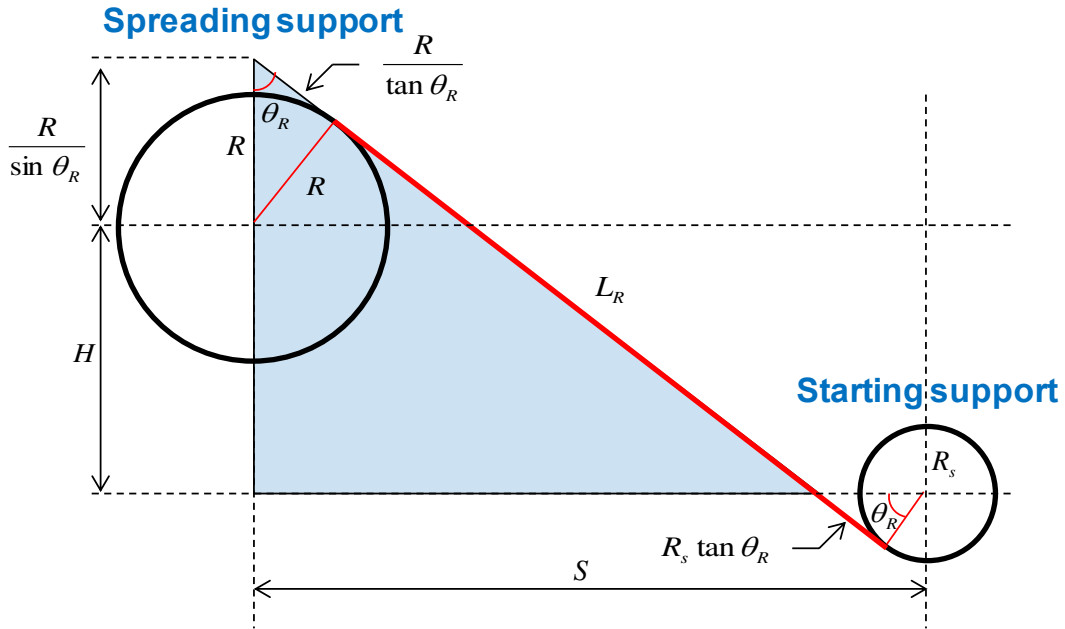


Figure 3.16: Trigonometric relations at the center line in spreading equation

$$\tan \theta_R = \frac{S - R_s / \cos \theta_R}{H + R / \sin \theta_R} \quad (3.20)$$

$$\cos \theta_R = \frac{H + R / \sin \theta_R}{L_R + R / \tan \theta_R - R_s \tan \theta_R} \quad (3.21)$$

For reasons of convenience, the spreading apparatus was specified by 100 mm for the horizontal distance (S), 20 mm for the vertical distance (H), 3 mm for the radius (R_s) of the starting support, and 13 mm for the radius (R) of the spreading support at the center line. Then, the tangent length (L_R) intersecting two supports at the center

line and its acute angle (θ_R) with the vertical line can be calculated as 100.72 mm and 69.66° by the above two trigonometric relations (see Figure 3.16). Thus, the path length of the center line is settled as 106.40 mm by adding the two arc lengths.

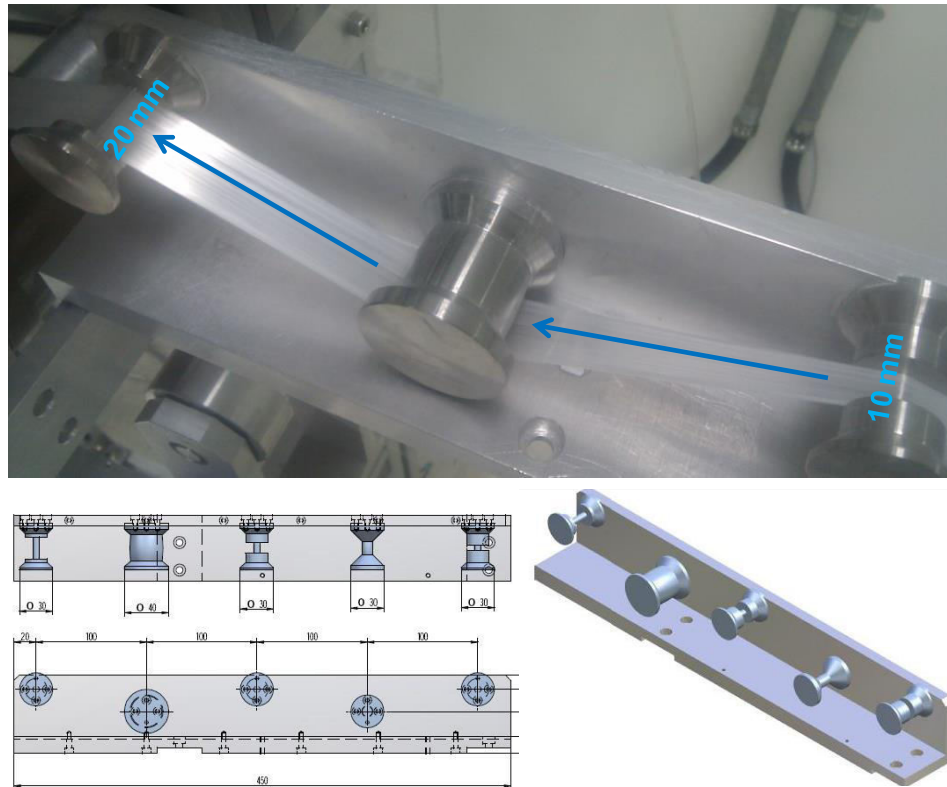


Figure 3.17: Stable spreading in accordance with newly derived equation by the lab scale device for single roving from 5 mm to 20 mm step-by-step [118]

Eventually, the radius (r) of the spreading support at $\pm x$ position is determined by a process of iteration to keep the same path length of 106.40 mm, depending on the designed widths of before and after spreading. Of course it influences on the tangent length (L_r) intersecting two supports at $\pm x$ position and its acute angle (θ_r) with the vertical line. If the widths are designed to spread from 10 mm to 20 mm, the radius (r) of the spreading support at ± 10 mm position is determined as 12.65 mm having the ratio (r/R) of 97.3%, so that the curvature on the spreading support is 7.0 m^{-1} . But, in the case of the equation proposed by Bates and Charrier, starting from a point, the corresponding radius (r) becomes 11.45 mm with the ratio (r/R) of 88.1% and the curvature of 30.3 m^{-1} . Thus, the newly derived spreading equation tends to result in a much smaller curvature that is strongly recommended to prevent the center-splitting-problem on a spreading support and for the stable spreading like in Figure 3.17.

Table 3.2: Comparison in design of spreading: at a stroke vs. step-by-step

Spreading (mm)	θ_R (°)	L_R (mm)	Path (mm)	θ_r (°)	L_r (mm)	r (mm)	r/R -	Curvature (m ⁻¹)
5 to 20	69.66	100.72	106.40	70.11	101.12	12.21	93.9%	15.8
5 to 10				69.71	100.76	12.91	99.3%	7.0
10 to 20				69.86	100.90	12.65	97.3%	7.0

H : 20 mm, S : 100 mm, R : 13 mm, R_s : 3 mm

Moreover, it is preferred to spread step-by-step rather than at a stroke. The spreading at a stroke from 5 mm width (before) to 20 mm width (after) is done by the curvature of 15.8 m⁻¹ on the spreading support, whereas the step-by-step spreading is done by the smaller curvature of 7.0 m⁻¹ on each of the two spreading supports, e.g. from 5 mm width (1st before) to 10 mm width (1st after), and subsequently from 10 mm width (2nd before) to 20 mm width (2nd after). The designed geometries based on the newly derived spreading equation are summarized in Table 3.2.

In the light of scale up, an idea of multilane spreading can be applied, which is done on a parallel structure with several sets of spreading and support bars. Each lane is composed of mostly the same geometry with the above lab scale device, except the partition walls (e.g. 4 mm gap). The spread fibers on every lane are placed between a pair of films and thermally fixed all together, and then slit to each lane and folded once or twice. The film thickness should be 20% thinner than for lab scale device, considering the 4 mm gap between lanes on 20 mm spreading.

3.2.3 Verification on impregnation quality

The impregnation quality of MLH-roving was verified with the plates that several plies of woven fabrics (see Table 3.3) had been impregnated and consolidated at the given conditions by the continuous compression molding (CCM) machine.

Table 3.3: Unbalanced (2/1) woven fabric made of MLH-roving

MLH-Roving	Unbalanced woven fabric
PP/GF45 vol. % (70 wt. %)	PP/GF45 vol. % (70 wt. %)
3450 TEX (2400 TEX GF+1050 TEX PP)	Warp/weft=2/1
(0.4 mm by 5 mm) and (0.2 mm by 10 mm)	(5.0 picks/inch) and (2.5 picks/inch)
	Unit thickness: 0.6 mm/fabric

The CCM machine is very appropriate for pilot-scale or mass production. As depicted in the process diagram of Figure 3.18, it is based upon the principle of the repeated pressurization and a quasi-continuous impregnation, by a mold consisting of both the heating and cooling zones. The compression pressure is applied with the aim of heat transfer and driving melt flow into the fiber reinforcement, while the pressure release is to give a chance of moving the material along the process direction. The repeated pressurization is one of the effectual ways to progressively get rid of the air trapped inside.

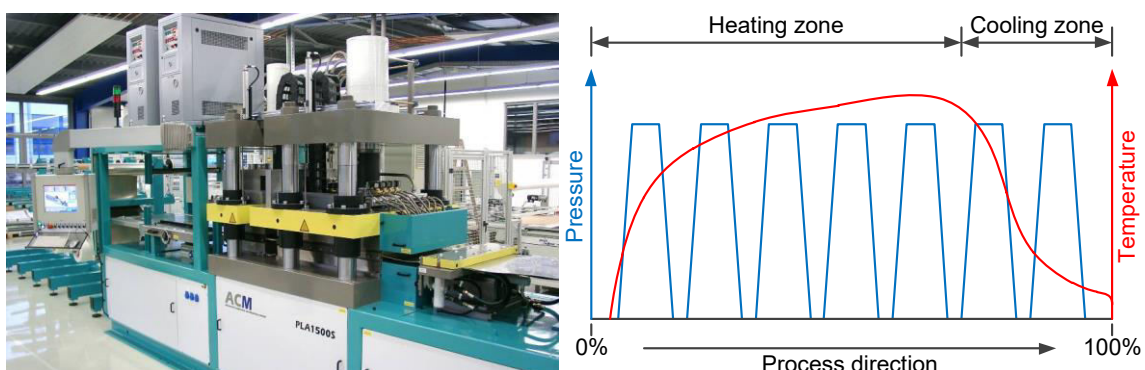


Figure 3.18: CCM machine at IVW GmbH (Germany) and its process diagram

Five plies of the unbalanced (2/1) woven fabrics made of PP/GF45 vol. % (70 wt. %) MLH-roving was loaded onto the CCM machine running at 10 m/h line speed and 25 bar pressure. Only the influence of temperature was investigated at 190, 210, 230,

and 250°C. The major direction of double reinforcement in unbalanced (2/1) woven fabric is toward the machine direction, and the plies are laid between the steel coils coated with the release agent of thermoset type. After released from the steel coils at the outlet of the CCM machine, the consolidated plate is cut to a given length at the next cutting unit. The impregnation quality was quantified by the three-point bending test for class III material in ISO 14125 that is the preferred class for multidirectional composites e.g. glass fiber systems. Bending tests are the most effective test method to see all kinds of undesirable failures including the shear failure between the plies of woven fabrics. In compliance with the test method, the dimensions of test specimen were setup into 3 mm thickness, 25 mm width to reduce a degree of variability, and 100 mm length. The span length was 60 mm (20 times the specimen thickness). The bending test was performed with the speed of 2.0 mm/min which is as equivalent as possible to the strain rate of 0.01 min⁻¹ on the outer surface of specimen. Using the load cell of 5 kN, the bending test continued within the valid strain limit of 3% that is the prescribed range for small deflection.

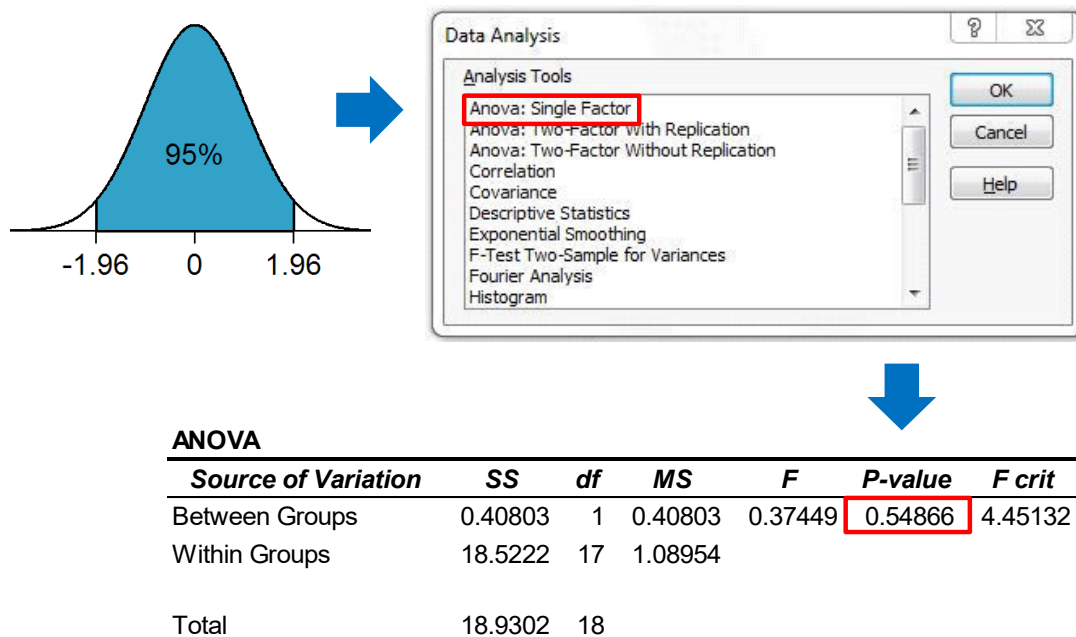


Figure 3.19: Statistical procedures for outlier verification and single-factor analysis of variance (ANOVA)

The design of experiments in each of the impregnation temperatures was made up of the two bending directions (tests on upper side and underside). This was intended to check the additional information whether the impregnation quality is asymmetric or symmetric. Each test set consisted of 10 specimens which had been machined in the

major or minor direction of the unbalanced (2/1) reinforcement. After bending tests in each test set, outliers were excluded through the verification with 95% probability on flexural modulus, strength and strain respectively. The statistical comparison between the two bending directions was done by single-factor analysis of variance (ANOVA) with 95% confidence level. Accordingly if the P-value is higher than 0.05, then there is no significant difference between the bending directions (refer to Figure 3.19). Also, the statistical comparison between two impregnation temperatures was done in the same manner, to define the advisable range of impregnation temperature.

3.2.4 Characterization on major direction

All the flexural properties in major direction were statistically symmetric with respect to bending direction except for the flexural strain at 190°C (1.43% on upper side and 1.64% on underside), being summarized in Table 3.4; as mentioned in the previous section, it was done through outlier verification with 95% probability and by single-factor ANOVA with 95% confidence level. The properties of two bending directions have merged into one in the case of P-value being higher than 0.05.

Table 3.4: Flexural properties with impregnation temperature (major direction)

Temperature	Flexural modulus	Flexural strength	Flexural strain
190°C	23.1 GPa (CV 4.5%)	312 MPa (CV 8.4%)	1.43%, 1.64% (CV 8.3%, 9.7%)
210°C	23.9 GPa (CV 2.7%)	370 MPa (CV 8.3%)	1.73% (CV 7.9%)
230°C	24.4 GPa (CV 4.2%)	438 MPa (CV 4.8%)	1.89 % (CV 6.4%)
250°C	24.2 GPa (CV 3.6%)	447 MPa (CV 5.1%)	1.91% (CV 5.8%)

CV: coefficient of variation

Unbalanced (2/1) woven fabric made of PP/GF45 vol. % (70 wt. %) MLH-roving

The other statistical comparison was performed between each pair of impregnation temperatures by single-factor ANOVA with 95% confidence level. Of those results, only the P-values between 230°C and 250°C were all significantly higher than 0.05 as summarized in Table 3.5. Accordingly, the properties of the two temperatures were merged, and the representative flexural properties for major direction were suggested as 24.3 GPa in modulus, 443 MPa in strength, and 1.90% in strain. First of all, the flexural modulus of 24.3 GPa is a very reasonable value because it is at 95% level of the theoretical value (25.7 GPa); the theoretical modulus was calculated by the rule of mixtures with the modulus of 1.72 GPa for PP [23] and 80.5 GPa for GF [24], in consideration of the fiber content and the orientation, like 45 vol. % and toward the major direction of unbalanced (2/1) layup [21][22]. The CV value of flexural modulus

is 3.9% in a very narrow range, whereas the other two CV values of flexural strength and strain are around 5% in a moderate range.

Table 3.5: Representative flexural properties (major direction)

Major direction	Flexural modulus	Flexural strength	Flexural strain
P-value	0.51	0.21	0.59
(230°C and 250°C)			
Representative value	24.3 GPa	443 MPa	1.90%
	(CV 3.9%)	(CV 5.0%)	(CV 6.1%)

CV: coefficient of variation

Unbalanced (2/1) woven fabric made of PP/GF45 vol. % (70 wt. %) MLH-roving

As graphically shown in Figure 3.20, the flexural properties are converging to each of the specific values. The amount of falling-off from representative values is calculated as 5% in modulus, 30% in strength (the most sensitive one), and 25% (on upper side) or 14% (on underside) in strain to 190°C.

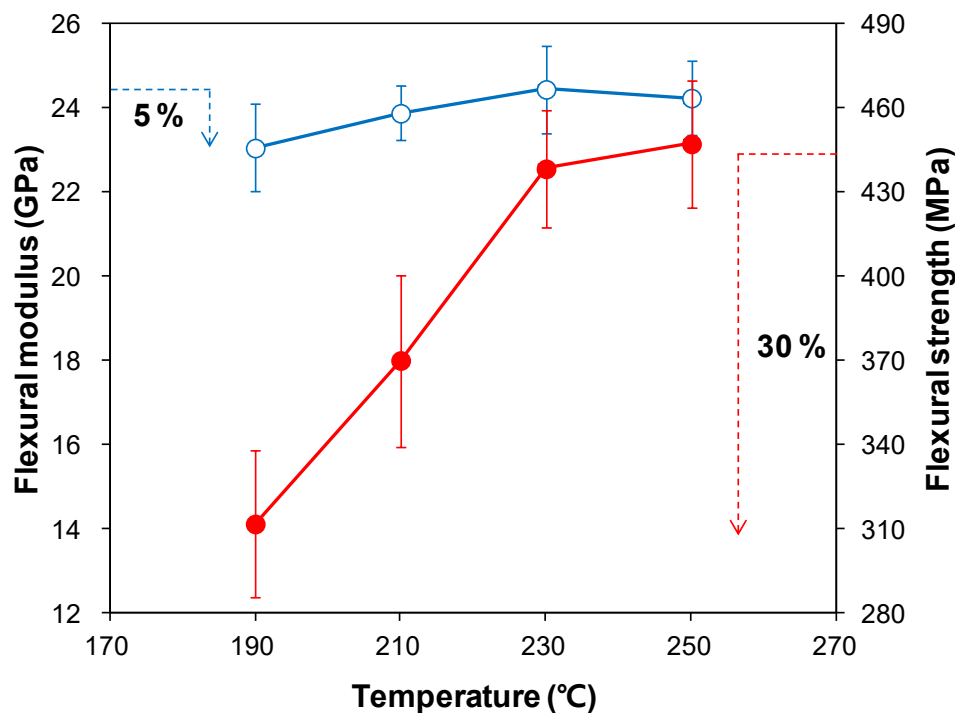


Figure 3.20: Variations in modulus and strength with impregnation temperature

The falling-off is deeply related to the flattened voids in the shape of cracks as shown in the cross-sectional view of the plate impregnated at 190°C (see yellow arrows in Figure 3.21) but no longer at 250°C (see Figure 3.22). And their influences gradually become obvious as the strain increases, whereas being not so critical in early stage.

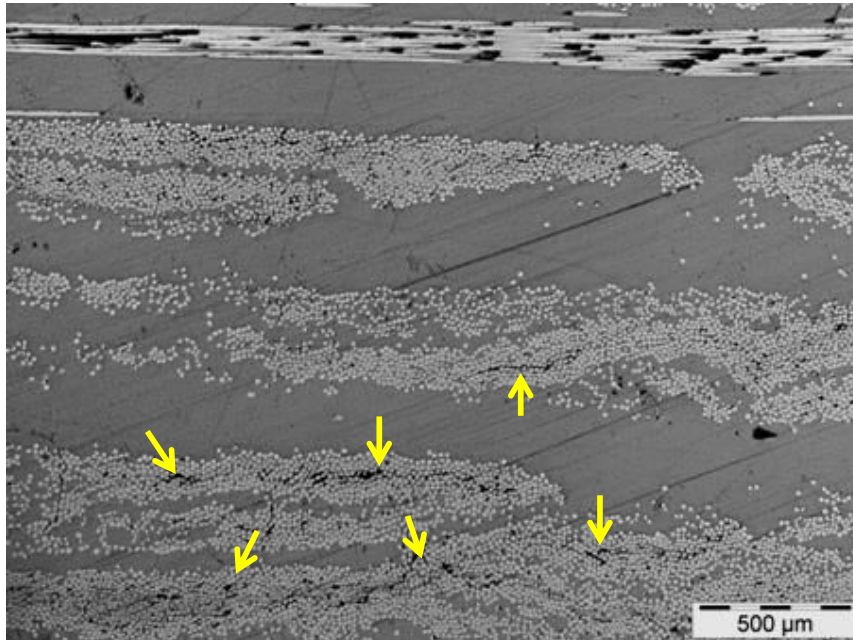


Figure 3.21: Cross-sectional view of plate impregnated at 190°C

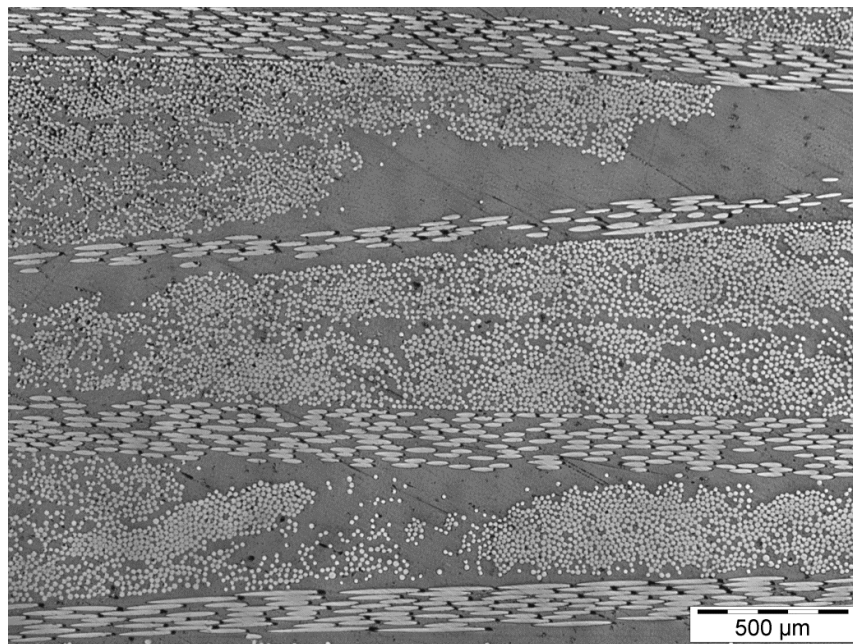


Figure 3.22: Cross-sectional view of plate impregnated at 250°C

To efficiently characterize the stress-strain behavior, the persistence (or bias) degree [96][97] was used just as the ratio of the experimental strength to the modulus-based strength (modulus times strain). As depicted in Figure 3.23, the persistence degree will be 100% if a stress-strain curve perfectly follows the straight line virtualized by its modulus. As for unbalanced (2/1) woven fabric made of PP/GF45 vol. % (70 wt. %) MLH-roving, the persistence degree in major direction increased with impregnation temperature, like 90% at 210°C, 95% at 230°C, and 96% at 250°C.

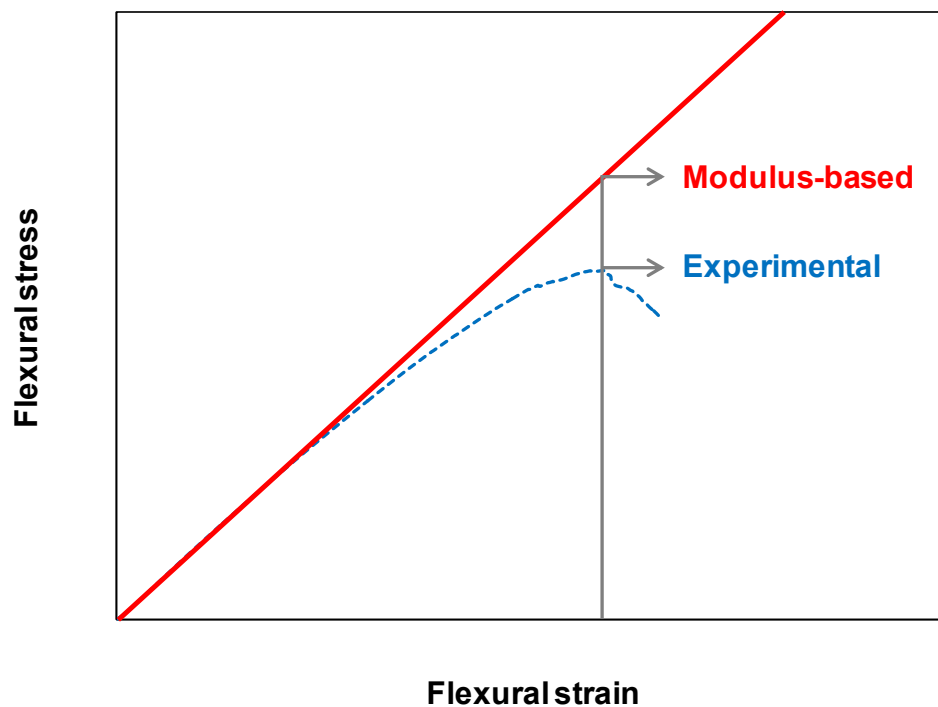


Figure 3.23: Persistence degree (or bias) as the ratio of experimental strength to modulus-based strength

In summary, the representative flexural properties for major direction, of unbalanced (2/1) woven fabric made of PP/GF45 vol. % (70 wt. %) MLH-roving, were determined at the impregnation temperature from 230°C to 250°C by CCM machine running at 10 m/h line speed and 25 bar pressure. Representativeness could be accepted with the modulus at 95% level of the theoretical value, and efficiently characterized by the persistence degree of above 95% for the stress-strain behavior. Consequently, the impregnation quality of MLH-roving was verified as being excellent, considering the case of pilot-scale or mass production.

3.2.5 Variation in minor direction

As summarized in Table 3.6, the representative flexural properties for minor direction were suggested as 13.9 GPa in modulus, 243 MPa in strength, and 2.07 % in strain at the impregnation temperature of 230°C; of course, there is no significant difference between the bending directions (on upper side and underside) in accordance with the statistical comparison by single-factor ANOVA with 95% confidence level. The flexural modulus of 13.9 GPa is likewise a very reasonable value because it is over 95% level of the theoretical value (14.4 GPa) calculated by the rule of mixtures having the fiber content of 45 vol. % and toward the minor direction of unbalanced (2/1) layup. Also, it has a narrow CV below 5%. Up to this point, it is similar with major direction.

Table 3.6: Representative flexural properties (minor direction at 230°C)

Minor direction	Flexural modulus	Flexural strength	Flexural strain
P-value (upper and under)	0.91	0.60	0.30
Representative value	13.9 GPa (CV 4.6%)	243 MPa (CV 14%)	2.07% (CV 9.7%)

CV: coefficient of variation

Unbalanced (2/1) woven fabric made of PP/GF45 vol. % (70 wt. %) MLH-roving

However, the other two CV values were three and two times wider, when compared with those of major direction lying in the moderate range of around 5%. These wider CV values seem to be somewhat related to the waving of fibers as depicted in Figure 3.24 with a dotted line along the minor direction. Also the sampling position for the specimens of flexural test (on upper side and underside) is marked together with the transparent and translucent rectangles. The transverse direction of CCM process, the same with the minor direction of unbalanced (2/1) fabric, is likely to be at high risks to the waving of fibers, because there is no adjunctively applied tension on the fibers. Moreover, the waving of fibers is caused by the dragging to load the fabrics into the CCM machine. Accordingly, the variation in minor direction might be unavoidable in an ordinary CCM process when using woven fabrics to make an impregnated and consolidated plate.

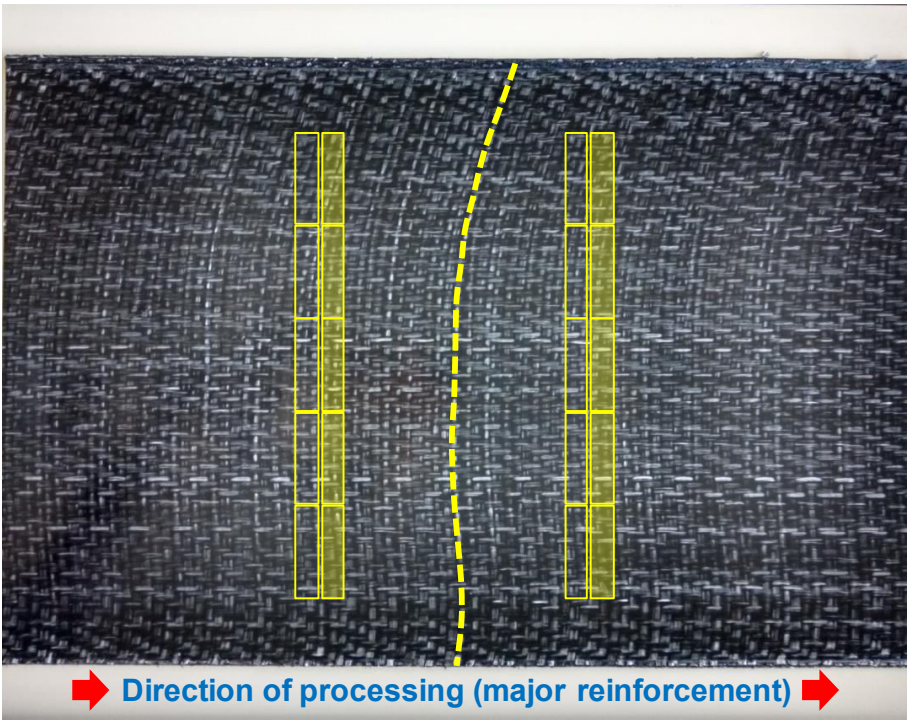


Figure 3.24: Sampling position and waving of fibers in minor direction

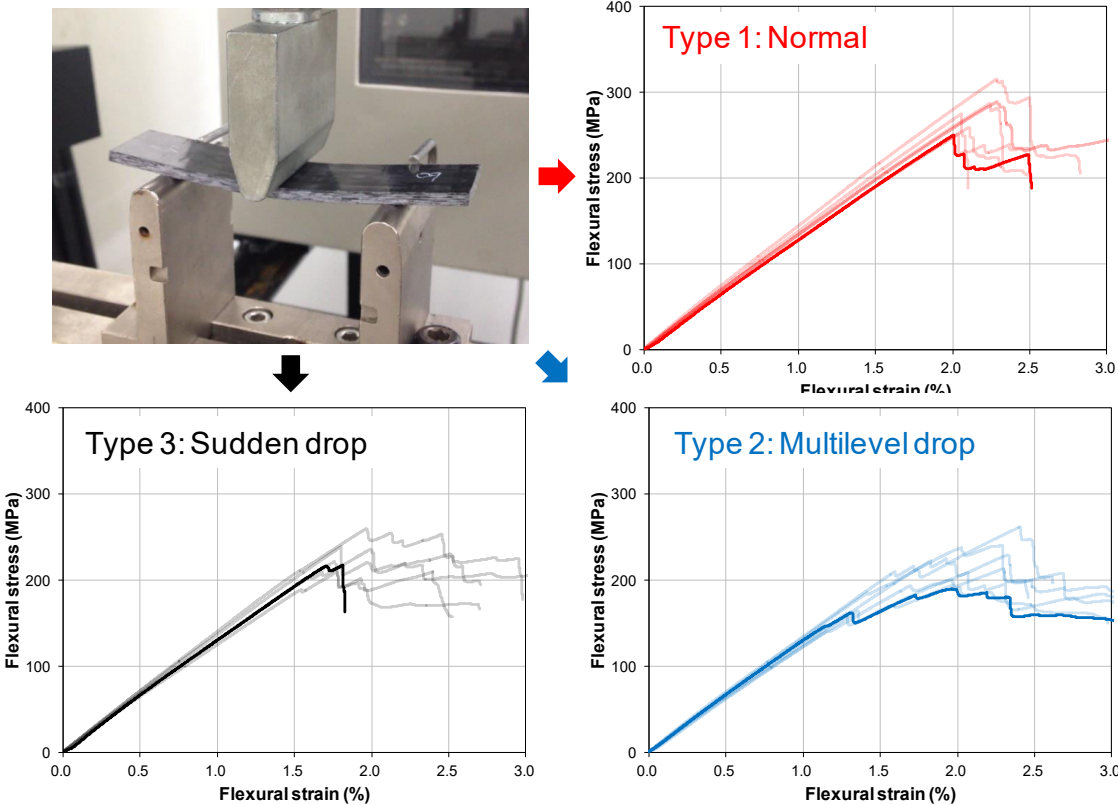


Figure 3.25: Classification of stress-strain curves into three types in minor direction

The stress-strain behavior of the minor direction can be classified into three types as shown in Figure 3.25. The number of each type is 7, 7, and 6 of 20 specimens that is evenly distributed. Type 1 is the quite normal behavior that has the strain of around 2.1% and the persistence degree of around 90%. It is very similar to the behavior of the major direction. Type 2 is named here as the multilevel-drop behavior that has the same level of strain with Type 1 but the lower persistence degree of around 75%. It might be directly related to the misalignment or the waving of fibers before and during impregnation. Type 3 is named here as the sudden-drop behavior that has the same level of persistence degree with Type 1 but the shorter strain. The sudden-drop might be due to the straightening phenomenon of crimps.

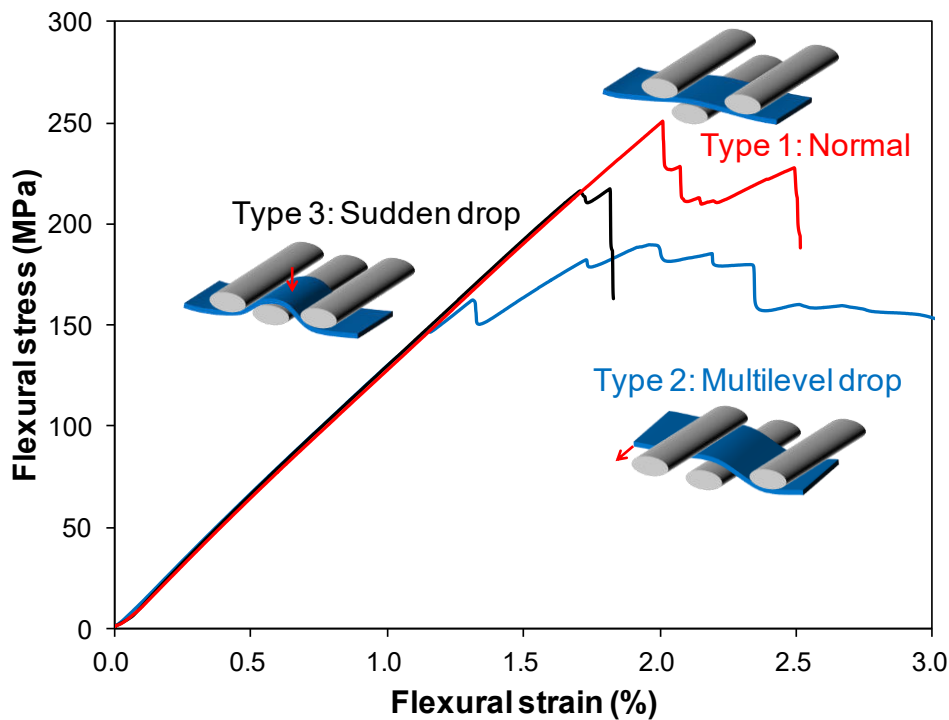


Figure 3.26: Three types of stress-strain behaviors in minor direction

The 10 mm width MLH-rovings in minor direction tend to form crimps easily, as there is no tension applied to the minor direction, and besides, as the 10 mm width MLH-rovings are more flexible than the 5 mm width MLH-rovings in major direction. Thus, as summarized in Figure 3.26, the minor direction (the transverse direction of CCM process) has the variation in stress-strain behavior due to the waving of fibers as well as the crimps of woven fabric, though having started with the same level of modulus.

3.3 Long Fiber Reinforcement

3.3.1 Concept of multilayered hybrid mat

As described in Section 2.1.2, conventional GMT materials are based on the lowered melt viscosity of matrix polymer for impregnation, so that those are inevitably limited in matrix polymer. And they have relatively low GF contents, such as from PP/GF15 wt. % to PP/GF45 wt. % in commercial aspects; merely from 6 vol. % to 22 vol. %. Hence, the concept of multilayered hybrid mat (MLH-mat) is aimed to realize a new GMT like material that is suitable for various matrix polymers and high GF contents. The MLH-mat consists of several plies of thermoplastic films and thin GF sublayers. In order to be isotropic as much as possible, each GF sublayer should have random directional fiber distribution as well as homogeneity in areal density.

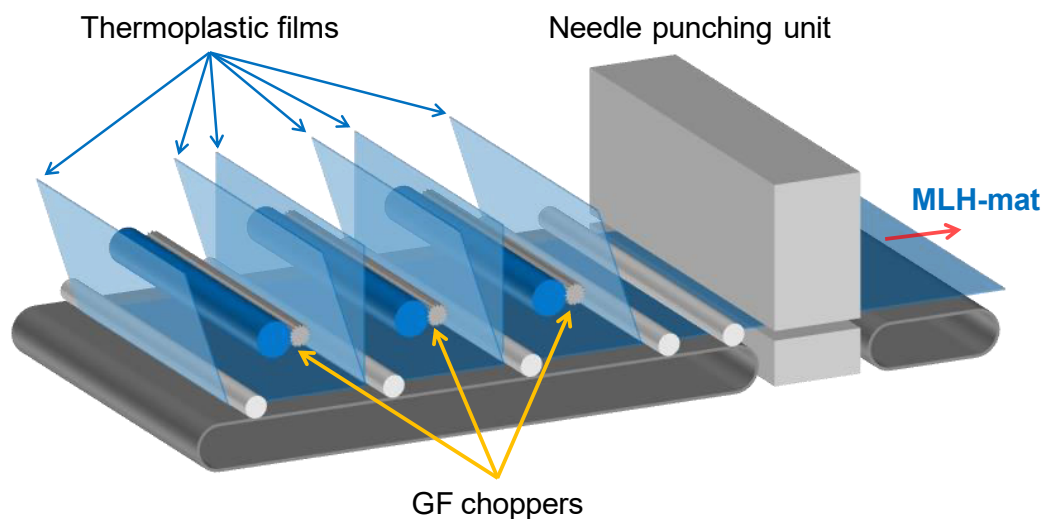


Figure 3.27: Manufacturing process of MLH-mat composed of several GF choppers and a needle punching unit [132]

The manufacturing process of MLH-mat is a kind of a modified chop-and-needle mat line. Multi-end rovings are being chopped on each film by a series of choppers, and then all needle-punched together with thermoplastic films as depicted in Figure 3.27 (also refer to Figure 3.28). For a long time, conventional GMT materials have been verified and optimized in order to be compatible with chop-and-needle mat lines. So, it is desirable to use the same specific grades of GF roving and to adopt the same mixed lengths of fibers like 25 and 37 mm. Almost all kinds of thermoplastic films are feasible in this MLH-mat, regardless of their melt viscosity. And the needle-punching process contributes to less cost by forming a combined MLH-mat as well as to better

impregnation quality by de-bundling of fibers in each sub-bundle. De-bundling is very helpful for impregnation in the next step to be done by CCM machine, double steel-belt press line, or whatever else.

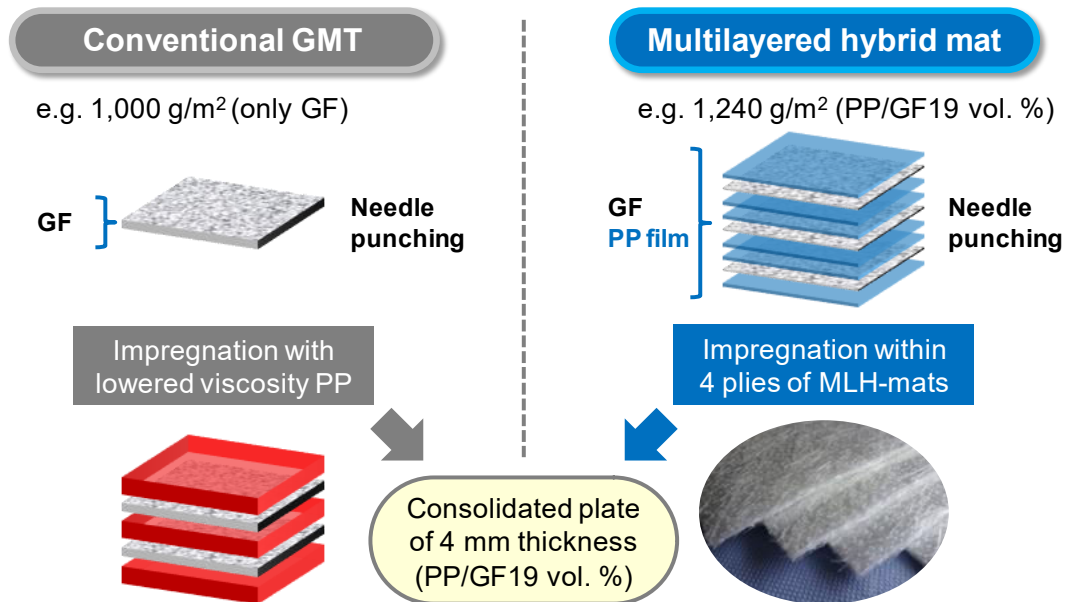


Figure 3.28: Comparison of MLH-mat with conventional GMT (PP/GF40 wt. %)

For a direct comparison between conventional GMT and MLH-mat, the unit MLH-mat of PP/GF19 vol. % (40 wt. %) was designed to have the areal density of 1240 g/m². It consists of 6 PP films and 3 GF sublayers as depicted in Figure 3.28. And the areal density of each GF sublayer was 165 g/m², which is at one sixth level compared to 1000 g/m² of GF mat for conventional GMT materials. The unit MLH-mat of PP/GF19 vol. % (40 wt. %) becomes 1.0 mm in thickness if fully impregnated and consolidated, whereas conventional GMT materials have the nominal thickness of 3.7–4.0 mm; this thickness is simply matched by adding four plies of the unit MLH-mats as described in Figure 3.28.

3.3.2 Changes of porosity along pressure

As mentioned in Section 3.1.4, the impregnation with thermoplastic matrix resins is done by means of heating and pressurizing tools. However, this kind of process often brings about the complicated, positive and negative effects on impregnation. As a result of compaction, especially, the porosity of fiber reinforcement decreases varying in a greater or less degree. Therefore, measuring the changes of porosity in fiber reinforcement along pressure becomes one of the important matters in order to trace and inspect the impregnation environment based on the Kozeny-Carman equation. Here the porosity changes of MLH-mat along pressure could be practically calculated from the entire-thickness changes as depicted in Figure 3.29 and Figure 3.30. The detailed explanations are as follows.

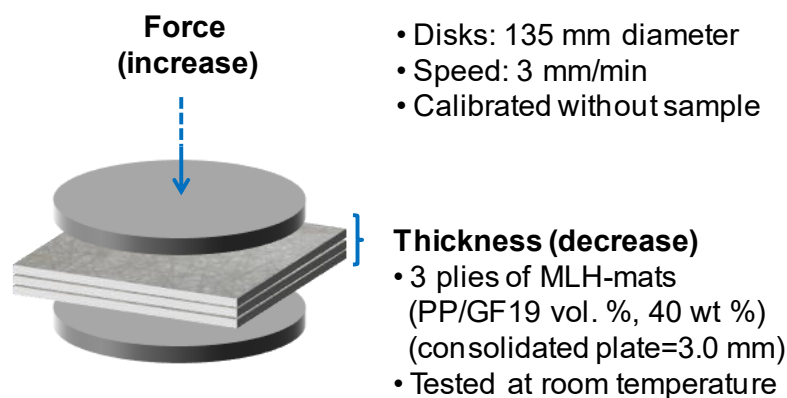


Figure 3.29: Thickness measurement of MLH-mats for porosity at room temperature

Being divided by the constant area of pressurizing disk, the volume of MLH-mat is regarded as the entire-thickness. And, testing at room temperature is closely related to the very beginning of impregnation, like just before melting of thermoplastic film in MLH-mat. The volume or entire-thickness of MLH-mat between the disks at a given pressure consists of three elements; fiber, air, and matrix polymer as shown with the stacked bar at the left of Figure 3.30. Of course, the primary concern is the porosity in fiber reinforcement that is the ratio of the air to the sum of air and fiber, and that should be completely replaced by matrix polymer. Meanwhile the two elements, fiber and matrix polymer, can be determined by the other information of fully impregnated and consolidated plate, on the assumption that they are not at all compressed by the pressure applied on MLH-mats. So, it probably tends to underestimate the proportion

of the air steadily as the pressure increases. Nevertheless, this approach is a very adequate and efficient way to inform about the porosity in fiber reinforcement of MLH-mat at a given pressure.

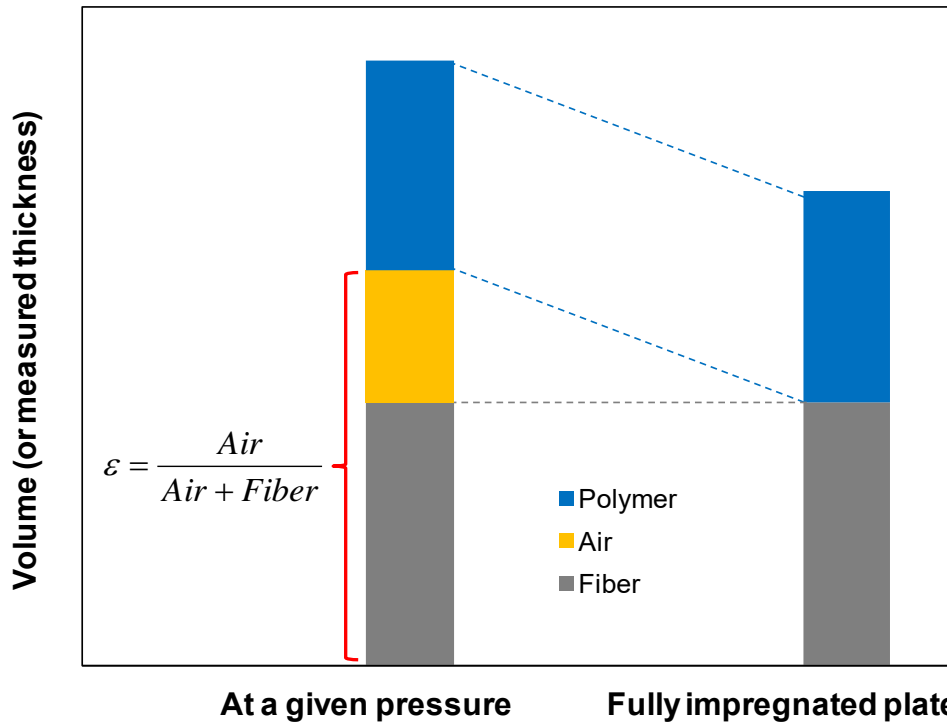


Figure 3.30: Porosity calculation from measured entire-thickness of MLH-mat at a given pressure and with information of its fully impregnated plate

Prior to compression tests on MLH-mats, the baseline was created up to 140 bar with the compression speed of 3 mm/min at room temperature. Of course, there was no sample between the rigid disks of 135 mm diameter. It is compulsory to compensate the measurement setup against the intrinsic displacement caused by pressurization. Thus, as shown in Figure 3.31, the intrinsic displacement turned out to be roughly 1.5 mm up to 100 bar, with the almost perfect linear fit of 99.9% R^2 . Under the same test conditions, three plies of the PP/GF19 vol. % (40 wt. %) MLH-mats were pressurized 3 times repeatedly. And the entire-thickness changes were plotted as shown in Figure 3.32 after the baseline correction. There is a rapid drop at the initial stage of each run. As the pressure increases, the entire-thickness converges to a specific value. Also, the curve itself might converge to a curve if the run is repeated more and more. The reproducibility was checked by the other test set. So, the average thicknesses of the two tests were taken for the porosity calculation in fiber reinforcement of the given MLH-mat.

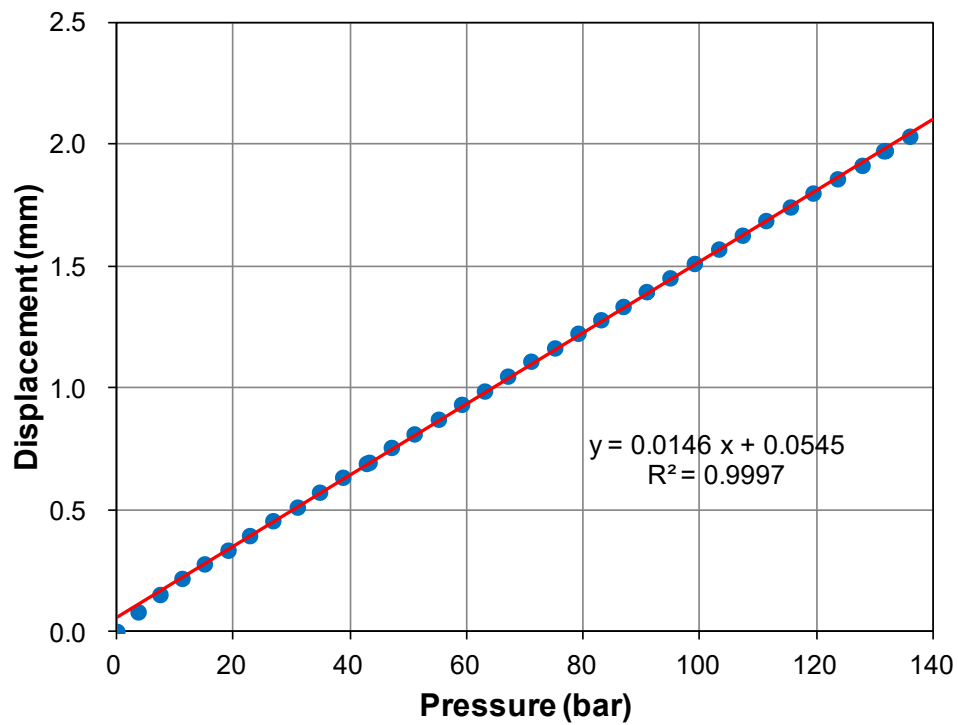


Figure 3.31: Baseline setting with no sample to compensate intrinsic displacement

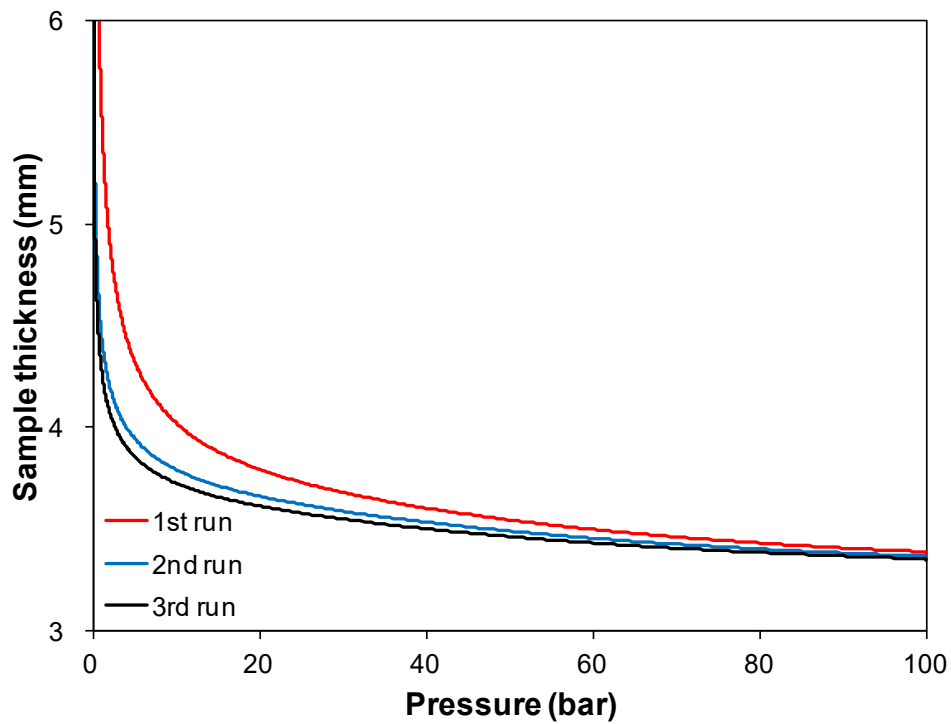


Figure 3.32: Thickness changes of PP/GF19 vol. % (40 wt. %) MLH-mat by repeated pressurization (after baseline correction)

The first run is more meaningful for the environment of impregnation, rather than the others that are partially recovered after being compressed by pressurization. The two representative porosities were carefully suggested here by the calculation from the entire-thickness changes in compression test on PP/GF19 vol. % (40 wt. %) MLH-mat. One is 54% porosity at 30 bar in first run, and the other is 37% porosity at 100 bar on average of runs as summarized in Figure 3.33. The porosity of 37% at 100 bar is treated as the lowest limit for MLH-mat of a random directional fiber distribution, which is naturally higher than the theoretical limits for very well aligned fibers; 21.5% or 9.3% by the square and hexagonal models when the inter-fiber spacing (s) is zero (refer to Figure 2.6 in Section 2.1.1).

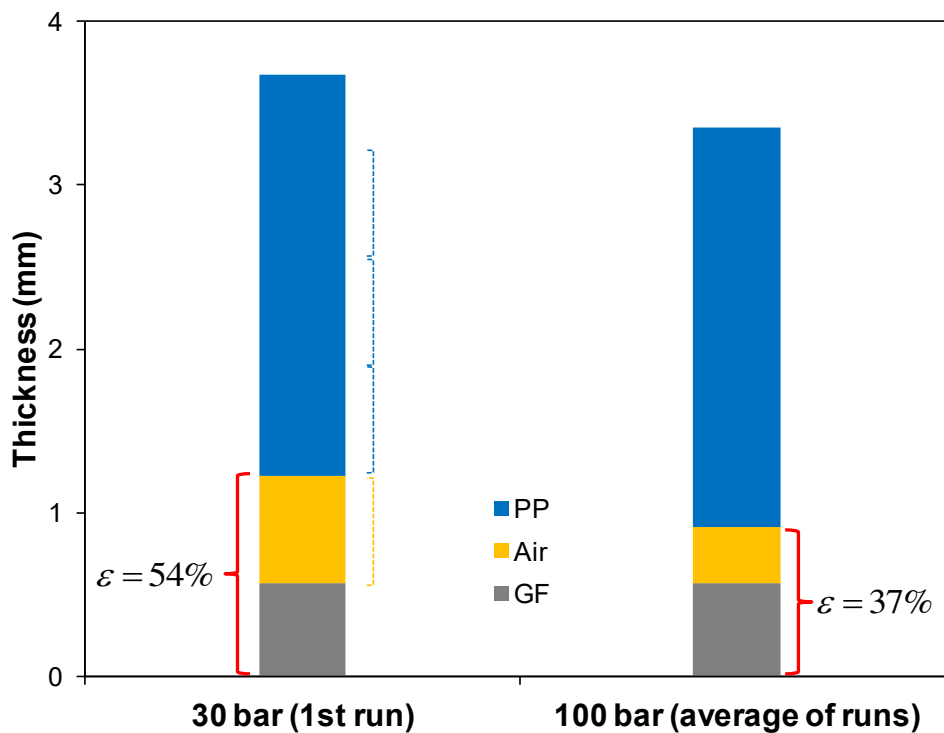


Figure 3.33: Representative porosities in fiber reinforcement of PP/GF19 vol. % (40 wt. %) MLH-mat at room temperature

The porosity of 54% at 30 bar is an appropriate one to describe a typical environment of impregnation with thermoplastic matrix resins, considering the process conditions ranging from 20 to 30 bar; cf. the porosity of 58% at 20 bar. Meanwhile, the amount of PP in PP/GF19 vol. % (40 wt. %) MLH-mat is more than three times the air, at 30 bar pressure and before impregnation, more strictly speaking at room temperature, as distinctly marked by the stacked bar in Figure 3.33. The surplus PP might not be involved in the following impregnation, which corresponds to the cross-sectional view

of an impregnated plate. It shows islandlike sub-bundles (see Figure 3.34) that are composed of 100 fibers, chopped in GF sublayers, and somewhat de-bundled during the needle-punching process.

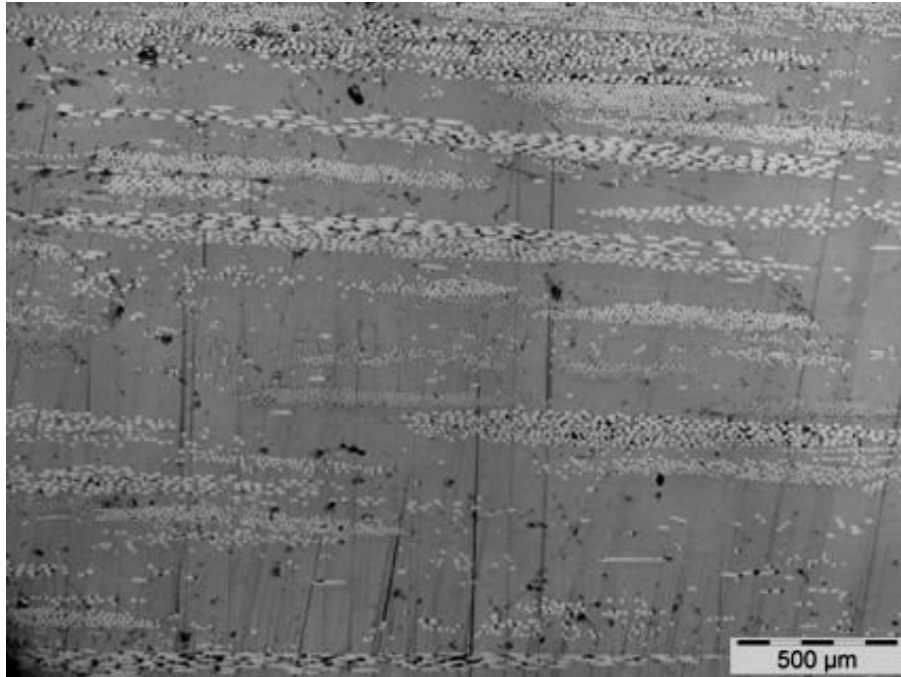


Figure 3.34: Cross-sectional view of impregnated PP/GF19 vol. % (40 wt. %) MLH-mat showing islandlike sub-bundles

Therefore, if the amount of PP in MLH-mat is gradually reduced to the amount of air, it is possible to have high GF contents, like about 45 vol. % as schematized in Figure 3.35; it is recommended to reduce PP evenly in each layer. The porosity at 20–30 bar matches the fiber content ranging 42 vol. % to 46 vol. % if fully impregnated, based on the result of PP/GF19 vol. % (40 wt. %) MLH-mat in first run of the compression test at room temperature. Furthermore, the environment of impregnation is not likely to be significantly influenced by the amount of matrix polymer in that the concept of MLH-mat is designed to have the similar level of areal density for GF sublayers.

As shown in Figure 3.36, a cross-sectional view of impregnated PP/GF45 vol. % (70 wt. %) MLH-mat no longer has islandlike sub-bundles, contrary to Figure 3.34. Still, it is necessary to confirm the concept of MLH-mat by checking the impregnation quality. The flexural properties will be measured and characterized as a way to check if the impregnation quality could be maintained at high fiber contents. The modulus is the only characteristic value that can be estimated with theoretical basis. So, the stress-strain behaviors will be characterized by the persistence degree.

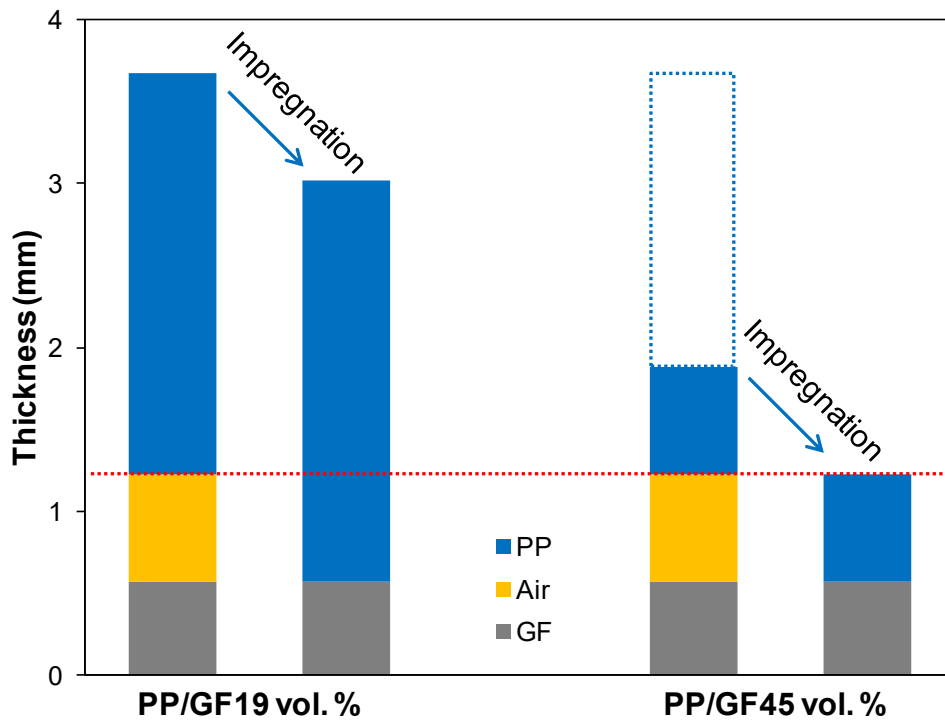


Figure 3.35: MLH-mat of high GF content about 45 vol. % can be reached if PP is reduced to the amount of air at 30 bar pressure

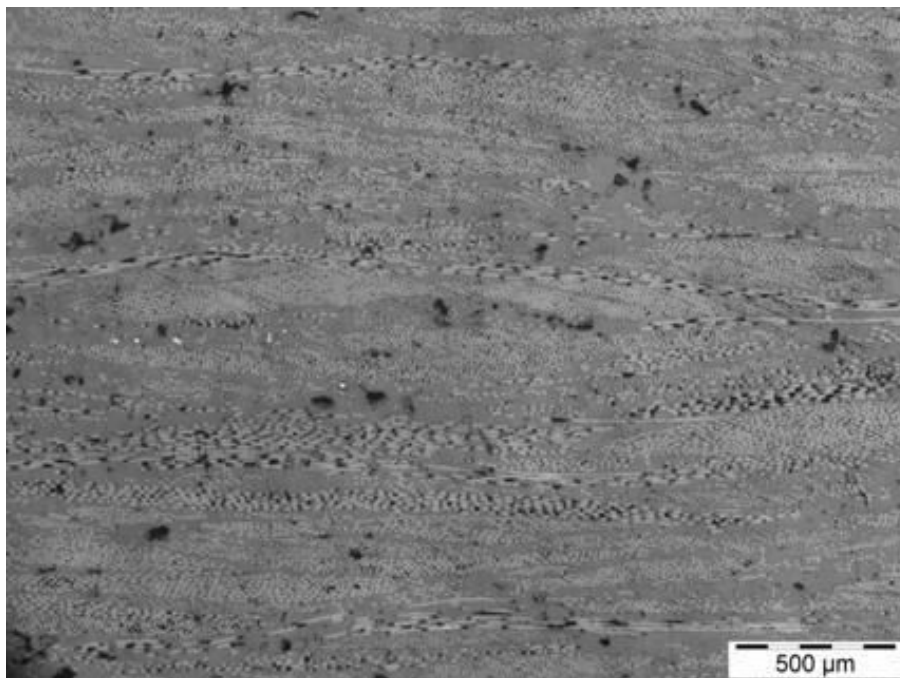


Figure 3.36: Cross-sectional view of impregnated PP/GF45 vol. % (70 wt. %) MLH-mat showing no longer islandlike sub-bundles

3.3.3 Preparation and impregnation

Several grades of MLH-mats were prepared with the specifications described in Table 3.7, three PP/GF grades and four PA6/GF grades having the glass fiber content from 19 vol. % to 50 vol. %. Each MLH-mat gets a unit thickness of 0.60 to 1.00 mm in the case of a fully impregnated and consolidated plate, and also consists of several GF sublayers having an areal density between 140 and 165 g/m². The present work is using the films of 29 μm thickness for PP grades and of 25 μm for PA6 grades, as a way of experimental simplification. As a detailed example, PP/GF32 vol. % (57 wt. %) and PP/GF45 vol. % (70 wt. %) MLH-mats are commonly using two-ply PP films of 29 μm thickness and have the same numbers of GF sublayer, as depicted in Figure 3.37. But, those MLH-mats are somewhat different in the number and configuration of PP film, and each areal density of GF sublayers are fine-tuned to 141 and 149 g/m².

Table 3.7: Specification of MLH-mat for PP/GF and PA6/GF grades

Grade	Unit MLH-mat		
	Areal density	Thickness	GF sublayers
PP/GF19 vol. % (40 wt. %)	1240 g/m ²	1.00 mm	165 g/m ² ×3 EA
PP/GF32 vol. % (57 wt. %)	1230 g/m ²	0.85 mm	141 g/m ² ×5 EA
PP/GF45 vol. % (70 wt. %)	1060 g/m ²	0.63 mm	149 g/m ² ×5 EA
PA6/GF19 vol. % (35 wt. %)	1270 g/m ²	0.90 mm	150 g/m ² ×3 EA
PA6/GF37 vol. % (58 wt. %)	1075 g/m ²	0.64 mm	156 g/m ² ×4 EA
PA6/GF42 vol. % (63 wt. %)	1145 g/m ²	0.65 mm	144 g/m ² ×5 EA
PA6/GF50 vol. % (70 wt. %)	1125 g/m ²	0.60 mm	157 g/m ² ×5 EA

Homogeneity of GF sublayers in areal density was verified by an indirect and simple manner, which starts with the step to measure each weight of unit MLH-mats cut to 338 mm width and 478 mm length. So, the coefficient of variation (CV) value on unit MLH-mat was calculated to be 0.9% for PP/GF32 vol. % (57 wt. %) and 1.2% for PP/GF45 vol. % (70 wt. %). Dividing CV values on unit MLH-mat by each GF weight percent is used to determine CV values on GF sublayers; based on the assumption that PP films are of a uniform areal density. Thus, their CV values on GF sublayers become 1.5% and 1.7% respectively, in an extremely narrow range.

Reproducibility was verified on PP/GF45 vol. % (70 wt. %) MLH-mat. The statistical comparison between the two production dates was done by single-factor ANOVA with 95% confidence level, and the P-value was 0.10; the CV value on GF sublayers of the other production is 2.9%. All the MLH-mats in Table 3.7 have been controlled not to exceed 5% in CV value on GF sublayers.

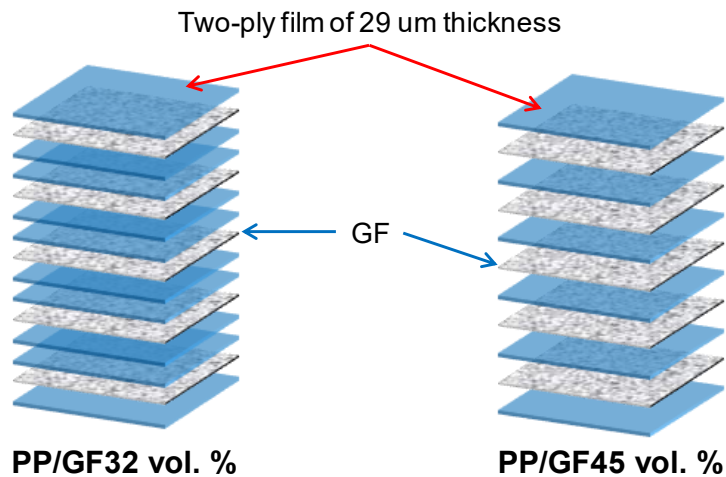


Figure 3.37: Configuration details: PP/GF32 vol. % (57 wt. %) and PP/GF45 vol. % (70 wt. %) using films of the same thickness

Each role of MLH-mats is as follows. PP/GF19 vol. % (40 wt. %) is assigned for direct comparison with conventional GMT materials. PP/GF45 vol. % (70 wt. %) is for the fiber volume content assumed to have it when being pressurized and impregnated at 30 bar pressure (refer to Figure 3.35); cf. although the exact value is 46 vol. %. Then, PP/GF32 vol. % (57 wt. %) is simply positioned at the midpoint between the two fiber volume percent. PA6/GF19 vol. % (35 wt. %) has the same fiber volume content with PP/GF19 vol. % (40 wt. %). PA6/GF42 vol. % (63 wt. %) is assumed to have the fiber volume content at 20 bar pressure. PA6/GF37 vol. % (58 wt. %) is positioned at the midpoint between 32 vol. % and 42 vol. %. However, PA6/GF50 vol. % (70 wt. %) is reserved to see what will happen beyond 45 vol. %. For a better understanding, all the positions are graphically marked in Figure 3.38.

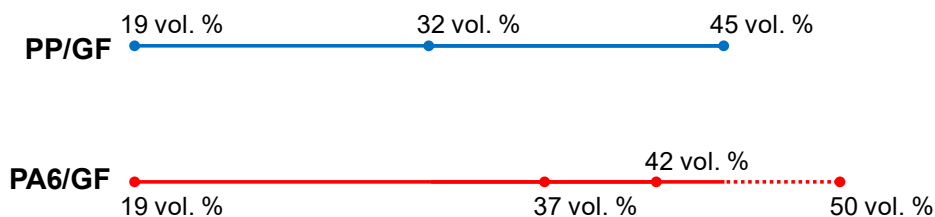


Figure 3.38: Fiber volume contents of MLH-mats (PP/GF and PA6/GF grades)

To make impregnated and consolidated plates, four to seven plies of unit MLH-mats, being cut to 338 mm by 478 mm, were placed into the compression mold (340 mm by 480 mm) already preheated at the given temperature⁹ like 200°C for PP/GF grades [133] or 250°C for PA6/GF grades [134]. The numbers of plies were predetermined to make consolidated plates of around 4 mm thickness as recommended in ISO 14125 for class II material (e.g. GMT, SMC, BMC, and DMC)¹⁰ [95]. Right after closing the mold, the compression pressure was applied for 5 min at 10 bar and continued for 5 min at 30 bar with maintaining the given temperature. This two-step pressurization is aimed to serve a mild impregnation condition. It allows the matrix resin to start melt at a relatively low pressure avoiding a heavy compaction. Then, the mold was cooled down to 40°C with 4°C/min rate, holding the compression pressure at 30 bar, in order to take the consolidated plate out of the mold.

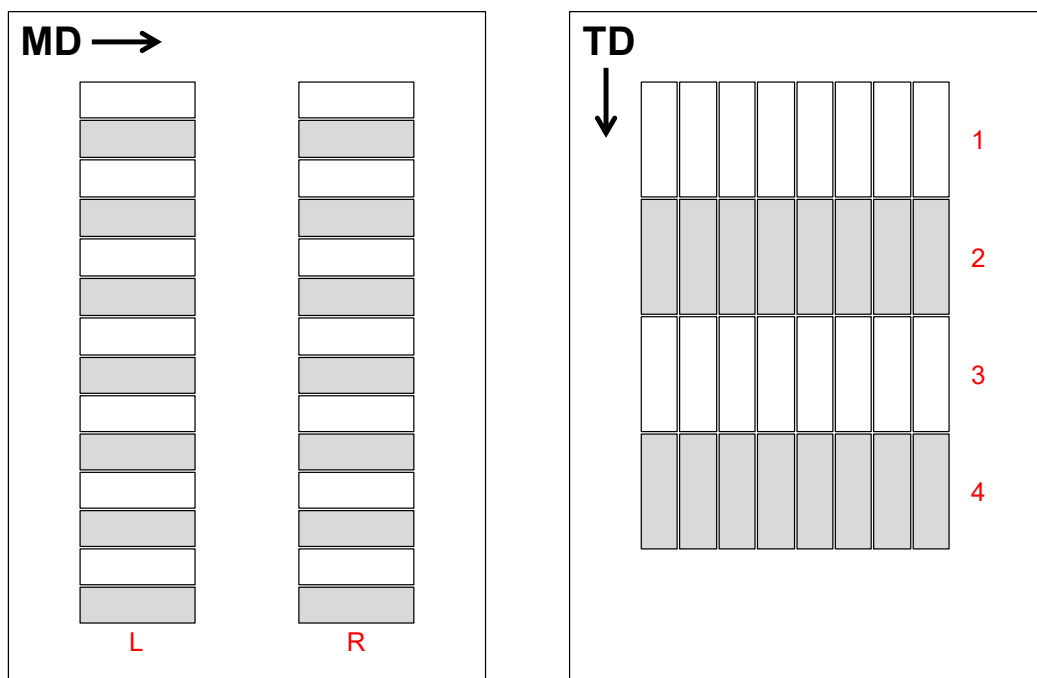


Figure 3.39: Sampling positions for bending tests along machine direction (MD) and transverse direction (TD)

⁹ The temperature was determined to be the lowest one at an interval of 10°C in the recommended range of 191 to 232°C for PP/GF grades or 245 to 280°C for PA6/GF grades, considering thermal stability.

¹⁰ Glass mat reinforced thermoplastic (GMT), Sheet molding compound (SMC), Bulk molding compound (BMC), and Dough molding compound (DMC)

Specimens for three-point bending tests were extracted out of each impregnated and consolidated plate, with the size of 25 mm width and 80 mm length as recommended in the standard test method. As depicted in Figure 3.39, the sampling positions in a plate were labeled as L and R along machine direction (MD), or 1, 2, 3, and 4 along transverse direction (TD). The position marked in gray and white corresponds to the classification for bending directions, upper side (P) and underside (D). The labels of test sets were summarized in Table 3.8, and each set consists of 7 or 8 specimens.

Table 3.8: Labels of test sets by sampling positions and bending directions

Machine direction (MD)	L	R		
Upper side (P)	LP	RP		
Underside (D)	LD	RD		
Transverse direction (TD)	1	2	3	4
Upper side (P)	1P	-	3P	-
Underside (D)	-	2D	-	4D

The bending test was performed with the speed of 1.5 mm/min which is as equivalent as possible to the strain rate of 0.01 min^{-1} on the outer surface of specimen. And the span length was 60 mm (16 times the specimen thickness). Using the load cell of 5 kN, the bending test continued within 3.8% strain limit that is valid for small deflection. In the same way described in Section 3.2.3, statistical procedures (outlier verification and single-factor ANOVA) were basically performed to determine the representative properties of all MLH-mats in Table 3.7.

3.3.4 Evaluation and characterization

MLH-mat of high fiber content

To verify the potentiality that MLH-mat could have higher GF contents and of course maintain a good impregnation quality, firstly PP/GF45 vol. % (70 wt. %) MLH-mat was evaluated through flexural properties. Figure 3.40 shows all the stress-strain curves associated with sampling positions and bending directions after outlier verification; a black curve of each test set is treated as the most representative one (refer to Table 3.8 for each label). Besides, the average values and CV values of each test set are summarized in Table 3.9, being 13.9–14.4 GPa in modulus, 212–218 MPa in strength, and 2.06%–2.19% in strain. The CV values of strain were much wider than the others.

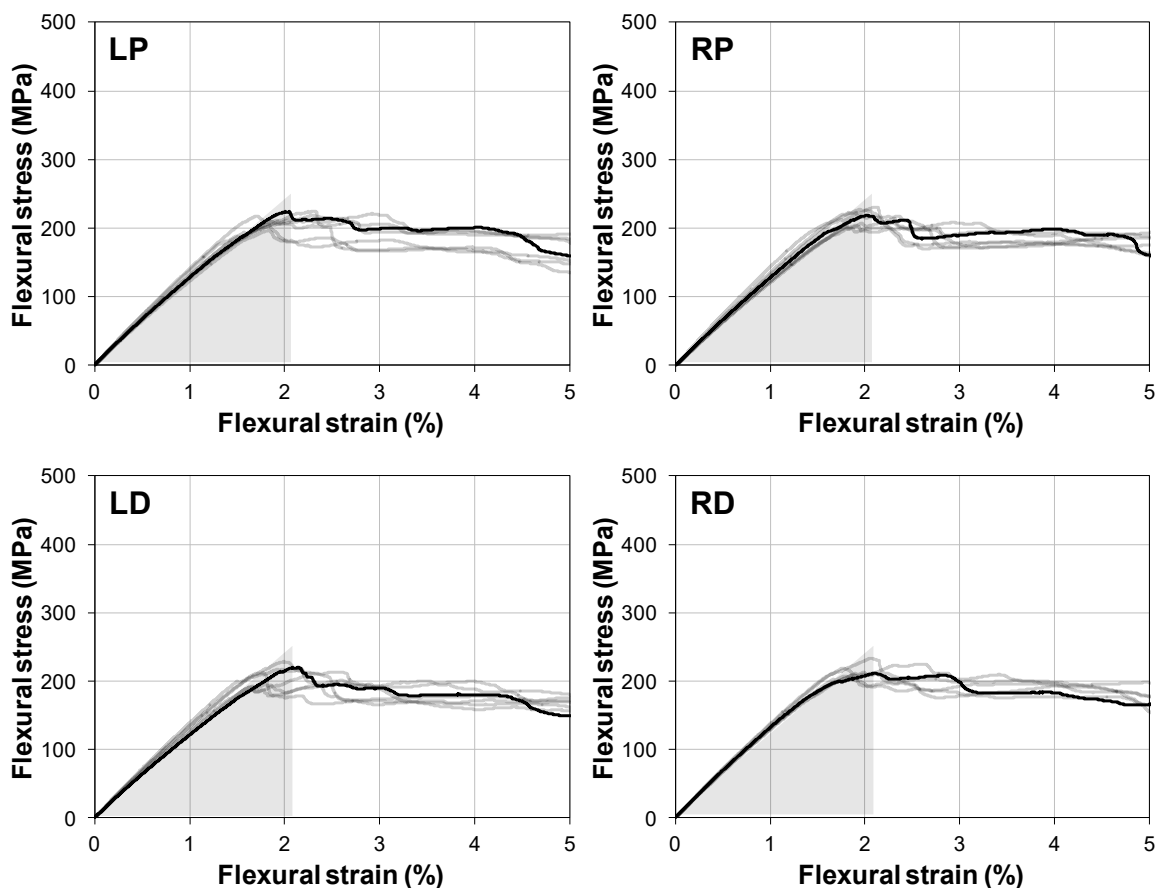


Figure 3.40: Flexural stress-strain curves of PP/GF45 vol. % (70 wt. %) MLH-mat

The representative flexural properties should be determined by statistical procedures as in the following. In the case of sampling positions, it is preferred to use two-factor ANOVA without replication and to perform on each bending direction separately, e.g. LP vs. RP and LD vs. RD. As shown in Table 3.10, all the P-values were above 0.05,

so that there is no significant difference in sampling positions with 95% confidence level. Thus, after merging into each bending direction, single-factor ANOVA was done between bending directions (upper side and underside); the P-values in Table 3.11 indicate that there is no significant difference between bending directions as well. The representative flexural properties of PP/GF45 vol. % (70 wt. %) MLH-mat, therefore, could be suggested after merging all the test sets, as 14.1 GPa in modulus, 215 MPa in strength, and 2.13% in strain. The flexural modulus of 14.1 GPa is a reasonable value despite being at 89% level of the theoretical value (15.8 GPa) calculated by the rule of mixtures for quasi-isotropic layup ($0^\circ/90^\circ/\pm 45^\circ$) of continuous fiber [21][22].

Table 3.9: Flexural properties of PP/GF45 vol. % (70 wt. %) MLH-mat

Flexural property	LP	RP	LD	RD
Modulus (GPa)	14.1	14.1	13.9	14.4
CV	(4.5%)	(6.0%)	(5.6%)	(2.6%)
Strength (MPa)	214	217	212	218
CV	(5.1%)	(5.2%)	(5.8%)	(4.3%)
Strain (%)	2.18	2.06	2.19	2.09
CV	(18%)	(8.6%)	(15%)	(14%)

Table 3.10: Two-factor ANOVA without replication on sampling positions

P-value	LP vs. RP	LD vs. RD
Flexural modulus	Inside: 0.68 / between: 0.93	Inside: 0.22 / between: 0.25
Flexural strength	Inside: 0.95 / between: 0.71	Inside: 0.12 / between: 0.17
Flexural strain	Inside: 0.42 / between: 0.45	Inside: 0.35 / between: 0.51

Table 3.11: Representative value: PP/GF45 vol. % (70 wt. %) MLH-mat

Representative	PP/GF45 vol. % (70 wt. %)	P-value
Flexural modulus	14.1 GPa (CV 4.8%)	0.96
Flexural strength	215 MPa (CV 5.0%)	0.92
Flexural strain	2.13% (CV 14%)	0.84

Isotropy check on MLH-mat

The isotropy check as a random directional fiber distribution was done on PA6/GF37 vol. % (58 wt. %) MLH-mat by a comparison of flexural properties between machine direction (MD) and transverse direction (TD); the test sets were LP, RP, LD, and RD along MD, and 1P, 3P, 2D, and 4D along TD (refer to Table 3.8 for each label). After statistical procedures up to single-factor ANOVA on bending directions, the flexural properties for MD and TD could be suggested respectively as summarized in Table 3.12 and Table 3.13. Moreover, all the CV values were quite narrow. The P-values in Table 3.14 by single-factor ANOVA with 95% confidence level mean that there is no significant difference between MD and TD. The direction MD and TD are regarded as having the biggest difference. So, PA6/GF37 vol. % (58 wt. %) MLH-mat is isotropic enough not to check again for other directions such as $\pm 45^\circ$.

Table 3.12: Machine direction after single-factor ANOVA on bending directions

Machine direction (MD)	PA6/GF37 vol. % (58 wt. %)	P-value
Flexural modulus	13.9 GPa (CV 4.2%)	0.13
Flexural strength	372 MPa (CV 3.8%)	0.24
Flexural strain	3.22% (CV 4.5%)	0.29

Table 3.13: Transverse direction after single-factor ANOVA on bending directions

Transverse direction (TD)	PA6/GF37 vol. % (58 wt. %)	P-value
Flexural modulus	13.5 GPa (CV 4.4%)	0.15
Flexural strength	368 MPa (CV 3.7%)	0.91
Flexural strain	3.30% (CV 5.2%)	0.49

Table 3.14: Representative value: PA6/GF37 vol. % (58 wt. %) MLH-mat

Representative	PA6/GF37 vol. % (58 wt. %)	P-value
Flexural modulus	13.6 GPa (CV 4.4%)	0.13
Flexural strength	369 MPa (CV 3.8%)	0.36
Flexural strain	3.26% (CV 5.0%)	0.05

The representative flexural properties of PA6/GF37 vol. % (58 wt. %) MLH-mat could be suggested as 13.6 GPa in modulus, 369 MPa in strength, and 3.26% in strain by merging MD and TD; very similar stress-strain curves as shown in Figure 3.41. The flexural modulus is at 93% level of the theoretical value (14.6 GPa); it is a better level compared to 89% level of PP/GF45 vol. % (70 wt. %) MLH-mat.

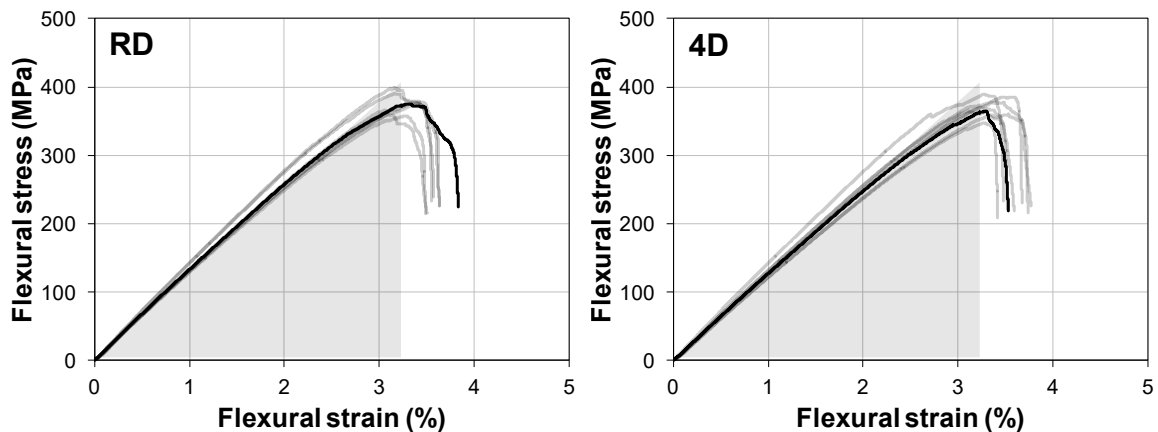


Figure 3.41: Flexural stress-strain curves of PA6/GF37 vol. % (58 wt. %) MLH-mat

Longer strain of PA6/GF grade

The two MLH-mats, PP/GF45 vol. % (70 wt. %) and PA6/GF37 vol. % (58 wt. %), are equivalent in density (1.68 g/cm^3) and employing the same grade of GF (Advantex[®] boron-free ECR grade of Owens Corning) that is just different in chemical sizing for each matrix polymer; there are no significant differences in mechanical properties¹¹ between PP and PA6 matrix polymers [23][135] compared with those of GF [24]. Their flexural stress-strain behaviors are quite different as compared in Figure 3.42. Although having the similar values in flexural modulus, PA6/GF37 vol. % (58 wt. %) MLH-mat continues 1.53 times longer than PP/GF45 vol. % (70 wt. %) MLH-mat in flexural strain. After reaching flexural strengths (maximum stress), the PA6/GF MLH-mat shows a sudden drop in stress, whereas PP/GF MLH-mat shows a long lasting stress. From another point of view, the persistence (or bias) degree of the PA6/GF MLH-mat is calculated (refer to Figure 3.23 in Section 3.2.4) to be 83% that is

¹¹ The values of tensile modulus are 1.72 GPa for PP, 2.76 GPa for PA6, and 80.5 GPa for GF. The values of tensile strength are 32 MPa for PP, 76 MPa for PA6, and 3450 MPa for GF.

somewhat higher than 72% of the PP/GF MLH-mat. Basically, persistence degree is a function of fiber orientation affecting stress-to-strain ratio; cf. as for the unbalanced (2/1) woven fabric made of PP/GF45 vol. % (70 wt. %) MLH-roving, it was 95% for major direction (see Section 3.2.4) and 71% to 92% for minor direction (see Section 3.2.5). Anyhow, PA6/GF37 vol. % (58 wt. %) MLH-mat is 1.72 times the flexural strength of PP/GF45 vol. % (70 wt. %) MLH-mat, which is caused by longer flexural strain as well as by higher persistence degree. Practically, it implies that the PA6/GF MLH-mat can provide high chances of light weight over 40% where flexural strength is a dominant point.

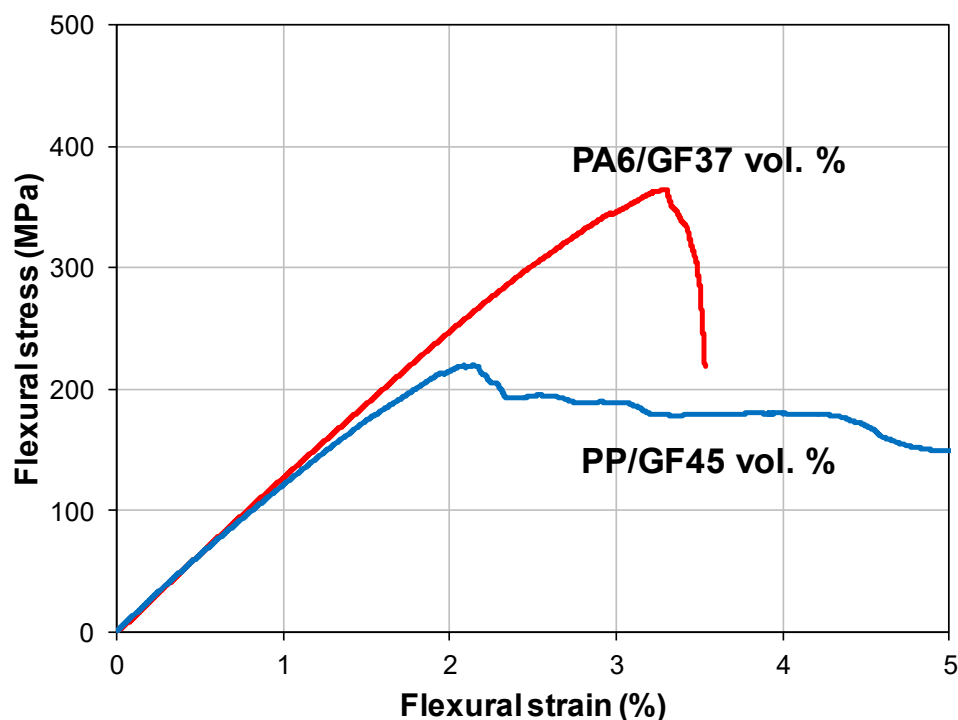


Figure 3.42: Comparison of flexural stress-strain curve between PP/GF45 vol. % (70 wt. %) and PA6/GF37 vol. % (58 wt. %)

PP/GF MLH-mat vs. PA6/GF MLH-mat

As summarized in Table 3.15 to Table 3.19, the representative values on five more MLH-mats could be suggested with P-values after statistical procedures up to single-factor ANOVA on bending directions. It is obvious that all the stress-strain curves in Figure 3.43 follow the same behaviors characterized in Figure 3.42 as a long lasting stress for PP/GF MLH-mat and a sudden drop in stress for PA6/GF MHL-mat. When compared at the same fiber content of 19 vol. %, the PA6/GF MLH-mat has a longer flexural strain than the PP/GF MLH-mat despite having the same level of modulus.

Table 3.15: Representative value: PP/GF19 vol. % (40 wt. %) MLH-mat

Representative	PP/GF19 vol. % (40 wt. %)	P-value
Flexural modulus	7.0 GPa (CV 8.3%)	0.66
Flexural strength	174 MPa (CV 8.8%)	0.16
Flexural strain	3.47% (CV 8.9%)	0.51

Table 3.16: Representative value: PP/GF32 vol. % (57 wt. %) MLH-mat

Representative	PP/GF32 vol. % (57 wt. %)	P-value
Flexural modulus	10.1 GPa (CV 5.0%)	0.97
Flexural strength	210 MPa (CV 4.8%)	0.23
Flexural strain	2.91% (CV 13%)	0.75

Table 3.17: Representative value: PA6/GF19 vol. % (35 wt. %) MLH-mat

Representative	PA6/GF19 vol. % (35 wt. %)	P-value
Flexural modulus	7.2 GPa (CV 8.5%)	0.94
Flexural strength	227 MPa (CV 7.3%)	0.09
Flexural strain	3.91% (CV 5.4%)	0.52

Table 3.18: Representative value: PA6/GF42 vol. % (63 wt. %) MLH-mat

Representative	PA6/GF42 vol. % (63 wt. %)	P-value
Flexural modulus	14.9 GPa (CV 5.9%)	0.98
Flexural strength	373 MPa (CV 5.9%)	0.80
Flexural strain	3.08% (CV 9.3%)	0.82

Table 3.19: Representative value: PA6/GF50 vol. % (70 wt. %) MLH-mat

Representative	PA6/GF50 vol. % (70 wt. %)	P-value
Flexural modulus	17.8 GPa (CV 5.1%)	0.35
Flexural strength	328 MPa (CV 5.5%)	0.11
Flexural strain	2.48% (CV 10%)	0.23

The other set of MLH-mats shows that the PA6/GF MLH-mat is about 1.68 times the flexural strength of the PP/GF MLH-mat if having the same level of flexural strain. So, to figure out the general tendencies of flexural modulus and flexural strain with fiber volume content, the values are depicted and fitted by linear least squares, separately for PP/GF MLH-mats and PA6/GF MLH-mats. But, the PA6/GF50 vol. % (70 wt. %) MLH-mat was excluded as it resulted in a lower flexural strength than expected. It is somewhat predicted in Section 3.3.2 that a fiber content beyond 46 vol. % might be inadequate to the impregnation at 30 bar pressure (cf. 42 vol. % at 20 bar pressure).

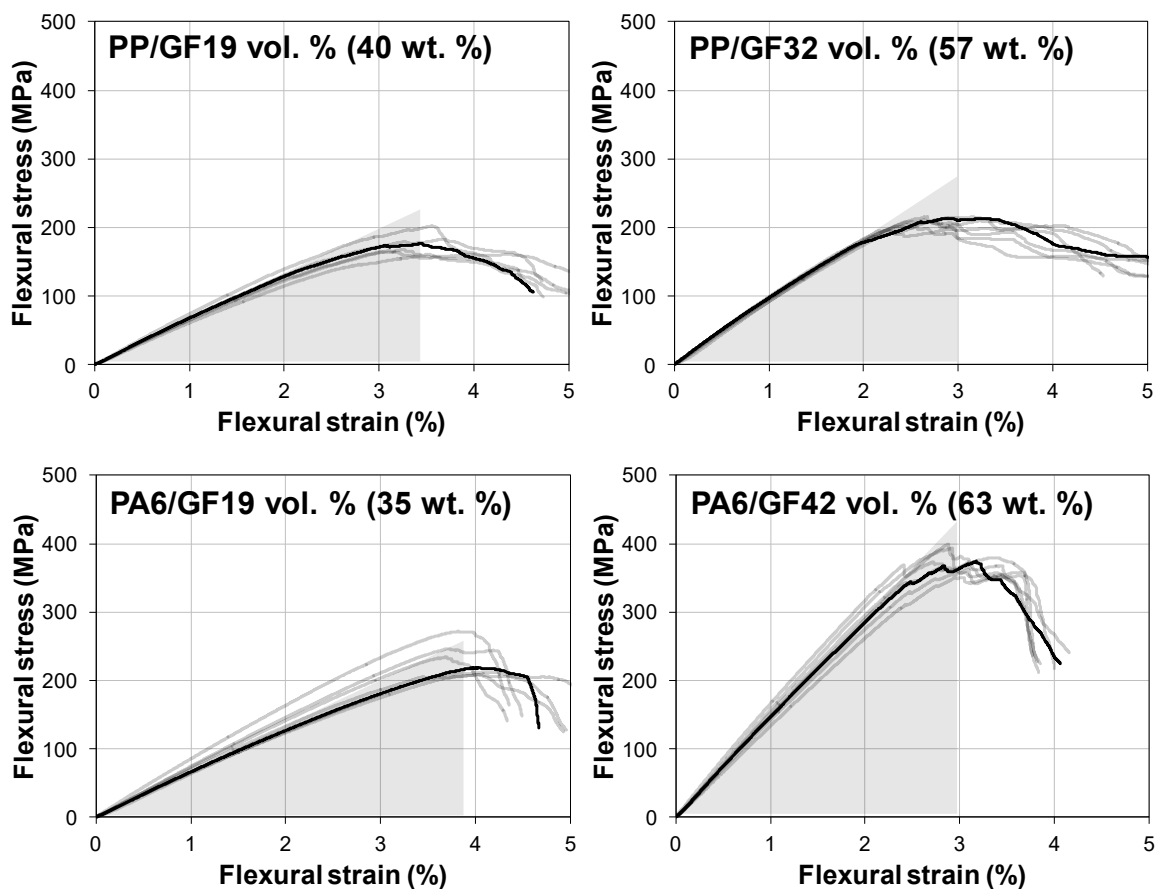


Figure 3.43: Flexural stress-strain curves of PP/GF and PA6/GF MLH-mats

Each linear trend-line has a good coefficient of determination (R^2) as shown in Figure 3.44 and Figure 3.45, being over 0.97. Naturally, flexural modulus increases with fiber volume content according to the rule of mixtures, with almost the same slope from each modulus of matrix polymer (y-intercept). Meanwhile, flexural strain decreases from a flexural strain (y-intercept), e.g. 4.5%, but with different slopes. The PA6/GF MLH-mats show a gentle slope of 64% level, compared to the PP/GF MLH-mats.

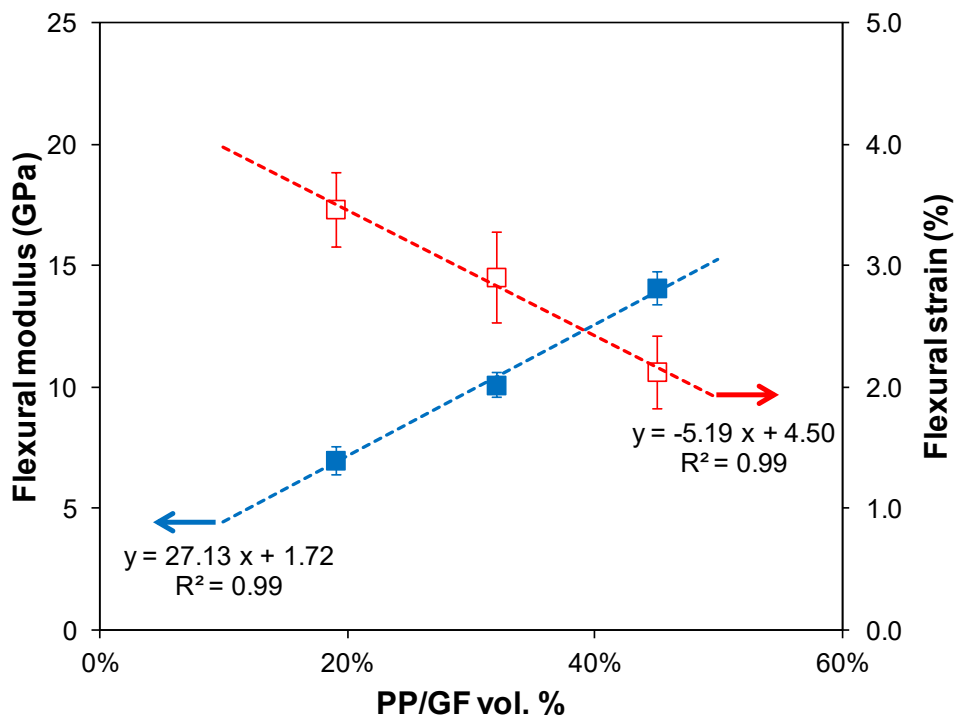


Figure 3.44: Tendency of modulus and flexural strain for PP/GF MLH-mats

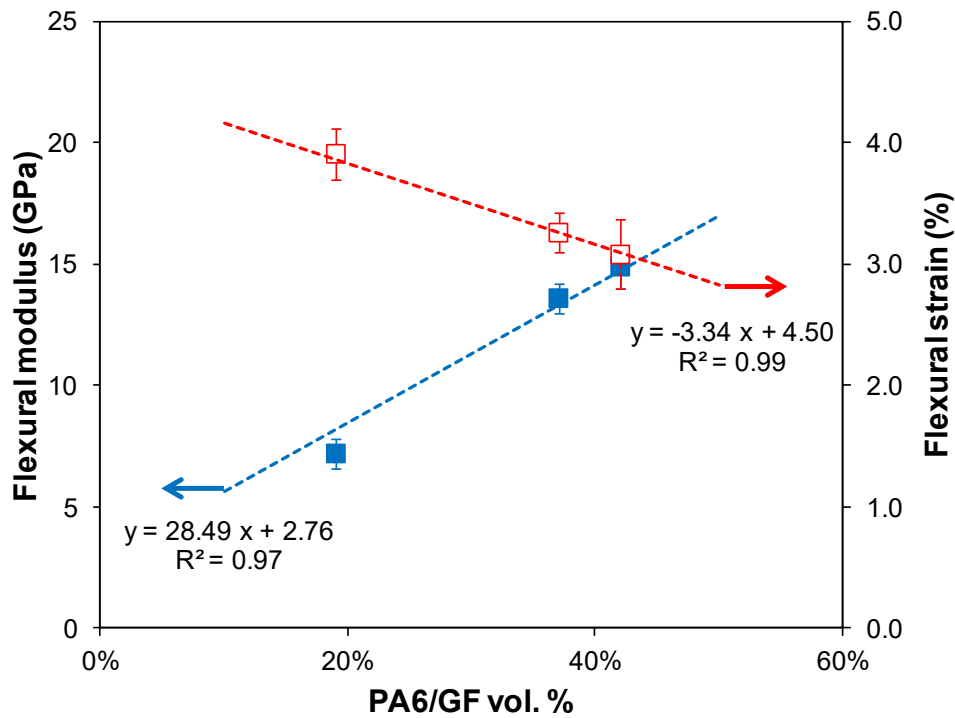


Figure 3.45: Tendency of modulus and flexural strain for PA6/GF MLH-mats

Normally, flexural strain is directly proportional to adhesive properties between matrix polymer and glass fiber against shear deformation, and inversely proportional to fiber volume content. And it is influenced by fiber orientation and fiber discontinuity (or fiber length) with the result that the PA6/GF MLH-mats show the persistence degree of 82% with a very narrow CV of 1.7%, being higher than 72% (almost constant) of the PP/GF MLH-mats. So, the characteristic persistence degree implies that flexural strength increases linearly with fiber volume content.

Reheating stability

MLH-mats, conventional GMT materials, and consolidated plates of continuous fiber reinforcement should be reheated in an oven for thermoforming or hybrid molding a component. A lot of effort has gone into preventing or delaying thermal decomposition of resin, ranging from process condition in oven to chemical additives like antioxidant in resin. However, swelling a kind of physical phenomenon came to the fore as the serious problem in LFT materials, especially GMT and LFT-D; the longer the fiber length and the higher the fiber content, basically the more serious the swelling.

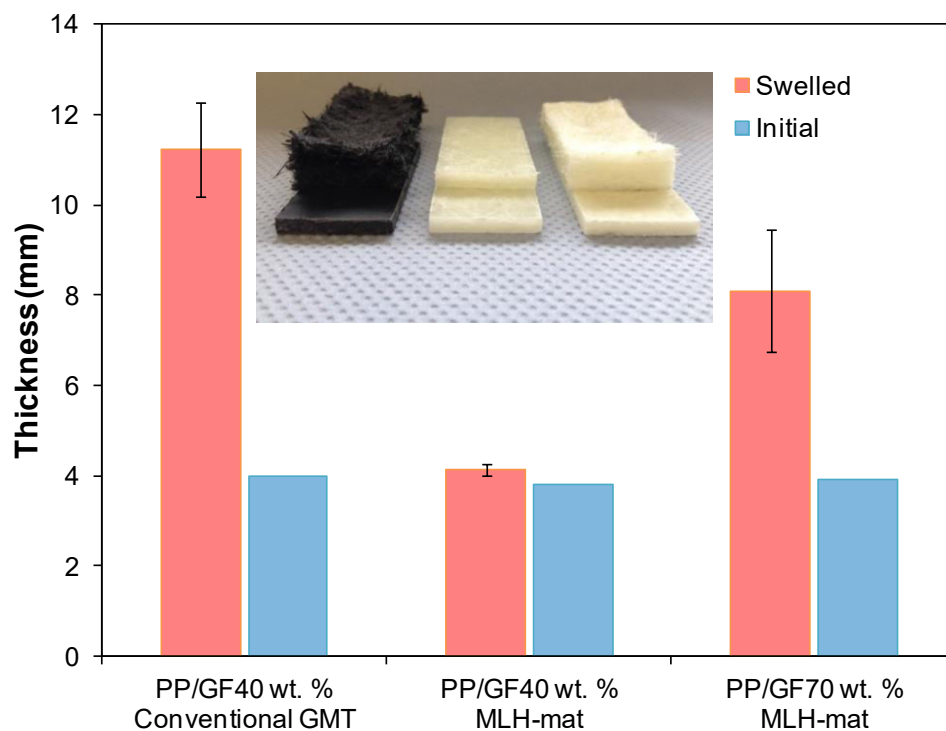


Figure 3.46: Comparison of reheating stability in oven by a degree of swelling

The swelling during heating leads to a material of higher surface area only to result in a smoking and burning material eventually, or at least too much air inside to produce

a good surface quality without any silver streaks in a component. The swelling test was done by heating at 220°C for 5 min and immediately quenched in a cold water bath; the specimens before and after tests are shown as the stacked ones at bottom and top sides, respectively with the graph (see Figure 3.46). The MLH-mats showed little swelling at 40 wt. % compared to the conventional GMT material and even less swelling at 70 wt. %. MLH-mats have excellent reheating stability.

4 Crash Application

On the materials newly developed and verified in Chapter 3, the crash behavior and performance will be investigated by dynamic crash test imposing a given amount of impact energy at once. By taking into account the matters that crash test specimens have not yet been standardized, the present work is obliged to adopt one of the most widely used shapes, named a welded round-hat tube for the evaluation of material itself. Actually, the test specimens of any shapes tend to pursue real components as far as possible, but are often faced with a difficulty in formability. This is the reason why there have been so many shapes of test specimens that are customized case by case [136][137], nevertheless those are somewhat different with real components.

This chapter focuses on the crash behavior and performance, especially of the long fiber reinforced PP/GF and PA6/GF materials which have high GF contents of around 45 vol. %. These materials are, of course, compared with the woven fabric of PP/GF material that is reinforced with the same amount of continuous fiber, in order to define what the main differences are in crash behavior and performance. Because there is at least no need of weaving or placement (tape-laying) process, long fiber reinforced thermoplastic materials are basically better in cost aspects. Moreover, their inherent flowability could help give the design flexibility (or formability) such as variations of wall thickness, ribs for design stiffness, and insert-molding for simple assembly. The crash behavior is being described here in detail as the mode of ‘splaying and lamina-bending followed by inside-wrinkling and outside-tearing’, which was categorized as splaying mode by Hamada et al. (or lamina-bending by Farley et al.). Above all, the distinct difference in the crushed features between continuous fiber- and long fiber reinforced thermoplastic materials will serve as a sensible guideline on how to obtain the best crash performance.

4.1 Dynamic Crash Test

4.1.1 Specimen preparation

The test specimens are the shape of a welded round-hat tube, and the geometry is depicted in Figure 4.1. A sufficient width of linear flange is required occasionally as a way to prevent undesirable failures in the welding zones during crash test, but brings

about a negative influence on the value of specific energy absorption (SEA) in some degree [92][93]; the SEA gets lower as the width of linear flanges is wider. The linear flanges of 20 mm width take up a significant proportion in the test specimen, 33% in area or 20% in length which is simply calculated on the cross-section perpendicular to the direction of crash test; here the length is closely related to the crash behavior of splaying, and the area is to the other behaviors depicted in Figure 4.7 (Section 4.2).

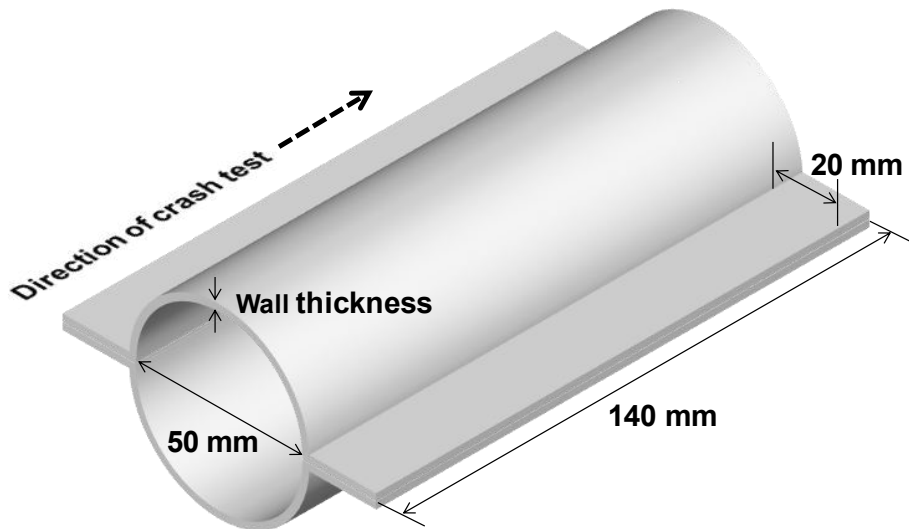


Figure 4.1: Geometry of test specimen (welded round-hat tube)

The test specimens were manufactured through the procedures [92][93][94] (see Figure 4.2) from thermoforming to vibration welding processes with fully impregnated and consolidated plates of 340 mm by 480 mm size. The procedure of preparing the plates is the same with of Section 3.3.3, except the numbers of plies (4 mm thickness for bending test, but 2.0–2.5 mm for crash test).

Step 1 to 3: A consolidated plate is fastened to the sledge frame with several tension coil-springs, and put into the infrared (IR) heating zone with a thermocouple inserted at a side of the plate in order to measure the temperature change.

Step 4 and 5: After reaching a given temperature and holding time, the plate having reached a thermoformable state is quickly conveyed by the sledge frame and placed on the mold for the next step of compression molding.

Step 6: The thermoformed sheet is cut to the given dimension as a set of two halves starting from the center of the plate as far as possible.

Step 7: The vibration welding process is carried out between the faced linear-flanges of two halves through the small amplitude of 1.20 mm and the high frequency of 240 Hz under the load of 12 kN, until reaching the welding depth of 0.50 mm.

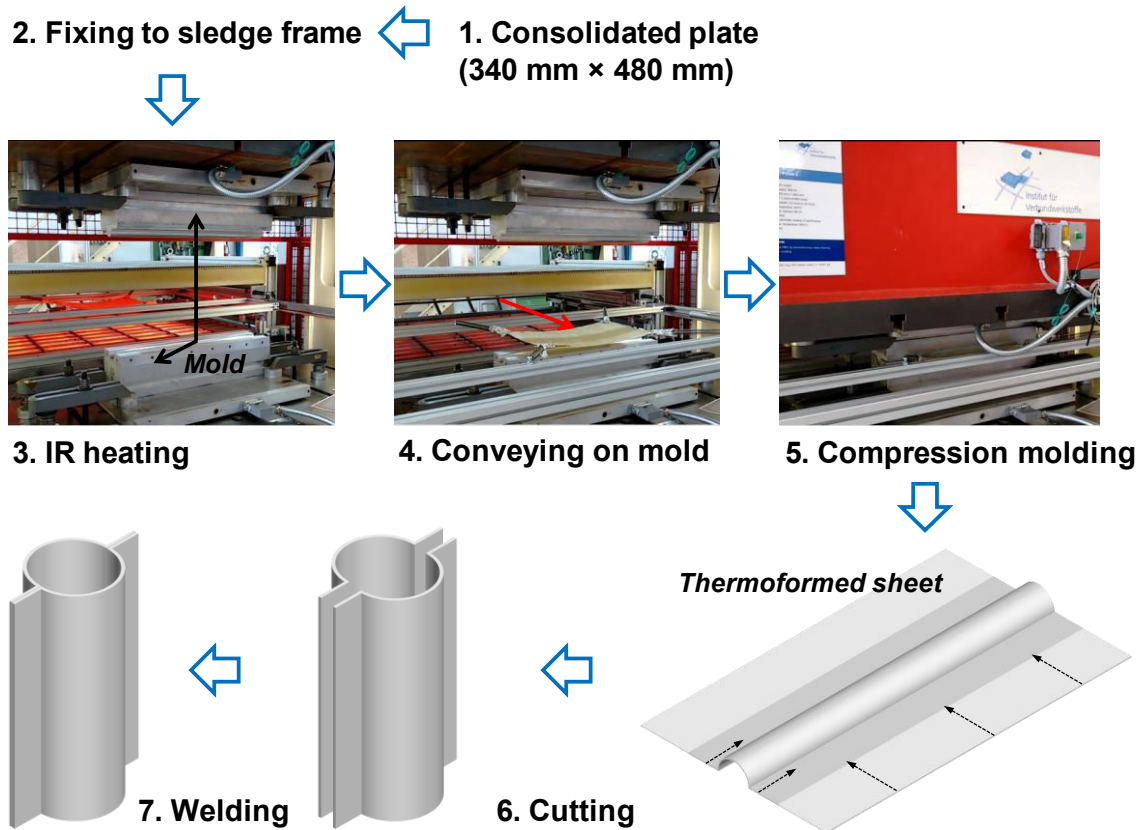


Figure 4.2: Manufacturing procedures for test specimen (welded round-hat tube)

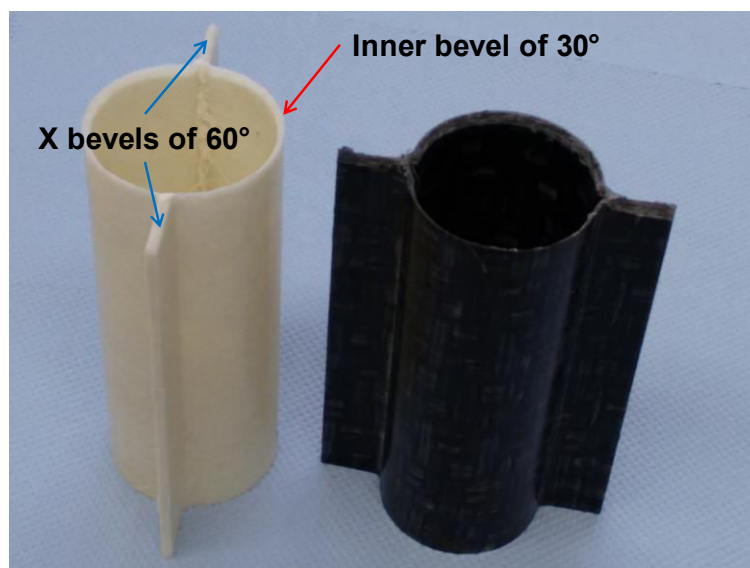


Figure 4.3: Trigger with inner and X bevels at one end of a test specimen

Finally, the trigger is created only at one end of a test specimen as shown in Figure 4.3, with one inner bevel of 30° along the circumference and two X bevels of 60° on the linear flanges. Trigger aims to initiate a stable and progressive failure developed from highly stressed regions where compressive resistance is relatively lower. Thus, trigger can avoid any undesirable failures such as mid-length collapse or local tube-wall buckling [67][138][139][140]. The proportion of trigger in the specimens is small enough not to influence on the value of SEA. It takes 1.3%–1.6% in volume or weight when calculated with a specimen that has a wall thickness in the range of 2.0–2.5 mm and the length of 140 mm. In spite of creating triggers, the weakest point of the test specimens is the zones made by vibration welding of a welded round-hat tube. Table 4.1 shows the information about the test specimens for crash tests to overview each code and material classification.

Table 4.1: Overview of test specimens

Specimen code	Material classification	Description
PP-70fM-1, 2, 3, 4	MLH-roving PP/GF4 vol. % (70 wt. %)	Major direction (warp) Section 4.2
PP-70fm-1, 2, 3, 4	MLH-roving PP/GF4 vol. % (70 wt. %)	Minor direction (weft) Section 4.2
PP-70-1, 2, 3, 4	MLH-mat PP/GF45 vol. % (70 wt. %)	Section 4.3
PP-70H-1, 2, 3, 4	MLH-mat and MLH-roving PP/GF45 vol. % (70 wt. %)	Alternately layered Section 4.3
PA-70-1, 2, 3, E	MLH-mat PA6/GF50 vol. % (70 wt. %)	E: lower impact velocity Section 4.4
PA-63-1, 2, 3, 4	MLH-mat PA6/GF42 vol. % (63 wt. %)	Section 4.4

4.1.2 Test and evaluation method

The dynamic crash tests were conducted by the test rig [92][93][94][141], of which the mass was fixed at 61 kg whereas the impact velocity was set in accordance with the level of crashworthiness; like 8.3 m/s or 9.5 m/s imposing the kinetic energy of 2.1 kJ or 2.7 kJ. In contrast to quasi-static test, the crushing speed in dynamic crash test decreases spontaneously as the test specimen dissipates the impact energy, from a given impact velocity to rest. This implies that more attention needs to be paid to the sensitivity of materials to strain rate. Also, as shown in Figure 4.4, there is a kind of elastic spring-back just after the zero speed at the maximum displacement. To fulfill the behavior of stable and progressive crushing, the load-displacement curve should be of tiny fluctuation while maintaining a constant load level until maximum displacement as far as possible [4]. Namely, the ideal curve resembles the shape of a rectangle [142] as marked in Figure 4.4.

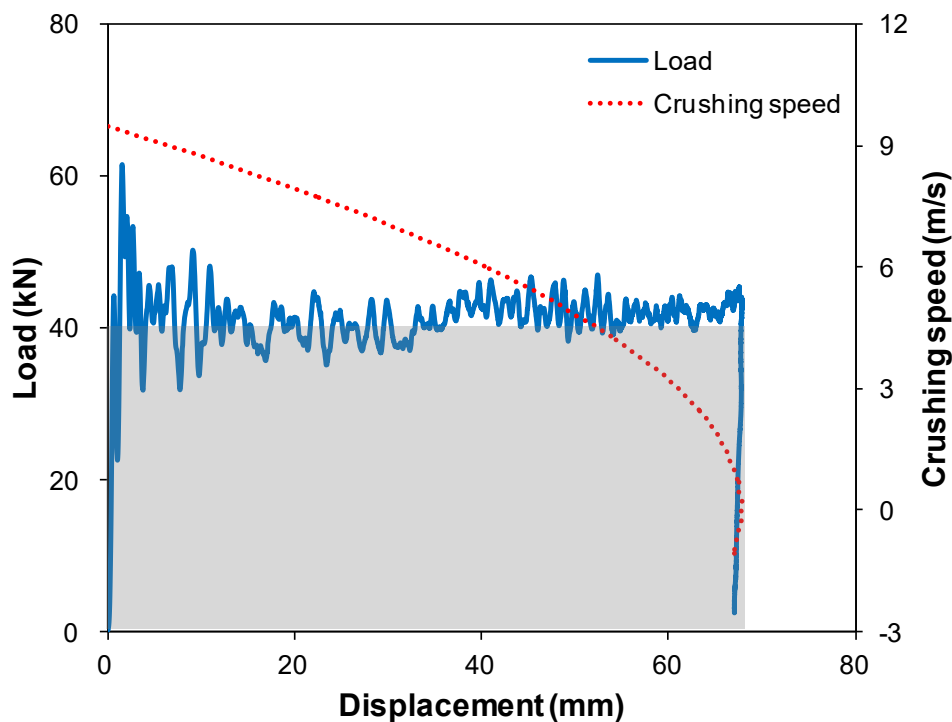


Figure 4.4: Load-displacement and crushing speed in dynamic crash test

The area of a rectangle is equivalent to the applied impact energy, and its height can be interpreted into the mean load. Also, the load uniformity is defined as the ratio of the maximum load to the mean load, which can be used to indicate the risk on overall structure that is normally caused by a sudden delivery of too much force at the initial

stage of crushing [5][75]. The most practical index SEA has the unit of J/g, and it is defined as the ratio of the applied impact energy to the crushed mass of material in the following equation.

$$SEA = \frac{E}{\rho \int_0^{\delta} A(l) dl} \quad (4.1)$$

Where:

- E is the applied impact energy as a form of kinetic energy that is calculated by the given mass and the impact velocity;
- ρ is the density of the test specimen;
- δ is the maximum displacement;
- $A(l)$ is the function of the cross-sectional area that is perpendicular to the length of test specimen (same to the direction of crash test).

SEA can be simplified if the function of the cross-sectional area is constant, into the applied impact energy (E) divided by the weight (W) of the test specimen and the ratio of the maximum displacement (δ) to the length (L) of the test specimen.

$$SEA = \frac{E}{\rho A \int_0^{\delta} dl} = \frac{E}{\rho A \delta} = \frac{E}{\rho AL \cdot \left(\frac{\delta}{L}\right)} = \frac{E}{W \cdot \left(\frac{\delta}{L}\right)} \quad (4.2)$$

Sometimes the volumetric energy absorption (VEA), with the unit of J/cm³, can be used more effectively for the comparison of crashworthiness apart from density effect. It is simply calculated by multiplying the specimen density to SEA, and it must be a critical index to volume-limited applications as well. For example, the result of quasi-static tests between PEEK/CF (AS4 carbon fiber) and PEEK/GF (S2 glass fiber) drew a practical conclusion that PEEK/CF showed 20% higher SEA than PEEK/GF [143]. But it becomes merely 3% enhancement in VEA. Therefore, this result implies that the performance of PEEK/CF is primarily related to the lower density of carbon fiber rather than to any other benefits in crash behavior.

4.2 Woven Fabric of PP/GF

First of all, the crashworthiness was investigated on the continuous fiber reinforced PP/GF45 vol. % (70 wt. %) material of unbalanced (2/1) woven fabric that is made of MLH-roving. According to the direction of the weaving pattern, it was classed into two kinds of specimen groups and labeled as PP-70fM and PP-70fm respectively. Each direction of crash test is the same with major direction (warp) of double reinforcement or minor direction (weft); refer to Figure 3.11 in Section 3.2.1.

The test specimens were prepared with four plies of unbalanced (2/1) woven fabrics to have a wall thickness of 2.4 mm; if fully impregnated and consolidated, the plate thicknesses are multiples of 0.6 mm. Upon the two specimen groups, the dynamic crash tests were conducted with the impact velocity of 8.3 m/s imposing a kinetic energy of 2.1 kJ. The load-displacement curves were very close to the ideal one of rectangular shape regardless of specimen groups as plotted in Figure 4.5 and Figure 4.6. The crashworthiness of PP-70fM (major direction) is summarized in Table 4.2 with the representative values, such as 43 J/g for SEA, 72 J/cm³ for VEA and 65 MPa for mean stress. In the case of PP-70fm, those are 40 J/g for SEA, 66 J/cm³ for VEA and 61 MPa for mean stress (see Table 4.3); the test specimen of No. 4 split into two halves owing to a poor but unpredictable welding property between the faced linear-flanges, and marked as 'Weld NG'.

The statistical comparison, based on single-factor ANOVA with 95% confidence level, tells that PP-70fM for major direction has higher representative values than PP-70fm for minor direction; namely, there is 7.5% drop of SEA in minor direction compared to major direction. This drop might be deeply related to the relatively weak compressive stiffness normally brought about by an insufficient wall thickness [8][88][89][90] or by an unsuitable fiber orientation [5][8][86][87]; cf. the drops of SEA in quasi-static test that are caused by an unsuitable fiber orientation (like $\pm 45^\circ$ to crash direction) were 31% (specimen V vs. VI) [5], 27% (specimen No. 36 vs. 29) or 18% (specimen No. 59 vs. 58) [8], and 29% (batch No. 07 vs. 09) or 8.9% (batch No. 01 vs. 06) [86][87].

Accordingly, the crashworthiness in unbalanced (2/1) woven fabric made of PP/GF45 vol. % (70 wt. %) MLH-roving might be affected by the direction, so that it results in a somewhat higher value along the major direction of double reinforcement. However, the representative values and the load-displacement curves are insufficient to explain concretely why this drop is happening and to characterize all the behaviors.

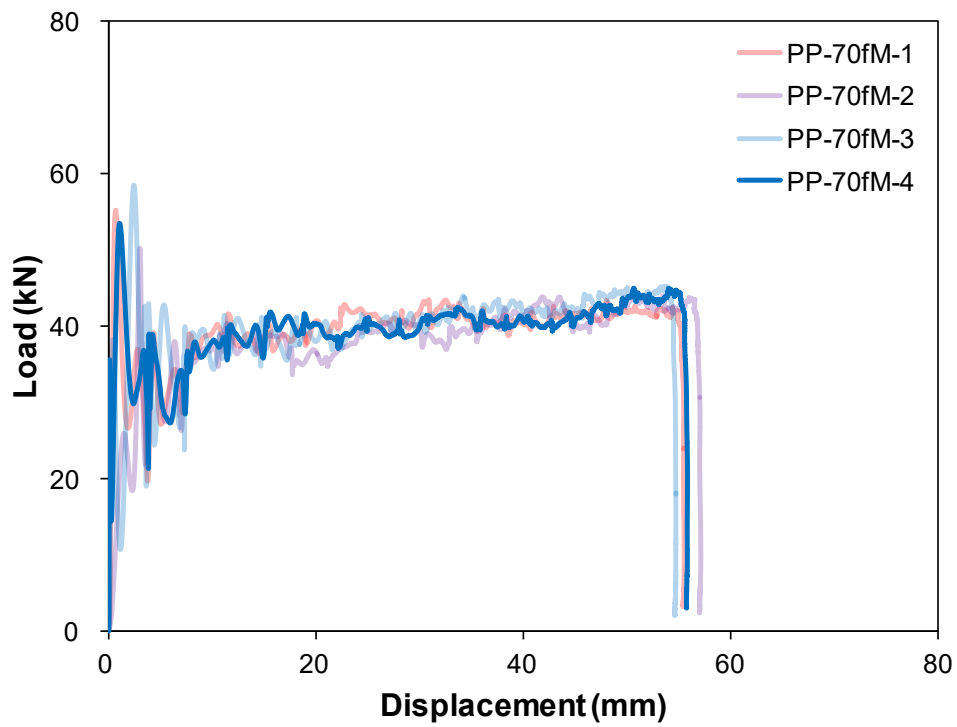


Figure 4.5: Load-displacement of PP-70fM; major direction of unbalanced (2/1) woven fabric made of PP/GF45 vol. % (70 wt. %) MLH-roving

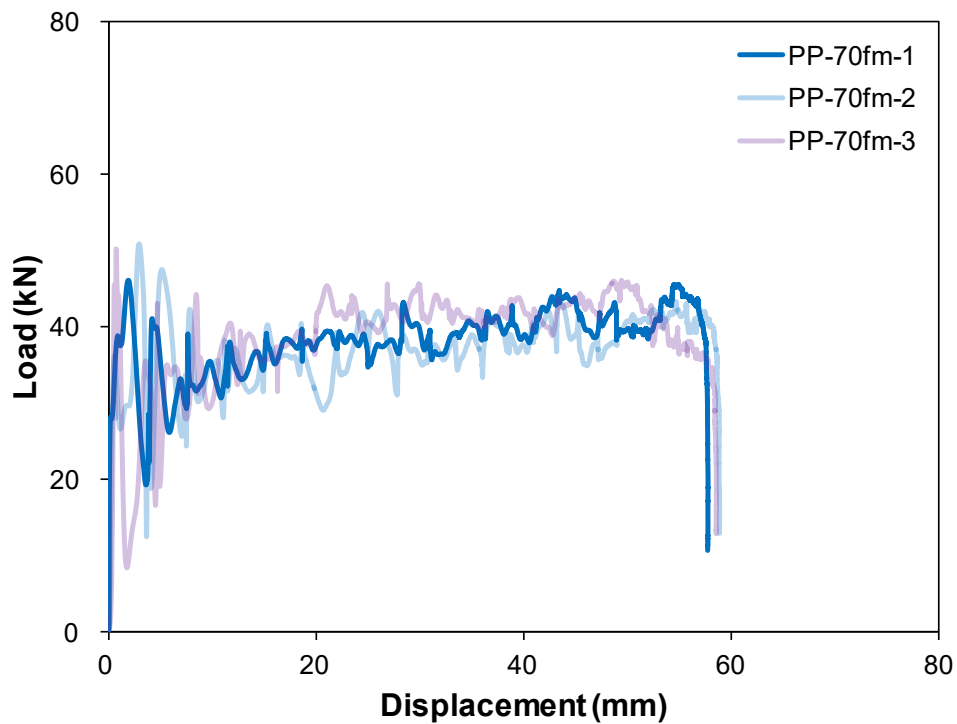


Figure 4.6: Load-displacement of PP-70fm; minor direction of unbalanced (2/1) woven fabric made of PP/GF45 vol. % (70 wt. %) MLH-roving

Table 4.2: Crashworthiness of PP-70fM: major direction of unbalanced (2/1) woven fabric made of PP/GF45 vol. % (70 wt. %) MLH-roving

PP-70fM	Average	No. 1	No. 2	No. 3	No. 4
Velocity (m/s)		8.31	8.32	8.29	8.33
Applied energy (J)		2111	2116	2101	2121
Specimen weight (g)		123.8	123.3	123.9	123.1
Displacement (mm)		55.49	57.03	54.72	55.78
Mean stress(MPa)	64.5	64.8	63.2	65.4	64.8
Load uniformity	1.43	1.45	1.35	1.52	1.41
SEA (J/g)	42.9	43.0	42.1	43.4	43.2
VEA (J/cm ³)	71.7	71.8	70.4	72.4	72.2
Remark		OK	OK	OK	OK

Table 4.3: Crashworthiness of PP-70fm; minor direction of unbalanced (2/1) woven fabric made of PP/GF45 vol. % (70 wt. %) MLH-roving

PP-70fm	Average	No. 1	No. 2	No. 3	No. 4
Velocity (m/s)		8.28	8.22	8.28	8.25
Applied energy (J)		2096	2066	2096	2081
Specimen weight (g)		125.1	125.4	127.1	123.8
Displacement (mm)		57.76	58.85	58.55	94.64
Mean stress(MPa)	60.9	61.8	59.8	61.0	-
Load uniformity	1.37	1.27	1.44	1.40	-
SEA (J/g)	39.7	40.6	39.2	39.4	-
VEA (J/cm ³)	66.4	67.8	65.4	65.8	-
Remark		OK	OK	OK	Weld NG

The crash behavior of brittle fiber reinforced thermoplastic material can be described in more detail, see Figure 4.7, as the mode of 'splaying and lamina-bending followed by inside-wrinkling and outside-tearing'. Just after a crushing down of trigger portion, splaying starts out as the wall splitting into two parts of inward and outward laminas

near the middle of wall thickness [5][94]. By frictional sliding at the crushing plate, these laminae continue the lamina-bending with a curling down accompanying intra and inter lamina cracks. However, the additional features of inside-wrinkling and outside-tearing occur by wall curvatures of test specimen. This is the major reason why cylindrical tubes return higher values in crashworthiness than hexagonal, square and rectangular tubes showing the entire tearing at each corner [69][70]. Furthermore, the crashworthiness becomes higher as the radius of curvature is smaller; e.g. the dynamic crash test on cylindrical tubes made of Epoxy/CF woven fabric showed 17% enhancement in SEA, from 65 J/g for 80 mm diameter to 76 J/g for 50 mm diameter [91]. Consequently, a crash performance is a result of the complex interaction among compressive, interfacial, frictional, flexural and tensile properties involved to dissipate a given impact energy.

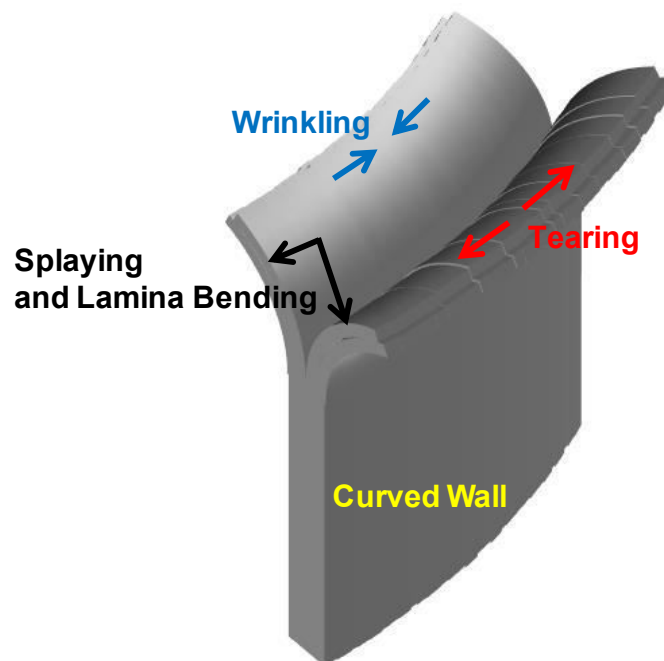


Figure 4.7: Crash behavior of brittle fiber reinforced thermoplastic materials as the mode of 'splaying and lamina-bending followed by inside-wrinkling and outside-tearing' [74][132]

As shown in Figure 4.8 and Figure 4.9, PP-70fM for major direction fulfills completely the crash behavior mentioned as the mode of 'splaying and lamina-bending followed by inside-wrinkling and outside-tearing'; an outside-tearing at the farthest points from the linear flanges. PP-70fm for minor direction tends to slightly deviate into a kind of crumpling or local buckling [81] as shown in Figure 4.10 and Figure 4.11, which must be avoided as far as possible for the better and stable crash performance.

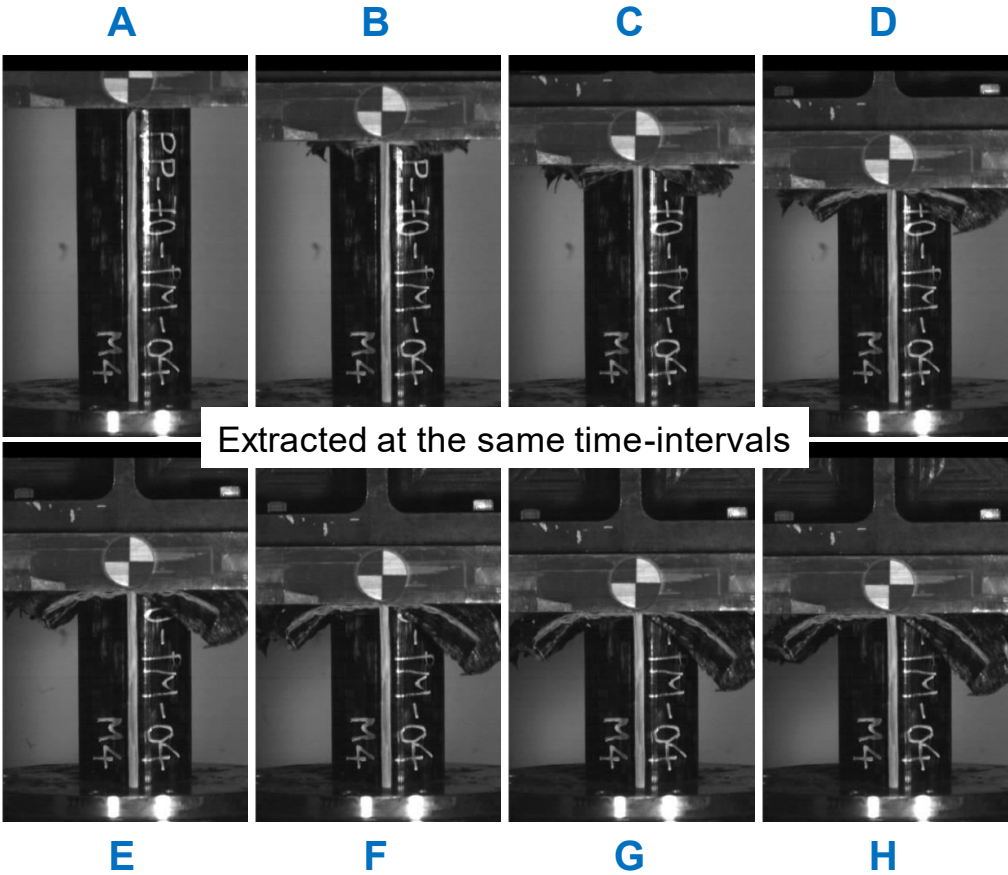


Figure 4.8: Crash behavior of PP-70fM; major direction of unbalanced (2/1) woven fabric made of PP/GF45 vol. % (70 wt. %) MLH-roving

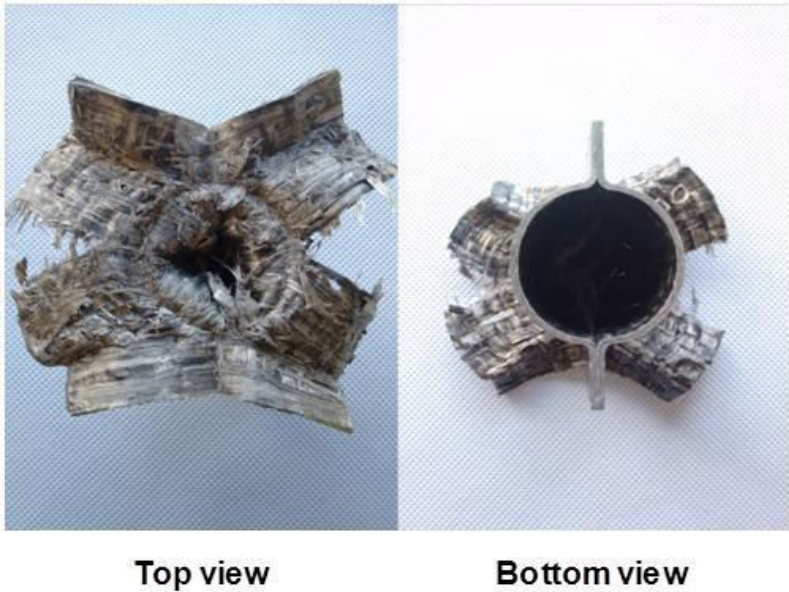


Figure 4.9: Crushed feature of PP-70fM; major direction of unbalanced (2/1) woven fabric made of PP/GF45 vol. % (70 wt. %) MLH-roving

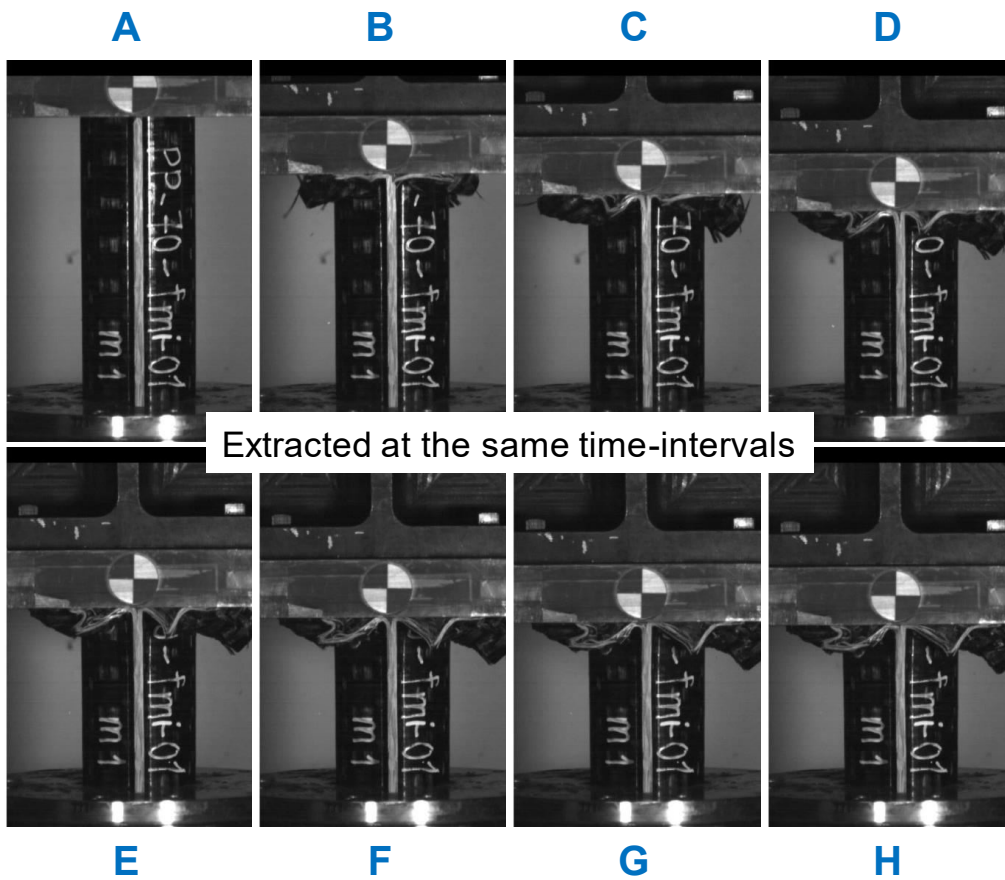


Figure 4.10: Crash behavior of PP-70fm; minor direction of unbalanced (2/1) woven fabric made of PP/GF45 vol. % (70 wt. %) MLH-roving

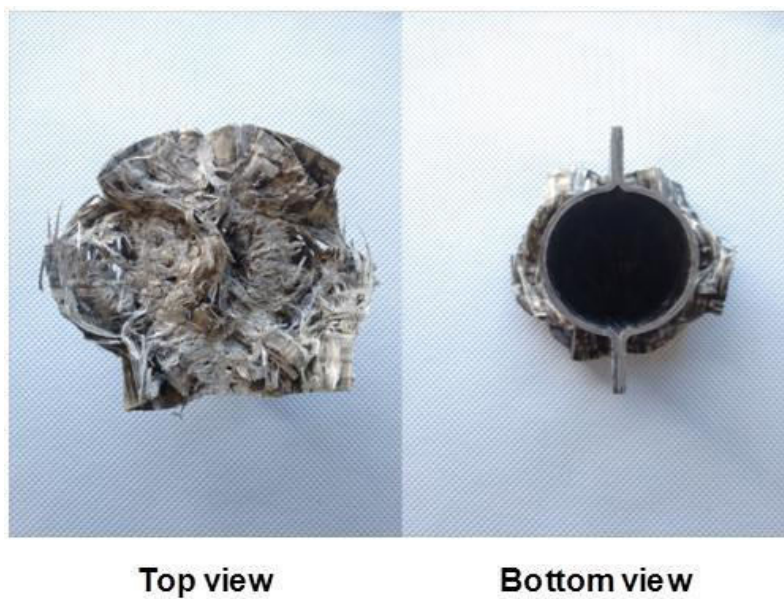


Figure 4.11: Crushed feature of PP-70fm; minor direction of unbalanced (2/1) woven fabric made of PP/GF45 vol. % (70 wt. %) MLH-roving

4.3 Random Mat of PP/GF

At least, the isotropic reinforcement can be free from unsuitable fiber orientation that sometimes doesn't fill up the perfect mode of 'splaying and lamina-bending followed by inside-wrinkling and outside-tearing'. Based on it, the dynamic crash tests were conducted with the same impact velocity of 8.3 m/s on the test specimens of PP-70 (2.5 mm wall thickness) made of PP/GF45 vol. % (70 wt. %) MLH-mat; i.e. PP-70 has the same fiber content with the continuous fiber reinforcement (PP-70fM and PP-70fm) in Section 4.2, but reinforced with long fiber of random directional distribution.

The load-displacement curves are plotted in Figure 4.12 and its crashworthiness is summarized in Table 4.4 with the representative values, such as 44 J/g for SEA, 74 J/cm³ for VEA, and 63 MPa for mean stress. These representative values might be at the same level with PP-70fM for major direction of continuous fiber reinforcement, in spite of being determined with just two data; cf. there were two test specimens of a poor but unpredictable welding property between the faced linear-flanges. And PP-70, as shown in Figure 4.13 and Figure 4.14, completely fulfills the mode of 'splaying and lamina-bending followed by inside-wrinkling and outside-tearing', but with a so-called gentle deformation.

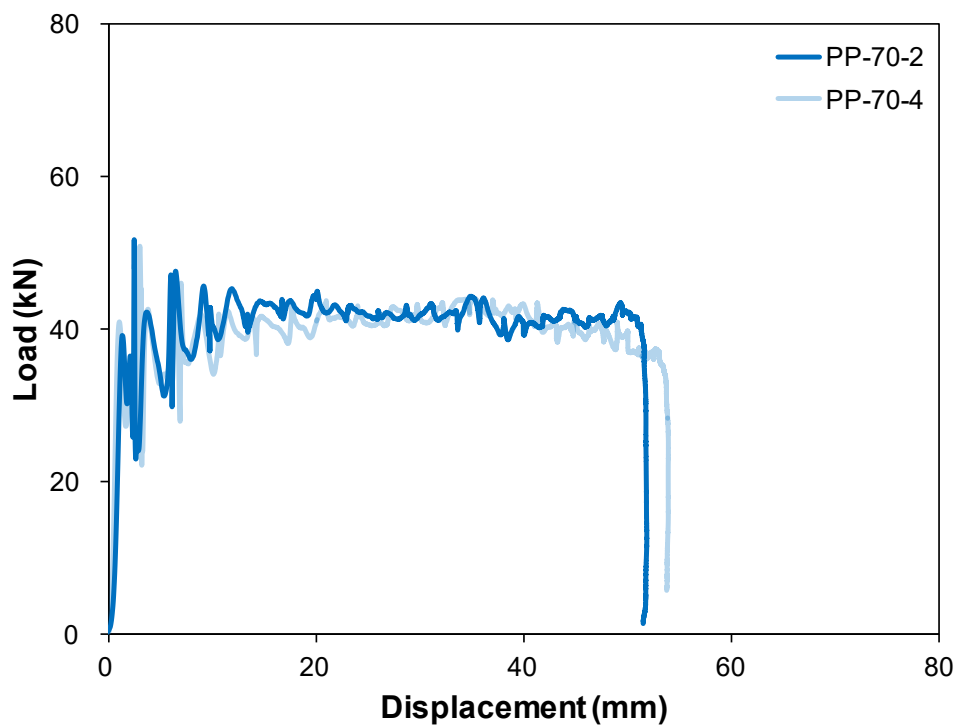


Figure 4.12: Load-displacement of PP-70; PP/GF45 vol. % (70 wt. %) MLH-mat

Table 4.4: Crashworthiness of PP-70; PP/GF45 vol. % (70 wt. %) MLH-mat

PP-70	Average	No. 1	No. 2	No. 3	No. 4
Velocity (m/s)		8.24	8.20	8.22	8.24
Applied energy (J)		2076	2056	2066	2076
Specimen weight (g)		124.3	125.6	123.7	121.9
Displacement (mm)		77.78	51.75	119.40	53.91
Mean stress(MPa)	63.4	-	64.4	-	62.4
Load uniformity	1.31	-	1.30	-	1.32
SEA (J/g)	44.2	-	44.3	-	44.2
VEA (J/cm ³)	73.9	-	73.9	-	73.8
Remark		Weld NG	OK	Weld NG	OK

In more detail, the lamina-bending of PP-70 tends to curl down more than that of PP-70fM, and its inside-wrinkling and outside-tearing seems to be of continuum that was not torn obviously like PP-70fM. The behavior of such gentle deformation might be directly related to the fact that thermoplastic materials are melted momentarily by the heat converted from kinetic energy during impact [93][94][144]. Also, it implies that long fiber reinforcement has the advantage of flowability compared with continuous fiber reinforcement of a limited drapability.

Additionally, the dynamic crash tests were conducted on the test specimens of PP-70H that is designed as the intermediate material alternately layered with PP-70fM and PP-70. It should be emphasized that the plate of PP-70H was impregnated and consolidated at the same time using woven fabrics of MLH-roving and non-woven MLH-mats, for both are a kind of ready-to-impregnate material. The crashworthiness is summarized in Table 4.5 with the representative values, such as 42 J/g for SEA, 71 J/cm³ for VEA, and 64 MPa for mean stress. On the basis of single-factor ANOVA with 95% confidence level, PP-70H has statistically the same representative values with PP-70fM. Moreover, as shown in Figure 4.15, the crushed feature of PP-70H is definitely somewhere between PP-70fM (continuous fiber reinforcement) and PP-70 (long fiber reinforcement).

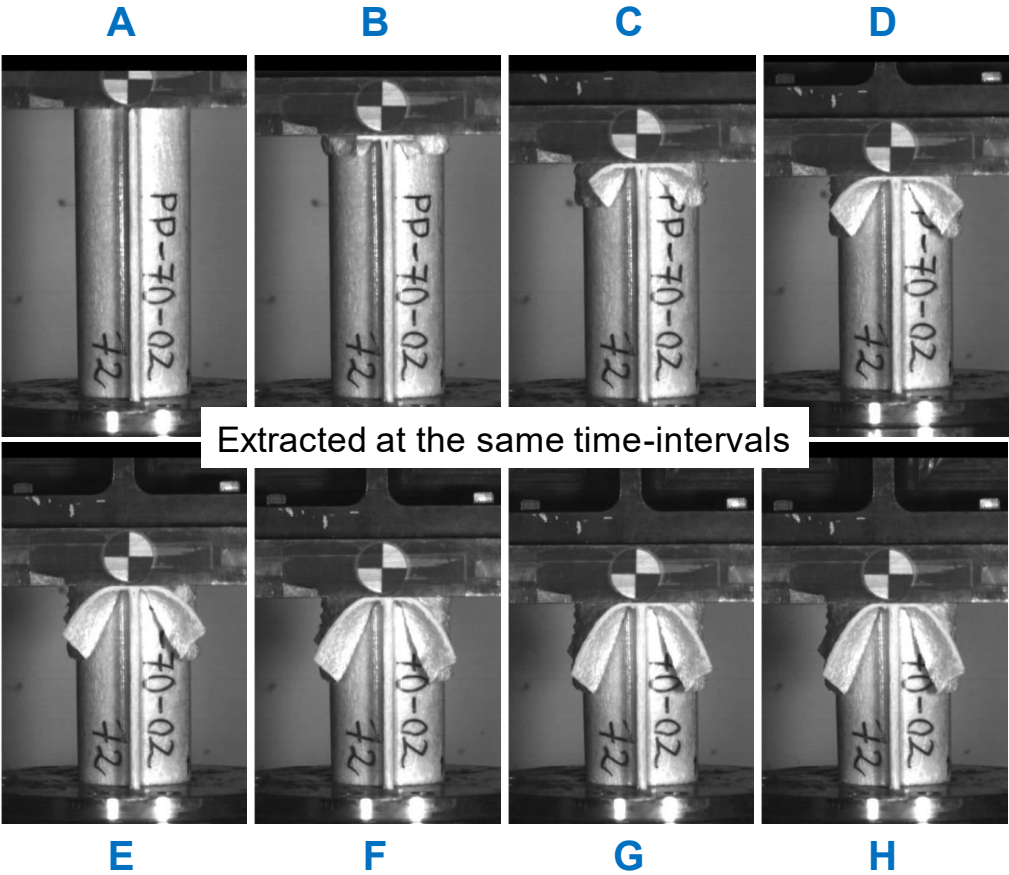


Figure 4.13: Crash behavior of PP-70; PP/GF45 vol. % (70 wt. %) MLH-mat

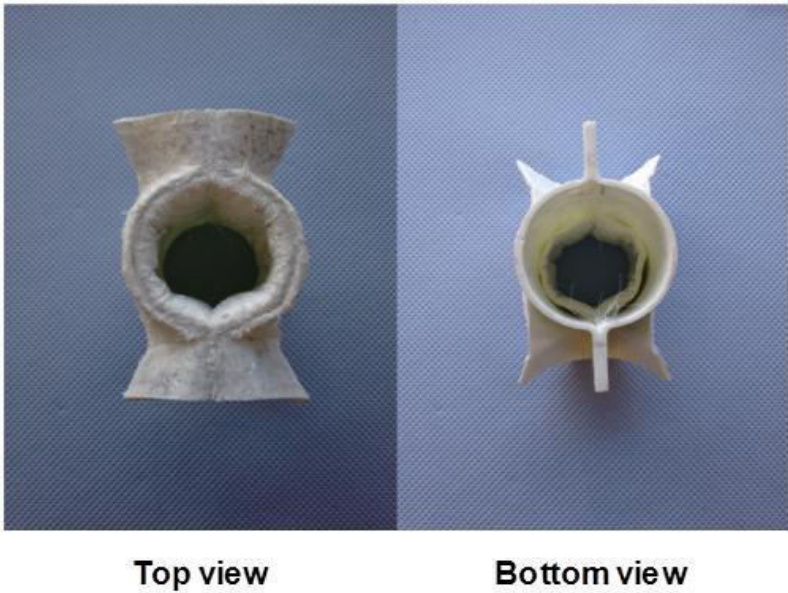


Figure 4.14: Crushed feature of PP-70; PP/GF45 vol. % (70 wt. %) MLH-mat

Table 4.5: Crashworthiness of PP-70H; PP/GF45 vol. % (70 wt. %) intermediate between MLH-roving and MLH-mat

PP-70H	Average	No. 1	No. 2	No. 3	No. 4
Velocity (m/s)		8.49	8.45	8.31	8.49
Applied energy (J)		2203	2183	2111	2203
Specimen weight (g)		124.7	129.0	127.3	127.7
Displacement (mm)		56.56	56.80	54.96	57.72
Mean stress(MPa)	63.9	64.7	63.8	63.8	63.4
Load uniformity	1.55	1.66	1.58	1.36	1.60
SEA (J/g)	42.4	43.7	41.7	42.2	41.9
VEA (J/cm ³)	70.8	73.0	69.6	70.5	69.9
Remark		OK	OK	OK	OK

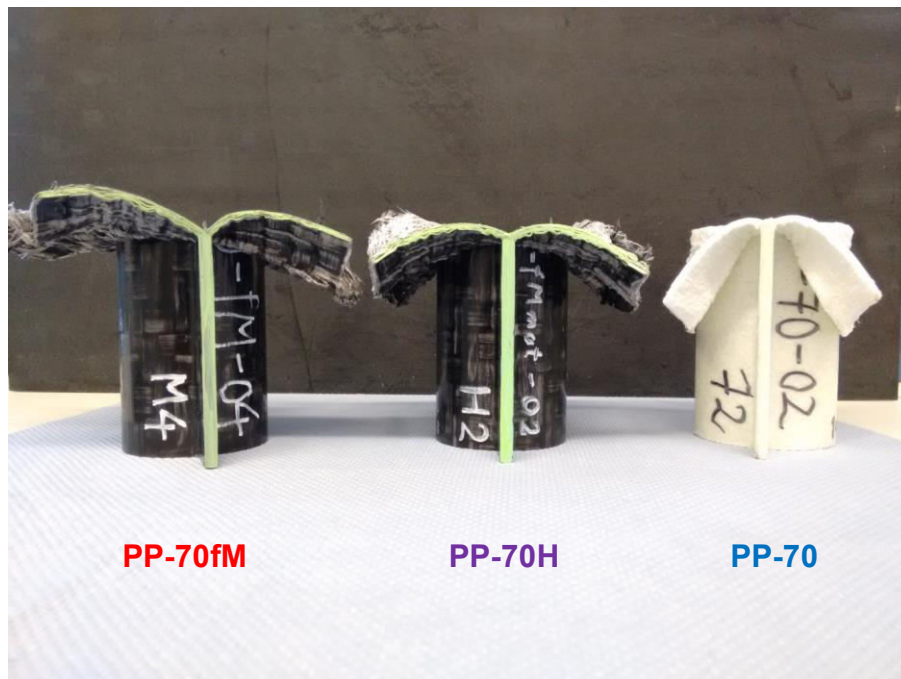


Figure 4.15: Comparison of crushed features; PP/GF45 vol. % (70 wt. %) materials

In short, there was no significant difference in SEA for PP-70fM (continuous fiber) of 42.9 J/g, PP-70 (long fiber) of 44.2 J/g, and PP-70H (mixed) of 42.4 J/g. Each has the same GF content of 45 vol. % and fulfills the desirable mode of 'splaying and lamina-bending followed by inside-wrinkling and outside-tearing'. Moreover, long fiber reinforcement is more freely deformed than continuous fiber reinforcement.

4.4 Random Mat of PA6/GF

As an example to investigate the influence of matrix polymer on crashworthiness, the dynamic crash tests were continued on the test specimens of PA-70 and PA-63 which are respectively made of PA6/GF50 vol. % (70 wt. %) MLH-mat and PA6/GF42 vol. % (63 wt. %) MLH-mat; cf. although holding the reasonable modulus, PA6/GF50 vol. % (70 wt. %) MLH-mat could not maintain its persistence degree. In accordance with the result of pretest, the impact velocity was raised to 9.5 m/s from 8.3 m/s, so that the imposed kinetic energy became 2.7 kJ. As compared in Figure 4.16, two curves of load-displacement are rectangular in shape and have the same height (mean load). Therefore, those two velocities return the same values of SEA (and VEA) by a linear relationship between applied impact energy and displacement; the higher the longer, but having the same ratio. More sufficient displacement can contribute to minimizing the inaccuracy which might be caused by the unstable portion of initial state.

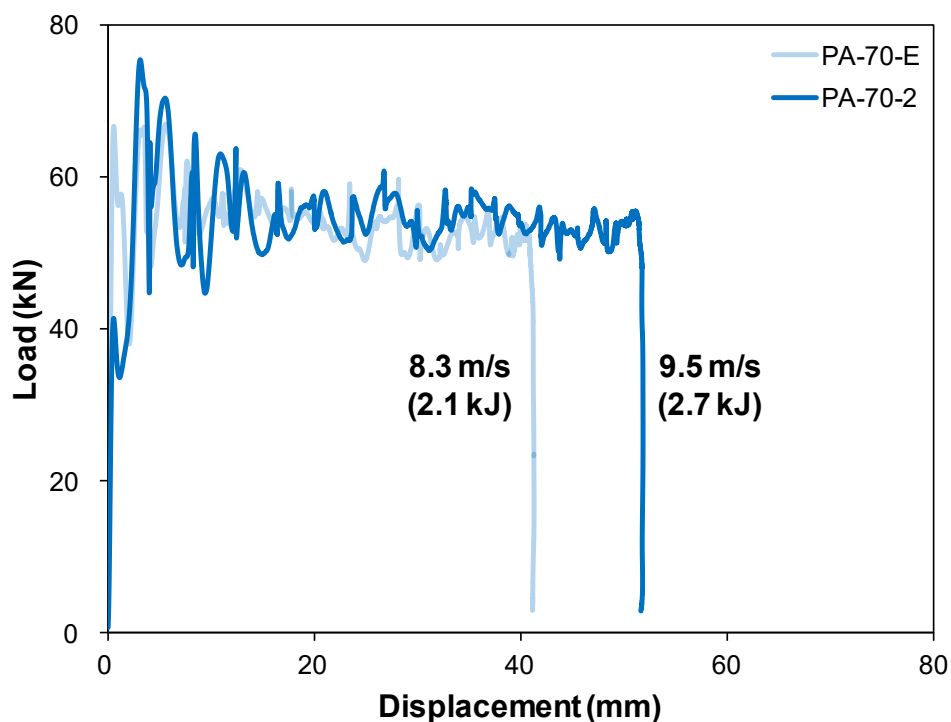


Figure 4.16: Influence of impact velocity on load-displacement curve

The load-displacement curves on PA-70 (2.5 mm wall thickness) are plotted in Figure 4.17. And its crashworthiness is summarized in Table 4.6, excluding the data of lower velocity marked as 'Low E', with the representative values, such as 50 J/g for SEA, 94 J/cm³ for VEA, and 83 MPa for mean stress. Also the crashworthiness of PA-63

(2.0 mm wall thickness) is summarized in Table 4.7 with the representative values, such as 52 J/g for SEA, 91 J/cm³ for VEA, and 85 MPa for mean stress.

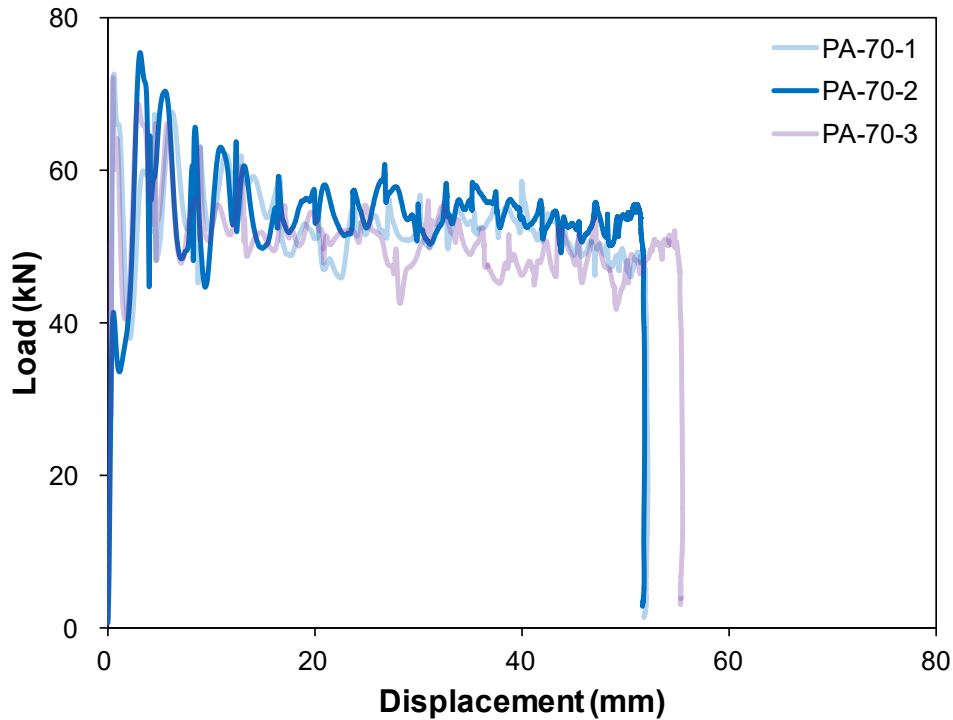


Figure 4.17: Load-displacement of PA-70; PA6/GF50 vol. % (70 wt. %) MLH-mat

Table 4.6: Crashworthiness of PA-70; PA6/GF50 vol. % (70 wt. %) MLH-mat

PA-70	Average	No. 1	No. 2	No. 3	No. E
Velocity (m/s)		9.35	9.42	9.44	8.35
Applied energy (J)		2673	2713	2724	2131
Specimen weight (g)		144.3	142.0	139.5	143.3
Displacement (mm)		52.07	51.75	55.42	41.35
Mean stress(MPa)	82.6	83.2	85.0	79.5	83.6
Load uniformity	1.44	1.41	1.44	1.47	1.30
SEA (J/g)	50.2	49.8	51.7	49.2	50.4
VEA (J/cm ³)	93.9	93.1	96.6	92.1	94.2
Remark		OK	OK	OK	Low E/OK

Table 4.7: Crashworthiness of PA-63; PA6/GF42 vol. % (63 wt. %) MLH-mat

PA-63	Average	No. 1	No. 2	No. 3	No. 4
Velocity (m/s)		9.65	9.47	9.47	9.47
Applied energy (J)		2863	2757	2757	2757
Specimen weight (g)		110.8	111.5	109.6	107.1
Displacement (mm)		68.60	66.78	68.81	71.36
Mean stress(MPa)	85.2	88.0	87.0	84.5	81.4
Load uniformity	1.51	1.46	1.58	1.54	1.45
SEA (J/g)	51.6	52.7	51.8	51.2	50.5
VEA (J/cm ³)	90.8	92.8	91.2	90.1	88.9
Remark		OK	OK	OK	OK

There are no significant differences in the representative values between PA-70 and PA-63, based on single-factor ANOVA with 95% confidence level. This corresponds with results of short-time scale behavior. Therefore, PA-70 and PA-63 can be merged into 51 J/g for SEA, 92 J/cm³ for VEA, and 84 MPa for mean stress which are treated as the representative values of PA6/GF MLH-mat having the GF content of around 45 vol. %. By changing the matrix polymer into PA6, the crashworthiness was improved 25% higher in VEA compared to PP/GF MLH-mat; 15% higher in SEA considering density effect. The crash behavior is characterized into the gentle deformation, the same with PP/GF MLH-mat, which fulfills the mode of ‘splaying and lamina-bending followed by inside-wrinkling and outside-tearing’ as shown in Figure 4.18 and Figure 4.19. So, the gentle deformation seems to be the common behavior of MLH-mat (or long GF reinforced thermoplastic material); it is distinctly different from continuous fiber reinforcement. Besides, the increase in crashworthiness of PA6/GF MLH-mat is mainly related to the longer strain and the higher modulus [8][143][145] than those of PP/GF MLH-mat (see Table 3.11, Table 3.18, and Table 3.19), as well as the higher melting temperature of matrix polymer; e.g. 220°C for PA6 and 163°C for PP. The law of Conservation of Energy means that energy can neither be created nor destroyed, and thus it can only transform from one to others, such as from the imposed kinetic energy to being dissipated into sound, friction, heat, and all kinds of deformation.

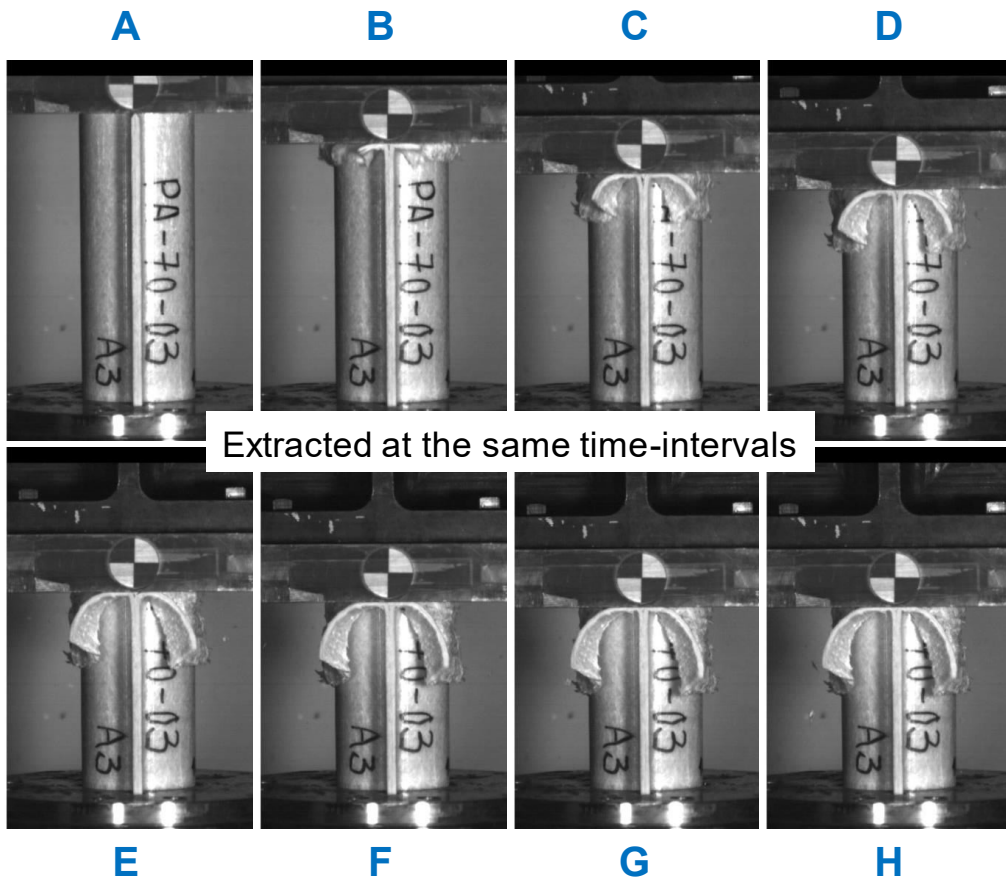


Figure 4.18: Crash behavior of PA-70; PA6/GF50 vol. % (70 wt. %) MLH-mat

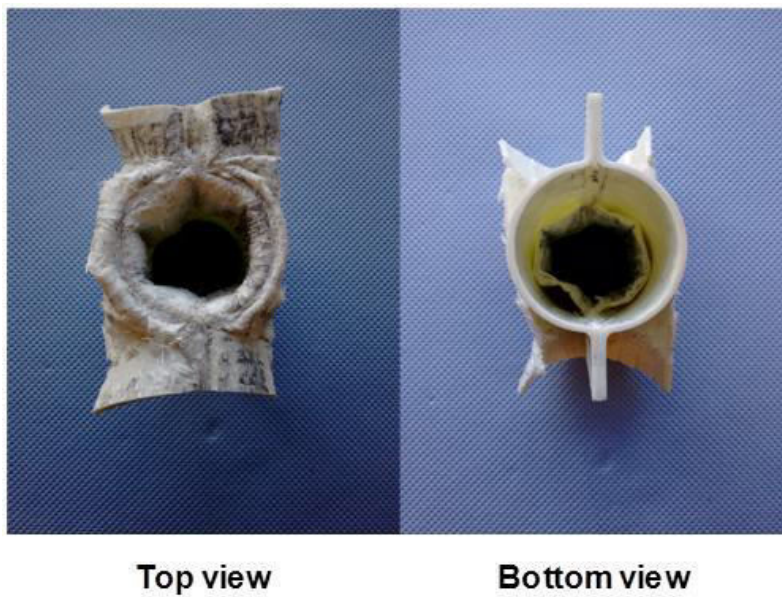


Figure 4.19: Crushed feature of PA-70; PA6/GF50 vol. % (70 wt. %) MLH-mat

5 Conclusions

Based on the same concept of multilayered hybrid (MLH) structure, continuous fiber- and long fiber reinforced thermoplastic materials are newly developed. Then, those materials are investigated as a promising candidate for the deformable parts in crash applications. The MLH structure corresponds to the concept of easier impregnation by minimizing the height of fiber reinforcement in the Kozeny-Carman equation. So, it heads toward the way to achieve a desirable level of impregnation quality without lowering a melt viscosity of thermoplastic matrix resin.

Continuous fiber reinforcement

As a continuous fiber reinforced thermoplastic material, the multilayered hybrid roving (MLH-roving) has been intended to combine the variety in intermediate product from commingled roving and the variety of material configuration from organic sheet. The MLH-roving is a fiber roving separated evenly into several sublayers by thermoplastic films through three sequential processes of spreading, fixing, and folding; a single-end glass fiber roving (4000 fibers of 17 μm in diameter) is successfully spread into 20 mm width based on the newly derived spreading equation. Based on the square and hexagonal models, the number of rows in fiber array becomes only 4–5 rows that is below half the level of continuous fiber reinforced thermoplastic materials available in the market; the lower the number of rows in fiber array, the easier the impregnation. Moreover, the MLH-roving can provide a variety of matrix polymer by using films and be free from the risks caused by irregularly distributed and movable fibers and from poor impregnation at every crossing point of warp and weft. The outward flow from inner layers is the most outstanding behavior of MLH-roving that can overcome any kind of hindrances caused by fiber compaction under pressure.

Newly derived spreading equation

If the widths are desired to spread from 10 mm to 20 mm, the radius of the spreading support at ± 10 mm position matches 12.65 mm with the curvature of 7.0 m^{-1} on the spreading support. But, in the case of starting from a point as proposed by Bates and Charrier, the corresponding radius becomes 11.45 mm with the curvature of 30.3 m^{-1} ; the bigger the curvature, the higher the risk of center-splitting-problem on spreading support. Also it is preferred to spread step-by-step rather than at a stroke, like from 5 mm to 10 mm, and then 10 mm to 20 mm.

Impregnation quality and characterization

The impregnation quality of PP/GF45 vol. % (70 wt. %) MLH-roving was verified with the plates of unbalanced (2/1) woven fabrics that are impregnated at 190–250°C and consolidated in a mass production scale. The representative flexural properties were suggested as 24.3 GPa in modulus, 443 MPa in strength, and 1.90% in strain for the major direction. The flexural modulus is a very reasonable value, being at 95% level of the theoretical value. And its stress-strain behavior was efficiently characterized by the persistence degree following the straight line with 95% that is virtualized by its modulus. But, the stress-strain behavior for the minor direction has a big variation caused by the waving of fibers and the crimps of woven fabric. The representative values were suggested as 13.9 GPa in modulus, 243 MPa in strength, and 2.07% in strain. And their behaviors are classified into three types like normal, multilevel drop, and sudden drop.

Long fiber reinforcement

The concept of multilayered hybrid mat (MLH-mat) aims to realize a new GMT like material that is quite suitable for various matrix polymers and high fiber contents. The MLH-mat consists of several plies of thin sublayers of glass fiber and thermoplastic films. And, each sublayer should have random directional fiber distribution as well as homogeneity in areal density, in order to be isotropic as much as possible.

Modified Kozeny-Carman equation for packed bed of fibers

The Kozeny-Carman equation has been used in the field of chemical engineering, in order to describe a flow in a packed bed composed of Raschig rings (equal in length and diameter). This equation must be modified for packed bed of fibers because of the length-to-diameter ratio being too far from 1. Eventually, the modified equation for packed bed of fibers consists of the constant 32, different from 72 in the Kozeny-Carman equation, with the tortuous degree of 1.0 (parallel) to 5 (transverse).

Impregnation quality and characterization

MLH-mats, three PP/GF grades and four PA6/GF grades, were prepared having the glass fiber content from 19 vol. % to 50 vol. %, and the areal density of sublayers between 140 and 165 g/m². Impregnation quality was verified to be good only up to the fiber content of 46 vol. %, assumed as the maximum value when impregnated at 30 bar and obtained from the compression test through entire-thickness changes; cf.

42 vol. % for impregnation at 20 bar. Homogeneity of glass fiber sublayers in areal density was verified as being in an extremely narrow range below 5% in coefficient of variation. Besides, the isotropy as a random directional fiber distribution was checked on PA6/GF37 vol. % (58 wt. %) MLH-mat with the set of flexural properties between machine direction and transverse direction. There is no significant difference between the two directions. PP/GF and PA6/GF MLH-mats showed quite different behaviors in flexural stress-strain. When having the similar values in flexural modulus, PA6/GF MLH-mat continues 1.53 times longer than PP/GF MLH-mat in flexural strain. The persistence degree of PA6/GF MLH-mat ranked 82% with a sudden drop behavior in stress, being higher than 72% of PP/GF MLH-mats with long lasting stress behavior. So, the general tendencies of flexural modulus and flexural strain with fiber volume content were well fitted by linear least squares, for PP/GF MLH-mats and PA6/GF MLH-mats. PA6/GF MLH-mat showed more gentle slope in flexural strain along fiber content, 64% level compared to PP/GF MLH-mat. Also, MLH-mats have an excellent reheating stability.

Crash behavior

On the newly developed materials, MLH-roving and MLH-mat, the crash behavior and performance were investigated by dynamic crash test imposing a given amount of impact energy at once. The dynamic crash test takes into account not only true circumstances but also the material sensitivity to strain rate. All the materials used here have the glass fiber content of around 45 vol. %, whatever reinforced with long fiber or continuous fiber. These materials showed the ideal load-displacement curves of rectangular shape and were characterized obviously as the mode of 'splaying and lamina-bending followed by inside-wrinkling and outside-tearing'. MLH-mats showed a gentle deformation due to flowability when momentarily melted by the crash energy. There was no significant difference in specific energy absorption (SEA) for all PP/GF materials; around 43 J/g for major direction of MLH-roving, MLH-mat, and mixed one. PA6/GF MLH-mats showed 51 J/g of SEA, which is 25% improvement in volumetric specific energy (apart from density effect) due to longer strain and higher modulus, as well as higher melting temperature.

6 References

- [1] P. -E. Bourban, N. Bernet, J. -E. Zanetto and J.-A. E. Månson, "Material phenomena controlling rapid processing of thermoplastic composites," *Composites Part A: Applied Science and Manufacturing*, vol. 32, no. 8, pp. 1045-1057, 2001.
- [2] M. Schemme, "LFT-development status and perspectives," *Reinforced Plastics*, vol. 52, no. 1, pp. 32-34, 36-39, 2008.
- [3] Hanwha Advanced Materials, "Products/Automotive materials/Stronglite (GMT) and Superlite (LWRT)," [Online]. Available: <http://hwam.co.kr/en/index.do>. [Accessed 12 June 2017].
- [4] H. Hamada and S. Ramakrishna, "A FEM method for prediction of energy absorption capability of crashworthy polymer composite materials," *Journal of Reinforced Plastics and Composites*, vol. 16, no. 3, pp. 226-242, 1997.
- [5] M. David, A. F. Johnson and H. Voggenreiter, "Analysis of crushing response of composite crashworthy structures," *Applied Composite Materials*, vol. 20, no. 5, pp. 773-787, 2013.
- [6] Bond Laminates: A company of the LANXESS group, "Advanced thermoplastic composites," 2013.
- [7] Owens Corning, "Product Information: TwinTEX® R PP (PP glass roving)," 2008.
- [8] S. Ochelski and P. Gotowicki, "Experimental assessment of energy absorption capability of carbon-epoxy and glass-epoxy composites," *Composite Structures*, vol. 87, no. 3, pp. 215-224, 2009.
- [9] T. Kraus, M. Kühnel and E. Witten, "Composites market report 2016-market developments, trends, outlook and challenges," CCeV and AVK, 2016.
- [10] M. Sauer, M. Kühnel and E. Witten, "Composites market report 2017-market

- developments, trends, outlook and challenges," CCEV and AVK, 2017.
- [11] M. Schemme, "Long glass fiber thermoplastics-Material classification and characterization," in *Langfaserverstärkte Thermoplaste im Automobil*, Würzburg, 2001.
- [12] F. Henning, H. Ernst, R. Brüssel, O. Geiger and W. Krause, "LFTs for automotive applications," *Reinforced Plastics*, vol. 49, no. 2, pp. 24-33, February 2005.
- [13] M. Schemme, "LFT status and perspectives," in *22. Nationales Symposium SAMPE Deutschland e.V.*, Fürth, 2016.
- [14] D. Emerson, D. Grauer, B. Hangs, M. Reif, F. Henning, A. Martsman and S. T. Jespersen, "Using UD glass tapes to improve impact performance of thermoplastic composites in automotive applications," in *SPE ACCE (Automotive Composites Conference and Exhibition)*, Troy, 2012.
- [15] Cato, "Tailored thermoplastic composite inserts for hybrid moulding," in *1st ICC (International Composite Congress)*, Stuttgart, 2015.
- [16] DIEFFENBACHER, "Tailored fiber placement LFT-D: flexible and economical process for the mass production of hybrid lightweight composites," in *1st ICC (International Composite Congress)*, Stuttgart, 2015.
- [17] M. Birrell, "IXIS-hybrid thermoplastic composite (HTPC) for horizontal automotive panels," in *SPE ACCE (Automotive Composites Conference and Exhibition)*, Troy, 2008.
- [18] L. M. Sherman, "The new lightweights: Injection molded hybrid composites spur automotive innovation," *Plastics Technology Magazine*, pp. 27-31, November 2012.
- [19] D. Häffelin, "Innovative processing of thermoplastic composites for Porsche Panamera brake pedal," in *Plastics in Automotive Engineering*, Mannheim, 2017.
- [20] M. H. Naitove, "Organic hybrid composites highlighted at K show," December

2010. [Online]. Available: <https://www.ptonline.com/articles/organic-hybrid-composites-highlighted-at-k-show>. [Accessed 10 July 2018].
- [21] T. G. P. Gutowski, "A brief introduction to composite materials and manufacturing processes," in *Advanced Composites Manufacturing*, ISBN 9780471153016, Wiley-Interscience, 1997, pp. 5-41.
- [22] B. Harris, "Elastic properties of fibre composites," in *Engineering Composite Materials*, 2nd ed., ISBN 9781861250322, Maney Publishing, 1999, pp. 33-60.
- [23] RTP Company, "Product data sheet and general processing conditions: Polypropylene (PP) unfilled," 2004.
- [24] Owens Corning, "Advantex® Boron-free ECR glass reinforcement properties," 2010.
- [25] Bond Laminates: A company of the LANXESS group, "Material Data Sheet: TEPEX® dynalite 104-RG600(x)/47% Roving Glass-PP Consolidated Composite Laminate," 2014.
- [26] K. van Rijswijk, Thermoplastic composite wind turbine blades, Delft: Technische Universiteit Delft, 2007.
- [27] C. Ó. Brádaigh, "Reactive thermoplastic composites-A potential game changer?," in *SAMPE UK and Ireland, Master Class*, Bristol, 2013.
- [28] E. Selver, Tow level hybridisation for damage tolerant composites, Manchester: University of Manchester, 2014.
- [29] M. Wysocki, R. Larsson and S. Toll, "Hydrostatic consolidation of commingled fibre composites," *Composites Science and Technology*, vol. 65, no. 10, pp. 1507-1519, 2005.
- [30] B. T. Åström, "Constituent materials," in *Manufacturing of polymer composites*, CRC Press, 1997, pp. 47-136.
- [31] Suprem SA, "Products," [Online]. Available: <https://www.suprem.ch>. [Accessed 24 March 2017].

-
- [32] SGL Group-The Carbon Company, "Unidirectional carbon fiber tape with thermoplastic matrix," 2017.
- [33] SGL Group-The Carbon Company, "Composite-Fiber and Materials: SIGRAFIL® Continuous carbon fiber tow," 2017.
- [34] Hexcel, "Product Data: HexTow® AS4 carbon fiber," 2014.
- [35] AGY, "Technical Paper: High strength glass fibers," 2006.
- [36] TenCate, "Cetex® TC910 Nylon 6 thermoplastic composite," 2017.
- [37] TenCate, "Cetex® TC1200 PEEK resin system," 2017.
- [38] Bond Laminates, "The world of TEPEX: Superior in Motion-Maximum performance with minimal resources," 2011.
- [39] G. Gardiner, "Aerospce-grade compression molding," July 2010. [Online]. Available: <https://www.compositesworld.com/articles/aerospace-grade-compression-molding>. [Accessed 28 May 2018].
- [40] Bond Laminates: A company of the LANXESS group, "Material data sheet: TEPEX® optilite 201-C200(x)/45% Carbon-PA6.6 Consolidated Composite Laminate," 2014.
- [41] Bond Laminates: A company of the LANXESS group, "Material data sheet: TEPEX® dynalite 102-RG600(x)/47% Roving Glass-PA6 Consolidated Composite Laminate," 2014.
- [42] T. Sontag, "Kosteneffizienter Leichtbau mit thermoplastischen Composites für die automobile Großserie," in *22. Nationales Symposium SAMPE Deutschland e.V.*, Fürth, 2016.
- [43] S. Ropers, "Bending characterization of textile composites," in *Bending Behavior of Thermoplastic Compoiste Sheets: Viscoelasticity and Temperature Dependency in the Draping Process*, ISBN 9783658175931, Springer, 2017, pp. 31-60.
- [44] M. Golzar, H. Brünig and E. Mäder, "Commingled hybrid yarn diameter ratio in

- continuous fiber-reinforced thermoplastic composites," *Journal of Thermoplastic Composite Materials*, vol. 20, no. 1, pp. 17-26, 2007.
- [45] M. M. B. Hasan, E. Staiger, M. Ashir and C. Cherif, "Development of carbon fibre/polyamide 6,6 commingled hybrid yarn for textile-reinforced thermoplastic composites," *Journal of Thermoplastic Composite Materials*, vol. 28, no. 12, pp. 1708-1724, 2015.
- [46] N. Wiegand and E. Mäder, "Commingled yarn spinning for thermoplastic/glass fiber composites," *Fibers*, vol. 5, no. 3, p. <https://doi.org/10.3390/fib5030026>, 2017.
- [47] Owens Corning, "Product Information: Thermopreg™ Fabrics (Commingled Polypropylen Glass Fabrics)," 2011.
- [48] P. Bates and I. Ekhtor, "Continuous consolidation of commingled glass and polypropylene roving," *Journal of Reinforced Plastics and Composites*, vol. 23, no. 13, pp. 1409-1424, 2004.
- [49] Owens Corning, "Composite Solutions: Reinforcement guide," 2011.
- [50] F. Hattum and S. Breugel, "LFT: the future of reinforced thermoplastics?," *Reinforced Plastics*, vol. 45, no. 6, pp. 42-44, June 2001.
- [51] P. Malnati, "Reinforced thermoplastics: LFRT/GMT roundup," August 2007. [Online]. Available: <https://www.compositesworld.com/articles/reinforced-thermoplastics-lfirtgmt-roundup>. [Accessed 12 June 2017].
- [52] P. Malnati, "Reinforced thermoplastics: LFRT vs. GMT," August 2007. [Online]. Available: <https://www.compositesworld.com/articles/reinforced-thermoplastics-lfirt-vs-gmt>. [Accessed 12 June 2017].
- [53] C. Tzoganakis, J. Vlachopoulos and A. E. Hamielec, "Production of controlled rheology polypropylene resins by peroxide promoted degradation during extrusion," *Polymer Engineering & Science*, vol. 28, no. 3, pp. 170-180, 1988.
- [54] GS Caltex Corporation, "Products/For Business/Polypropylene/LFT," [Online]. Available: <http://www.gscaltex.com/eng/>. [Accessed 18 May 2018].

- [55] "PlastiComp and Xenia to develop apps for carbon fiber TP composites," April 2015. [Online]. Available: <https://www.ptonline.com/articles/plasticomp-partners-with-xenia-to-develop-applications-for-carbon-fiber-thermoplastic-composites>. [Accessed 7 June 2018].
- [56] J. Markarian, "Long fibre reinforced thermoplastics continue growth in automotive," *Plastics, Additives and Compounding*, vol. 9, no. 2, pp. 20-22, 24, 2007.
- [57] T. Harmia, J. Hartikainen and M. Lindner, "Long fiber reinforced thermoplastic composites in automotive applications," in *Polymer Composites; from nano to macro scale*, Springer, 2005, pp. 255-262.
- [58] O. Geiger, F. Henning, P. Eyerer, R. Brüssel and H. Ernst, "LFT-D: materials tailored for new applications," *Reinforced Plastics*, vol. 50, no. 1, pp. 30-35, January 2006.
- [59] PlastiComp, "Pushtrusion: Direct in-line long fiber thermoplastic (D-LFT) compounding technology versus LFT pellets and GMT sheet".
- [60] M. Popella, "On the direct way to profitability: Production of long glass fiber reinforced thermoplastics in a one-step inline-compounding process," in *SPE ACCE (Automotive Composites Conference and Exhibition)*, Troy, 2007.
- [61] M. Graf, "Endless fiber reinforced long-fiber compound materials for the economical production of thermoplastic structural components," in *SPE ACCE (Automotive Composites Conference and Exhibition)*, Novi, 2014.
- [62] H. Jäger, "Lightweight material future is hybride...are carbon composites out now?," in *International Textile Conference*, Dresden, 2016.
- [63] T. Behr, "Material concepts for the car body of the future," in *International Textile Conference*, Dresden, 2016.
- [64] S. T. Taher, E. Mahdi, A. S. Mokhtar, D. L. Magid, F. R. Ahmadun and P. R. Arora, "A new composite energy absorbing system for aircraft and helicopter," *Composite Structures*, vol. 75, no. 1-4, pp. 14-23, 2006.

-
- [65] L. Peroni, M. Avalle and G. Belingardi, "Comparison of the energy absorption capability of crash boxes assembled by spot-weld and continuous joining techniques," *International Journal of Impact Engineering*, vol. 36, no. 3, pp. 498-511, 2009.
- [66] K. Friedrich and A. A. Almajid, "Manufacturing aspects of advanced polymer composites for automotive applications," *Applied Composite Materials*, vol. 20, no. 2, pp. 107-128, 2013.
- [67] A. G. Mamalis, D. E. Manolakos, M. B. Ioannidis and D. P. Papapostolou, "Crashworthy characteristics of axially statically compressed thin-walled square CFRP composite tubes: experimental," *Composite Structures*, vol. 63, no. 3-4, pp. 347-360, 2004.
- [68] G. C. Jacob, J. F. Fellers, S. Simunovic and J. M. Starbuck, "Energy absorption in polymer composites for automotive crashworthiness," *Journal of Composite Materials*, vol. 36, no. 7, pp. 813-850, 2002.
- [69] H. Zarei, M. Kröger and H. Albertsen, "An experimental and numerical crashworthiness investigation of thermoplastic composite crash boxes," *Composite Structures*, vol. 85, no. 3, pp. 245-257, 2008.
- [70] H. Zarei and M. Kröger, "Crashworthiness investigation and optimization of empty and foam filled composite crash box," in *Woven Fabric Engineering*, Sciyo, 2010, pp. 343-362.
- [71] C. Cutler, "Boldmethod," 13 January 2016. [Online]. Available: <http://www.boldmethod.com/blog/lists/2016/01/16-little-known-facts-about-the-airbus-a380/>. [Accessed 19 February 2018].
- [72] M. Waimer, D. Kohlgrüber, D. Hachenberg and H. Voggenreiter, "Experimental study of CFRP components subjected to dynamic crash loads," *Composite Structures*, vol. 105, pp. 288-299, 2013.
- [73] P. Steinle, M. Kriescher and H. E. Friedrich, "Innovative vehicle concept for the integration of alternative power trains," in *Stuttgarter Symposium*, Stuttgart, 2010.

-
- [74] G. Jung and S. Schmeer, "Material consideration for better crash parts: from metallic to fiber reinforced thermoplastic materials," *Composite Solutions*, no. 3, pp. 26-31, 2016.
- [75] M. R. Bambach, M. Elchalakani and X. L. Zhao, "Composite steel-CFRP SHS tubes under axial impact," *Composite Structures*, vol. 87, no. 3, pp. 282-292, 2009.
- [76] C. Priem, R. Othman, P. Rozycki and D. Guillon, "Experimental investigation of the crash energy absorption of 2.5D-braided thermoplastic composite tubes," *Composite Structures*, vol. 116, pp. 814-826, 2014.
- [77] J. Bouchet, E. Jacquelin and P. Hamelin, "Static and dynamic behavior of combined composite aluminum tube for automotive applications," *Composites Science and Technology*, vol. 60, no. 10, pp. 1891-1900, 2000.
- [78] M. R. Bambach, "Fibre composite strengthening of thin-walled steel vehicle crush tubes for frontal collision energy absorption," *Thin-Walled Structures*, vol. 66, pp. 15-22, 2013.
- [79] J. M. Babbage and P. K. Mallick, "Static axial crush performance of unfilled and foam-filled aluminum-composite hybrid tubes," *Composite Structures*, vol. 70, no. 2, pp. 177-184, 2005.
- [80] J. Bouchet, E. Jacquelin and P. Hamelin, "Dynamic axial crushing of combined composite aluminum tube: the role of both reinforcement and surface treatments," *Composite Structures*, vol. 56, no. 1, pp. 87-96, 2002.
- [81] G. L. Farley and R. M. Jones, "Analogy for the effect of material and geometrical variables on energy-absorption capability of composite tubes," *Journal of Composite Materials*, vol. 26, no. 1, pp. 78-89, 1992.
- [82] G. L. Farley and R. M. Jones, "Crushing characteristics of continuous fiber-reinforced composite tubes," *Journal of Composite Materials*, vol. 26, no. 1, pp. 37-50, 1992.
- [83] G. L. Farley and R. M. Jones, "Prediction of the energy-absorption capability of

- composite tubes," *Journal of Composite Materials*, vol. 26, no. 3, pp. 388-404, 1992.
- [84] S. Boria, A. Scattina and G. Belingardi, "Axial energy absorption of CFRP truncated cones," *Composite Structures*, vol. 130, pp. 18-28, 2015.
- [85] Y. Ma, T. Sugahara, Y. Yang and H. Hamada, "A study on the energy absorption properties of carbon/aramid fiber filament winding composite tube," *Composite Structures*, vol. 123, pp. 301-311, 2015.
- [86] A. Jackson, S. Dutton, A. J. Gunnion and D. Kelly, "Effect of manufacture and laminate design on energy absorption of open carbon fibre/epoxy sections," in *ICCM17*, Edinburgh, 2009.
- [87] A. Jackson, S. Dutton, A. J. Gunnion and D. Kelly, "Investigation into laminate design of open carbon-fibre/epoxy sections by quasi-static and dynamic crushing," *Composite Structures*, vol. 93, no. 10, pp. 2646-2654, 2011.
- [88] Q. Liu, H. Xing, Y. Ju, Z. Ou and Q. Li, "Quasi-static axial crushing and transverse bending of double hat shaped CFRP tubes," *Composite Structures*, vol. 117, pp. 1-11, 2014.
- [89] J. Meredith, E. Bilson, R. Powe, E. Collings and K. Kirwan, "A performance versus cost analysis of prepreg carbon fibre epoxy energy absorption structures," *Composite Structures*, vol. 124, pp. 206-213, 2015.
- [90] Q. Liu, Z. Ou, Z. Mo, Q. Li and D. Qu, "Experimental investigation into dynamic axial impact responses of double hat shaped CFRP tubes," *Composites Part B: Engineering*, vol. 79, pp. 494-504, 2015.
- [91] J. Obradovic, S. Boria and G. Belingardi, "Lightweight design and crash analysis of composite frontal impact energy absorbing structures," *Composite Structures*, vol. 94, no. 2, pp. 423-430, 2012.
- [92] M. R. S. Huisman, Experimental and numerical investigations for the prediction of the crashworthiness of layered quasi-isotropic thermoplastic composites, Kaiserslautern: Institut für Verbundwerkstoffe GmbH, 2001.

-
- [93] M. R. S. Huisman and M. Maier, "Investigation on the crash behaviour of knitted glass fibre reinforced poly (ethylene-terephthalate) structures," *International Journal of Crashworthiness*, vol. 5, no. 1, pp. 79-88, 2000.
- [94] A. Dehn, M. R. S. Huisman and M. Maier, "Effects of temperature on the crash behaviour of glass fiber reinforced polyamide 12," *International Journal of Crashworthiness*, vol. 4, no. 3, pp. 317-326, 1999.
- [95] ISO 14125:1998 (E) Fibre-reinforced plastic composites-Determination of flexural properties, International Organization for Standardization, 1998.
- [96] G. Jung, P. Mitschang and C. Park, "New GMT material suitable for various polymers and high glass fiber content," in *ECCM 16*, Seville, 2014.
- [97] G. Jung, P. Mitschang and C. Park, "New GMT material suitable for various polymers and high glass fibre content," *Plastics, Rubber and Composites*, vol. 44, no. 3, pp. 117-122, 2015.
- [98] F. M. White, "Differential relations for fluid flow," in *Fluid Mechanics*, 7th ed., ISBN 9780073529349, McGraw Hill, 2010, pp. 229-292.
- [99] R. B. Bird, W. E. Stewart and E. N. Lightfoot, "Velocity distributions in laminar flow," in *Transport Phenomena*, ISBN 9780471073925, John Wiley & Sons, 1960, pp. 34-70.
- [100] R. B. Bird, W. E. Stewart and E. N. Lightfoot, "Interphase transport in isothermal systems," in *Transport Phenomena*, ISBN 9780471073925, John Wiley & Sons, 1960, pp. 180-207.
- [101] W. McCabe, J. Smith and P. Harriott, "Flow past immersed objects," in *Unit Operations of Chemical Engineering*, 7th ed., ISBN 9780072848236, McGraw Hill, 2004, pp. 155-193.
- [102] G. Jung, H. Kim and S. Kim, "Preparation and characterization of lime-silica solids," *Industrial & Engineering Chemistry Research*, vol. 39, no. 5, pp. 1264-1270, 2000.
- [103] P. J. Bates, D. Taylor and M. F. Cunningham, "Compaction and transverse

- permeability of glass rovings," *Applied Composite Materials*, vol. 8, no. 3, pp. 163-178, 2001.
- [104] X. Chen and T. D. Papathanasiou, "On the variability of the Kozeny constant for saturated flow across unidirectional disordered fiber arrays," *Composites Part A: Applied Science and Manufacturing*, vol. 37, no. 6, pp. 836-846, 2006.
- [105] R. C. Lam and J. L. Kardos, "The permeability and compressibility of aligned and cross-ply carbon fiber beds during processing of composites," *Polymer Engineering & Science*, vol. 31, no. 14, pp. 1064-1070, 1991.
- [106] G. Bechtold and L. Ye, "Influence of fibre distribution on the transverse flow permeability in fibre bundles," *Composites Science and Technology*, vol. 63, no. 14, pp. 2069-2079, 2003.
- [107] T. G. Gutowski, Z. Cai, S. Bauer, D. Boucher, J. Kingery and S. Wineman, "Consolidation experiments for laminate composites," *Journal of Composite Materials*, vol. 21, no. 7, pp. 650-669, July 1987.
- [108] R. Gennaro, M. Christmann, A. Greco, G. Rieber, P. Mitschang and A. Maffezzoli, "Experimental measurement of transversal micro-and macro permeability during compression molding of PP/Glass composites," *Polymer Composites*, vol. 35, no. 1, pp. 105-112, 2014.
- [109] V. Michaud, R. Törnqvist and J.-A. E. Månson, "Impregnation of compressible fiber mats with a thermoplastic resin. Part II: Experiments," *Journal of Composite Materials*, vol. 35, no. 13, pp. 1174-1200, 2001.
- [110] D. Merhi, V. Michaud, L. Kämpfer, P. Vuilliomenet and J.-A. E. Månson, "Transverse permeability of chopped fibre bundle beds," *Composites Part A: Applied science and manufacturing*, vol. 38, no. 3, pp. 739-746, 2007.
- [111] P. J. Dumont, L. Orgéas, V. Michaud and D. Favier, "Experimental study of fiber-matrix separation during compression of glass mat thermoplastics," in *9th International Conference on Flow Processes in Composite Materials*, Montréal, 2008.

- [112] Korea Petrochemical Ind. Co., Ltd, "General homo PP film grade: Yuhwa Polypro 1088".
- [113] T. Abt and M. Sánchez-Soto, "A review of the recent advances in cyclic butylene terephthalate technology and its composites," *Critical Reviews in Solid State and Materials Sciences*, vol. 42, no. 3, pp. 173-217, 2017.
- [114] G. Jung, M. Park, Y. Yoon, H. Kim, J. Yun and C. Park, "Method for manufacturing hybrid composite with thermoplastics and continuous fiber". KR Patent 1234494, 12 February 2013.
- [115] G. Jung, M. Park, Y. Yoon, H. Kim, J. Yun and C. Park, "Method of preparing thermoplastics-continuous fiber hybrid composite". US Patent 8470114, 25 June 2013.
- [116] G. Jung, M. Park, Y. Yoon, H. Kim, J. Yun and C. Park, "Method for producing thermoplastic/continuous fiber hybrid complex". JP Patent 5345694, 23 August 2013.
- [117] G. Jung, M. Park, Y. Yoon, H. Kim, J. Yun and C. Park, "Method of preparing thermoplastics-continuous fiber hybrid composite". US Patent 9068284, 30 June 2015.
- [118] G. Jung and P. Mitschang, "Multilayered hybrid roving as a manufacturing concept of continuous fiber reinforced thermoplastic materials," *Journal of Thermoplastic Composite Materials*, vol. 31, no. 2, pp. 145-161, 2018.
- [119] G. Jung and H. Kim, "Apparatus of double steel belt press heated by high frequency induction method". KR Patent 1293892, 31 July 2013.
- [120] G. Jung and H. Kim, "High frequency induction heating double steel belt press apparatus". JP Patent 5528577, 25 April 2014.
- [121] G. Jung and H. Kim, "High frequency induction heating double steel belt press apparatus". US Patent 9210741, 8 December 2015.
- [122] G. Jung and H. Kim, "High frequency induction heating double steel belt press apparatus". EP Patent 2540475, 2 May 2018.

- [123] G. Jung, H. Kim, C. Choi and H. Kang, "Development of continuous fiber-reinforced thermoplastic composites based on multi-layered hybrid roving," in *ACCM 7*, Taipei, 2010.
- [124] Y. Gil, G. Jung, M. Christmann and H. Kim, "New material developments for large scale production in automotive sector," in *ICCM 18*, Jeju, 2011.
- [125] G. Jung, P. Mitschang and C. Park, "New semi-finished materials for producing structural components," in *International AVK Conference*, Düsseldorf, 2014.
- [126] S. Sihm, R. Y. Kim, K. Kawabe and S. W. Tsai, "Experimental studies of thin-ply laminated composites," *Composites Science and Technology*, vol. 67, no. 6, pp. 996-1008, 2007.
- [127] H. M. EL-Dessouky and C. A. Lawrence, "Ultra-lightweight carbon fibre/thermoplastic composite material using spread tow technology," *Composites Part B: Engineering*, vol. 50, pp. 91-97, 2013.
- [128] H. Diao, A. Bismarck, P. Robinson and M. R. Wisnom, "Production of continuous intermingled CF/GF hybrid composite via fibre tow spreading technology," in *ECCM 16*, Seville, 2014.
- [129] M. S. Irfan, V. R. Machavaram, R. S. Mahendran, N. Shotton-Gale, C. F. Wait, M. A. Paget, M. Hudson and G. F. Fernando, "Lateral spreading of a fiber bundle via mechanical means," *Journal of Composite Materials*, vol. 46, no. 3, pp. 311-330, 2012.
- [130] M. S. Irfan, V. R. Machavaram, R. C. Murray, F. N. Bogonez, C. F. Wait, S. D. Pandita, M. A. Paget, M. Hudson and G. F. Fernando, "The design and optimisation of a rig to enable the lateral spreading of fibre bundles," *Journal of Composite Materials*, vol. 48, no. 15, pp. 1813-1831, 2014.
- [131] P. J. Bates and J. M. Charrier, "Method for continuously coating fibers". US Patent 5236743, 17 August 1993.
- [132] G. Jung, S. Schmeer and P. Mitschang, "Crash behavior and performance of long fiber reinforced thermoplastic material in comparison with continuous fiber

- reinforcement," *International Journal of Crashworthiness*, vol. <https://doi.org/10.1080/13588265.2017.1345588>, 2017.
- [133] RTP Company, "Product data sheet and general processing conditions: PP/GF grades (short fiber and chemically coupled)," 2005/2006.
- [134] RTP Company, "Product data sheet and general processing conditions: PA6/GF grades (short fiber and heat stabilized)," 2010.
- [135] RTP Company, "Product data sheet and general processing conditions: Polyamide 6 (PA6) unreinforced," 2005.
- [136] V. S. Sokolinsky, K. C. Indermuehle and J. A. Hurtado, "Numerical simulation of the crushing process of a corrugated composite plate," *Composites Part A: Applied Science and Manufacturing*, vol. 42, no. 9, pp. 1119-1126, 2011.
- [137] G. Pitarresi, J. J. Carruthers, A. M. Robinson, G. Torre, J. M. Kenny, S. Ingleton, O. Velecela and M. S. Found, "A comparative evaluation of crashworthy composite sandwich structures," *Composite Structures*, vol. 78, no. 1, pp. 34-44, 2007.
- [138] S. T. Taher, A. A. Oshkour, R. Zahari, F. Mustapha and S. Basri, "On the crush behavior of an ultra light multi-cell foam-filled composite structure under axial compression," *Journal of Reinforced Plastics and Composites*, vol. 29, no. 3, pp. 391-408, 2010.
- [139] A. G. Mamalis, D. E. Manolakos, M. B. Ioannidis and D. P. Papapostolou, "On the response of thin-walled CFRP composite tubular components subjected to static and dynamic axial compressive loading: experimental," *Composite Structures*, vol. 69, no. 4, pp. 407-420, 2005.
- [140] A. G. Mamalis, D. E. Manolakos, M. B. Ioannidis and D. P. Papapostolou, "The static and dynamic axial collapse of CFRP square tubes: Finite element modelling," *Composite Structures*, vol. 74, no. 2, pp. 213-225, 2006.
- [141] M. Hörmann and M. Wacker, "Simulation of the crash performance of crash boxes based on advanced thermoplastic composite," in *5th European LS-DYNA*

Users' Conference, Birmingham, 2005.

- [142] C. Bisagni, G. D. Pietro, L. Frascini and D. Terletti, "Progressive crushing of fiber reinforced composite structural components of a Formula One racing car," *Composite Structures*, vol. 68, no. 4, pp. 491-503, 2005.
- [143] H. Hamada and S. Ramakrishna, "Effect of fiber material on the energy absorption behavior of thermoplastic composite tubes," *Journal of Thermoplastic Composite Materials*, vol. 9, no. 3, pp. 259-279, 1996.
- [144] S. Ochelski, P. Bogusz and A. Kiczko, "Heat effects measurements in process of dynamic crash of polymer composites," *Bulletin of the Polish Academy of Sciences: Technical Sciences*, vol. 60, no. 1, pp. 25-30, 2012.
- [145] J. Meredith, S. Cozien-Cazuc, E. Collings, S. Carter, S. Alsop, J. Lever, S. R. Coles, B. M. Wood and K. Kirwan, "Recycled carbon fibre for high performance energy absorption," *Composites Science and Technology*, vol. 72, no. 6, pp. 688-695, 2012.

7 Appendix

Betreute studentische Arbeiten

Es wurden keine studentische Arbeiten betreut.

Publikationen

Journale

G. Jung, P. Mitschang and C. Park, "New GMT material suitable for various polymers and high glass fibre content," *Plastics, Rubber and Composites*, vol. 44, no. 3, pp. 117-122, 2015.

G. Jung and P. Mitschang, "Multilayered hybrid roving as a manufacturing concept of continuous fiber reinforced thermoplastic materials," *Journal of Thermoplastic Composite Materials*, vol. 31, no. 2, pp. 145-161, 2018.

G. Jung, S. Schmeer and P. Mitschang, "Crash behavior and performance of long fiber reinforced thermoplastic material in comparison with continuous fiber reinforcement," *International Journal of Crashworthiness*, vol. <https://doi.org/10.1080/13588265.2017.1345588>, 2017.

Magazine

G. Jung, "Neue thermoplastische Halbzeuge für strukturelle Bauteile," *Carbon Composites Magazin*, no. 2, p. 15, 2014.

G. Jung, "Multi-layered hybrid rovings and mats," *CVC News*, no. 2, p. 19, 2014.

G. Jung and S. Schmeer, "Material consideration for better crash parts: from metallic to fiber reinforced thermoplastic materials," *Composite Solutions*, no. 3, pp. 26-31, 2016.

Symposien- und Konferenzbeiträge

P. Mitschang and G. Jung, "Activities in thermoplastic composite material in Europe," in *International Textile Fair*, Daegu, 2013.

G. Jung, P. Mitschang and C. Park, "New GMT material suitable for various polymers and high glass fiber content," in *ECCM 16*, Seville, 2014.

G. Jung, P. Mitschang and C. Park, "New semi-finished materials for producing structural components," in *International AVK Conference*, Düsseldorf, 2014.

G. Jung, "Material consideration for better crash parts: from metallic to fiber

reinforced thermoplastic materials," in *2nd International Conference Lightweight Chassis and Body Design*, Berlin, 2016.

C. Goergen and G. Jung, "Composite material development: high content of long fiber reinforced thermoplastic," in *CCeV Thermoplastic*, Kaiserslautern, 2016.